UNIVERSITÀ DEGLI STUDI DI PADOVA

FACOLTÀ DI INGEGNERIA

DIPARTIMENTO DI TECNICA E GESTIONE DEI SISTEMI INDUSTRIALI

Gießerei Technologie Aalen

AALEN HOCHSCHÜLE FÜR TECHNIK UND WIRTSCHAFT

GIESSEREI TECHNOLOGIE AALEN

CORSO DI LAUREA MAGISTRALE IN INGEGNERIA DELL'INNOVAZIONE DEL PRODOTTO

INVESTIGATION ON THE EFFECTS OF INNOVATIVE MELT TREATMENTS ON MICROSTRUCTURE AND MECHANICAL BEHAVIOUR OF DIECAST AL ALLOYS

Relatori:

Prof. Dr. Ing. Lothar H. Kallien

Prof. Ing. Franco Bonollo

Laureando:

Alberto Dal Maso

Academic year 2011 − 2012

Indice

Compendio

Introduzione

La ricerca di materiali innovativi e dalle prestazioni sempre migliori sta avendo un ruolo chiave nello sviluppo di molti settori. Una delle strategie più spesso adottate per il miglioramento delle caratteristiche dei materiali è quella di unire due o più materiali complementari, che interagendo portino al raggiungimento di prestazioni superiori. Questo principio sta alla base della ricerca sui materiali compositi. Tra i materiali compositi, quelli a matrice metallica risultano interessanti sia per le prestazioni raggiungibili che per la varietà e versatilità dei processi in cui possono essere impiegati.

In questo lavoro sono riportati i risultati della sperimentazione di un trattamento effettuato su alluminio fuso con lo scopo di produrre ossido di alluminio in forma di particelle e di mantenerlo disperso all'interno del fuso, al fine di inglobarlo nel metallo, una volta solidificato.

L'impiego di Al_2O_3 come rinforzo si è dimostrato utile in due modi: come rinforzo meccanico, comporta un aumento della durezza, della resistenza e del modulo elastico delle leghe d'alluminio; come agente affinante, migliora le prestazioni delle leghe grazie all'ottenimento di una microstruttura più fine.

Oltre ad analizzare l'effetto del trattamento sull'alluminio puro, tre leghe Al-Cu sono state prodotte a partire dall'alluminio trattato. Le leghe realizzate sono state testate sia in colata in forma permanente, sia in pressocolata.

Il processo di pressocolata

Il processo di pressocolata è impiegato principalmente per la produzione di componenti in leghe a base Al, Mg o Zn. Consiste nell'iniezione ad altissima pressione di lega fusa in uno stampo in acciaio tramite l'azione di un pistone spinto da un circuito idraulico. Si tratta di un processo dall'elevata produttività, impiegato da decenni, nella sua versione moderna, per la realizzazione di componenti in grandi volumi e con scarsi requisiti strutturali. Negli ultimi anni, la qualità raggiunta e il migliorato controllo del processo di pressocolata hanno permesso di realizzare getti con funzione strutturale, capaci di integrare molti componenti convenzionalmente

prodotti e assemblati in più fasi. La pressocolata trova larghissimo impiego nel settore automotive, in cui i volumi produttivi giustificano ampiamente gli investimenti necessari.

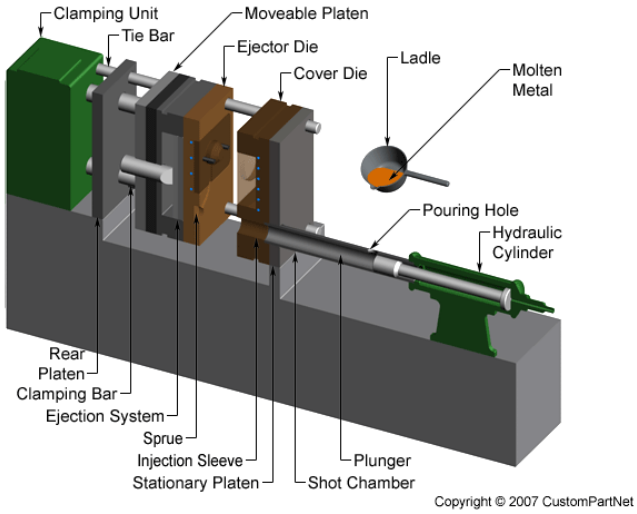

Figura 1: rappresentazione in sezione di una macchina da pressocolata

Recenti innovazioni nel processo di pressocolata, come l'introduzione del vuoto e l'utilizzo leghe allo stato semi-solido, hanno portato ad ulteriori miglioramenti nella qualità dei getti realizzati.

Leghe Al-Cu

Le leghe Al-Cu sono tra le più resistenti leghe di alluminio. Sono impiegate sia come leghe da deformazione plastica, sia come leghe da fonderia. La loro elevata resistenza a frattura e il buon livello di allungamento a rottura derivano dal processo di rafforzamento per precipitazione di fasi secondarie, ottenuto con trattamenti di invecchiamento artificiale o naturale dopo solubilizzazione.

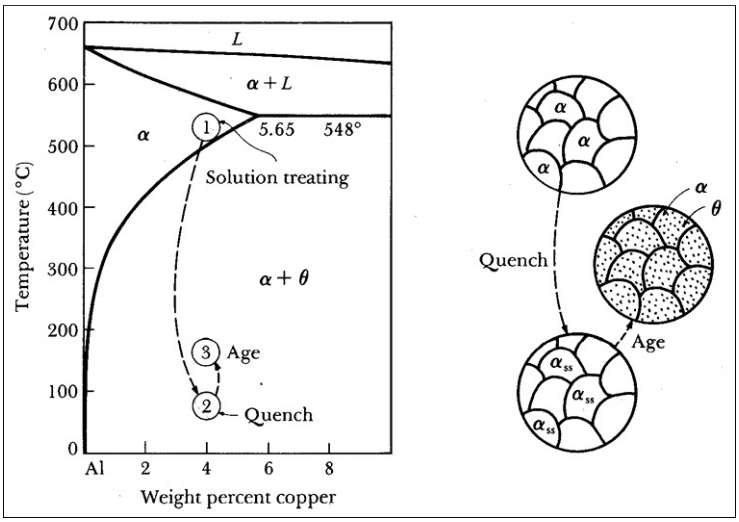

Figura 2: illustrazione del processo di rafforzamento per precipitazione

Le prestazioni di queste leghe si apprezzano in un ampio intervallo di temperature, per cui sono spesso impiegate in applicazioni criogeniche o ad alta temperatura. Le leghe Al-Cu soffrono, tuttavia, di alcune debolezze: hanno un'elevata tendenza alla criccatura a caldo, che ne impedisce l'utilizzo in pressocolata e ne limita la saldabilità, e hanno una ridotta resistenza alla corrosione, a causa dell'interazione galvanica tra alluminio e rame a contatto con l'atmosfera. Se da un lato limitare la corrosione di queste leghe è possibile con l'uso di vernici o altri trattamenti superficiali, limitare la criccabilità a caldo risulta più complicato. Risultati positivi sono stati ottenuti aumentando la temperatura dello stampo e in generale promuovendo la formazione di una microstruttura globulare o equiassica.

Il trattamento

Il trattamento consiste nell'iniettare una miscela di argon e ossigeno in un bagno di alluminio fuso, tenuto in agitazione per mezzo di una girante. Si ipotizza che l'ossigeno presente nelle bolle vada ad ossidare l'alluminio con cui viene a contatto e che la turbolenza indotta dalla girante possa rompere lo strato d'ossido creatosi, disperdendolo nel fuso mentre il gas inerte risale in superficie. L'impiego di argon contribuisce a formare un'atmosfera protettiva al di sopra del bagno fuso, per limitare l'ossidazione del fuso da parte dell'ossigeno presente in aria.

Per realizzare questo trattamento sono stati realizzati due impianti. In quello di dimensioni minori, costruito appositamente, il gas viene iniettato in un crogiolo all'interno di un forno a induzione tramite una girante realizzata per asportazione di

truciolo da un blocco di nitruro di boro, BN. La girante è incollata ad un tubo di ossido di alluminio, a sua volta unito ad un tubo di acciaio di 10 mm di diametro, montato sul mandrino di un miscelatore.

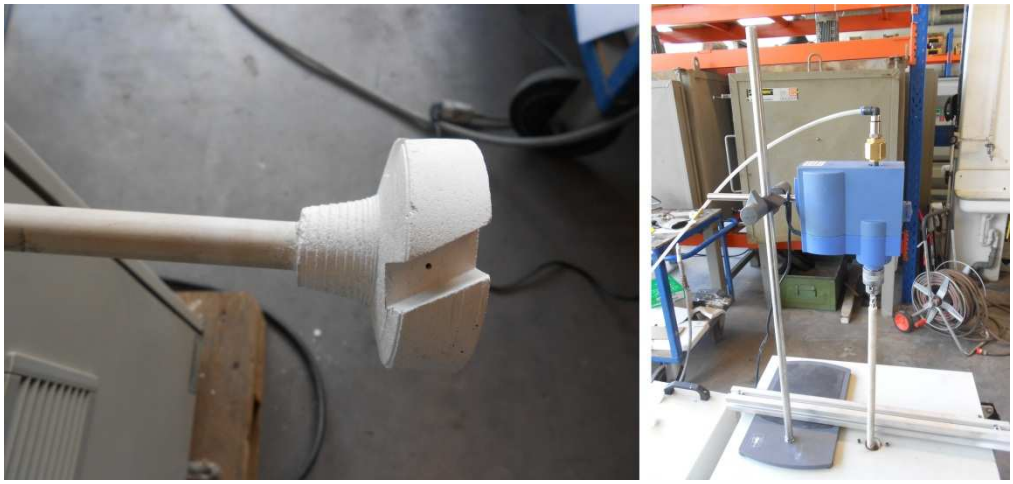

Figura 3: girante e miscelatore utilizzati nell'impianto più piccolo

La miscela di gas è realizzata a partire da una bombola contenente Ar e da una bombola di gas da saldatura PRAXAIR Stargon O8, costituito al 92 %vol. da Ar e all'8 %vol. da O_2. I due gas sono miscelati in un circuito controllato da due misuratori/regolatori di portata. La miscela in uscita entra nel tubo di acciaio per mezzo di un giunto rotante ed esce nel metallo fuso attraverso dei fori radiali realizzati sulla girante.

Il tubo di allumina si è rotto dopo 120 min ti utilizzo, probabilmente a causa di stress termici troppo elevati.

L'impianto più grande utilizza una normale unità di degasaggio dell'alluminio, con lievi modifiche alla girante per adattarla alle esigenze del trattamento. Il sistema di miscelazione del gas è il medesimo.

Durante il trattamento, sulla superficie del fuso e attorno alle giranti si accumula una scoria costituita da ossido e alluminio solidificato. Tale scoria sembra prodotta dall'agglomerarsi delle bolle che, una volta ossidata la superficie, galleggiano verso il pelo libero del fuso.

Figura 4: scoria formatasi sulla superficie del bagno fuso di alluminio fuso

Campioni prodotti

L'efficacia del trattamento è stata valutata misurando le proprietà meccaniche dei materiali ottenuti. Sono stati colati provini da trazione di sezione circolare mediante colata in conchiglia e piastre di 3 mm di spessore mediante processo di pressocolata, da cui sono stati ricavati provini da trazione di sezione rettangolare.

Il processo di pressocolata è stato eseguito con una macchina da 200 tonnellate di forza di serraggio, equipaggiata con un sistema a vuoto StatVac per l'estrazione dell'aria dallo stampo.

I getti ottenuti dalle leghe di Al-Cu presentano una elevata tendenza alla criccatura a caldo. Solo alzando la temperatura dello stampo in pressocolata si è ottenuta una riduzione sensibile del fenomeno.

Figura 5: piasta ottenuta per pressocolata con evidenti segni di criccatura a caldo

Materiali e trattamenti

Sono state testate 4 differenti leghe. La prima è l'alluminio puro in lingotti, come fornito dalla fonderia, che è stato sottoposto al trattamento di iniezione della miscela di gas. Le altre tre leghe sono state realizzate aggiungendo gli elementi all'alluminio puro dopo il trattamento del fuso.

Lega	Composizione, wt.%									
	Cu	Mn	Mg	Zn	Ti	Fe *	Si *	altri *		Al
								ciasc.	totale	
1	-	-	-	-	-	0.22	0.07	<0.007	0.06	bil.
2	4.61	-	-	-	-	0.22	0.07	<0.007	0.07	
3	4.99	0.45	0.37	-	-	0.24	0.08	<0.008	0.07	
4	4.98	0.42	0.27	0.1	0.023	0.20	0.28	<0.008	0.07	

Tabella 1: composizione chimica delle leghe testate (*=impurità)

Per ogni lega sono state testate diverse condizioni di trattamento e/o di colata. Nella tabella 2 sono riportati i parametri utilizzati con ciascuna lega.

Lega	Gas iniettato		Tempo di trattamento	Temp. del fuso	Impianto utilizzato		Processo di colata	
	Ar	Ar + 8 vol.% O_2			Ø 72 mm 650 rpm	Ø 185 mm 350 rpm	conchiglia	HPDC
1	●	●	0 – 15, 0 – 30, 45, 85, 120 min	730 °C	●	●	●	-
2	-	●	30 min	730 °C	-	●	●	●
3	-	●	30 min	730 °C	-	●	●	●
4	-	●	90 min	730 °C	-	●	●	●

Tabella 2: parametri di trattamento e processi di colata utilizzati per ciascuna lega

Lega 1

La lega 1 è stata testata realizzando dei provini in conchiglia di lega prelevata dal crogiolo durante i trattamenti. Le proprietà meccaniche sono state analizzate in funzione del tempo di trattamento, allo scopo di individuare l'evoluzione del materiale durante il processo.

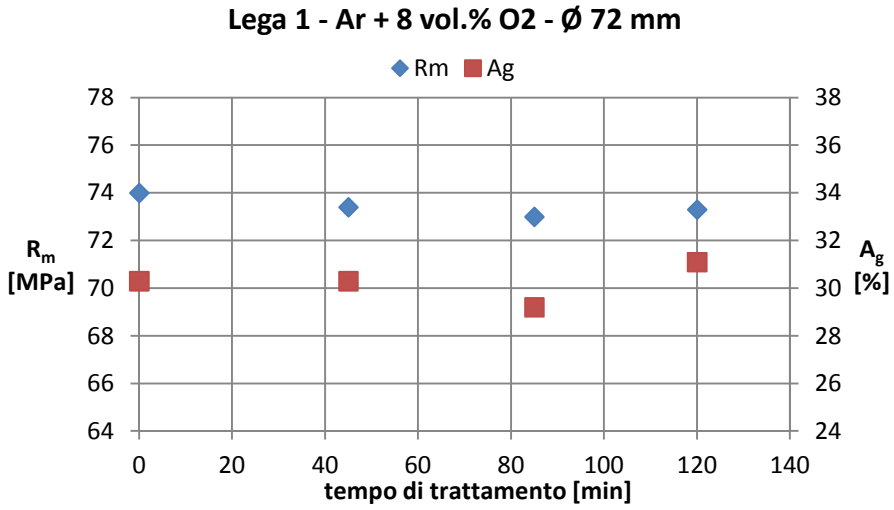

Figura 6: proprietà meccaniche della lega 1 - iniezione di Ar + O2 - girante da Ø 72 mm

In figura 6 sono riportate le proprietà meccaniche del materiale durante il trattamento con la girante più piccola. Nota: A_g indica l'allungamento permanente sotto carico massimo. Non si rilevano variazioni sostanziali delle prestazioni del materiale.

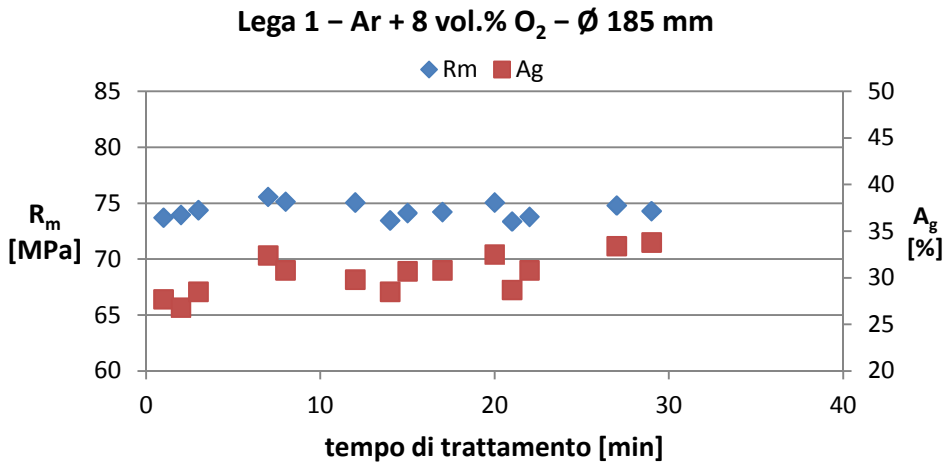

Figura 7: proprietà miccaniche della lega 1 - iniezione di Ar + O2 - girante da Ø 185 mm

In figura 7 sono riportate le proprietà meccaniche della lega 1 durante il trattamento con l'impianto più grande. Il carico di rottura rimane sostanzialmente invariato, mentre si osserva un andamento positivo dell'allungamento. Tuttavia, i valori ottenuti sono confrontabili con quelli del materiale sottoposto a trattamento con iniezione di solo argon. Il contenuto di porosità è stato valutato tramite tomografia computerizzata e correlato alla variabilità di prestazioni del materiale.

L'osservazione della microstruttura al microscopio ottico ha rivelato la presenza di un eutettico Al/Al_3Fe, presente sia nella lega non trattata sia in quella trattata. Non sono state osservate variazioni nella microstruttura dopo il trattamento.

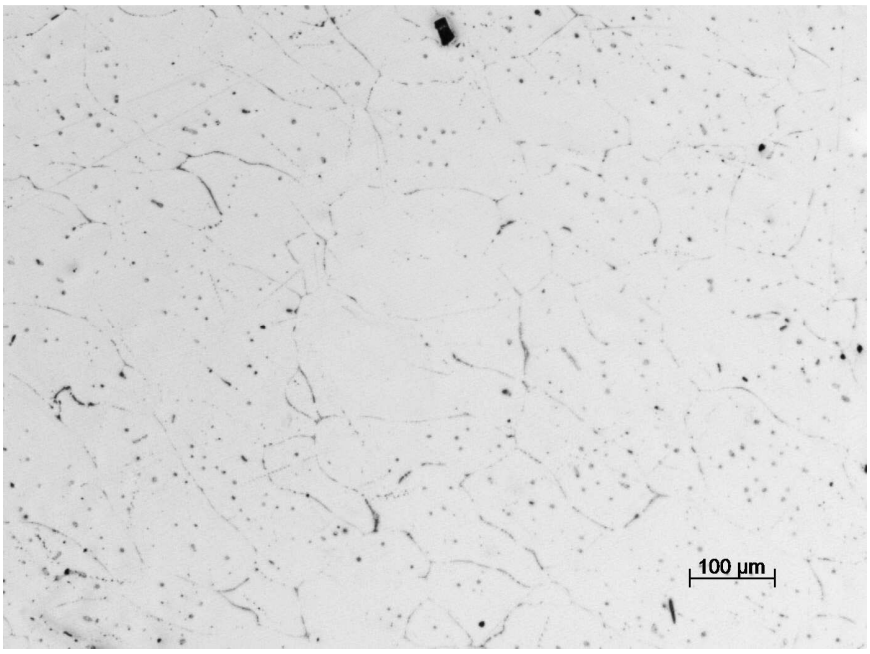

Figura 8: microstruttura della lega 1 dopo trattamento con iniezione di Ar + O_2

Lega 2

La lega 2 è stata testata sia in colata in conchiglia, sia in pressocolata. In entrambi i casi la lega si è dimostrata suscettibile di criccatura a caldo. Le prestazioni della lega migliorano sensibilmente grazie all'aggiunta di rame: UTS = 175 ÷ 181 MPa, YS = 48 ÷ 57 MPa, A = 8,6 ÷ 10,5%. Le prestazioni del materiale in forma permanente sono comparabili con quelle di una lega EN AC-21100 (UTS = 170 MPa, YS = 70 MPa, A = 5%). Solo il carico di snervamento risulta sensibilmente più basso. Le prestazioni della lega pressocolata raggiungono valori ancora più elevati, ma l'elevata presenza di cricche compromette la resistenza della maggior parte dei campioni testati.

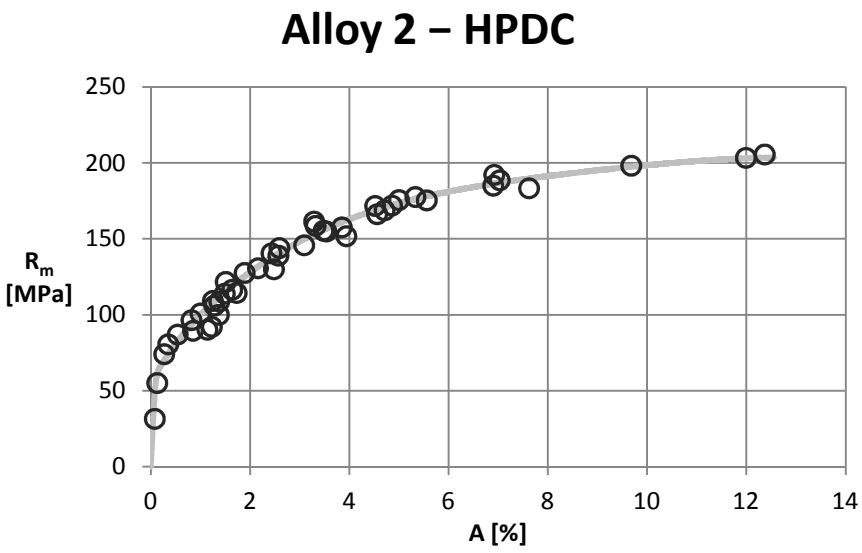

Figura 9: distribuzione dei punti di rottura dei provini di lega 2 pressocolata

La microstruttura si presenta dendritica, con presenza di fase $CuAl_2$ negli spazi interdendritici, assieme alla fase ricca in Fe già osservata nella lega 1.

Lega 3

La lega 3 è stata testata sia in conchiglia che in pressocolata. L'aggiunta di Mg e Mn, assieme ad un contenuto di Cu superiore, hanno determinato, nei provini colati in conchiglia, un aumento considerevole del carico di snervamento, che risulta triplicato, assieme ad un incremento del carico di rottura di circa 50 MPa, rispetto alla lega 2. Per contro, l'allungamento a rottura è ridotto al 3%. I risultati sono confrontabili con le specifiche della lega EN AC-21000 (UTS = 165 ÷ 195 MPa, YS = 195 ÷ 235 MPa, A = 1 ÷ 4 MPa). Le prestazioni della lega in pressocolata sono di poco superiori per quanto riguarda il carico di rottura, mentre l'allungamento, sebbene molto variabile a causa della difettosità, è in generale superiore, con picchi di oltre il 9 %. Anche nei getti in lega 3 è stata osservata una forte tendenza alla criccatura a caldo e una variabilità dei dati dovuta alla presenza di difetti.

La microstruttura della lega 3 si differenzia da quella della lega 2 per la presenza di piccole particelle di Mg solidificate in seno alla fase $CuAl_2$ e la formazione di una fase ricca in Fe e Mn.

Lega 4

La lega 4 è stata testata, come la lega 2 e la lega 3, sia in conchiglia, sia in pressocolata. La sua composizione non si differenzia molto da quella della lega 3. Le proprietà meccaniche della lega colata in conchiglia sono allineate con quelle della lega 3, con un allungamento a rottura del leggermente superiore (3,5 ÷ 3,7 %) e un carico di snervamento di poco inferiore (137 ÷ 147 MPa). I provini ottenuti per pressocolata sono stati testati sia in condizione "as-cast", sia dopo trattamento T4. I primi mostrano proprietà meccaniche migliori rispetto a quanto visto per la lega 3, complice una riduzione della criccatura a caldo ottenuta aumentando la temperatura dello stampo, con allungamenti che arrivano quasi sempre oltre il 6 % e in più casi superano il 9 %. Anche il carico di rottura è in genere più alto.

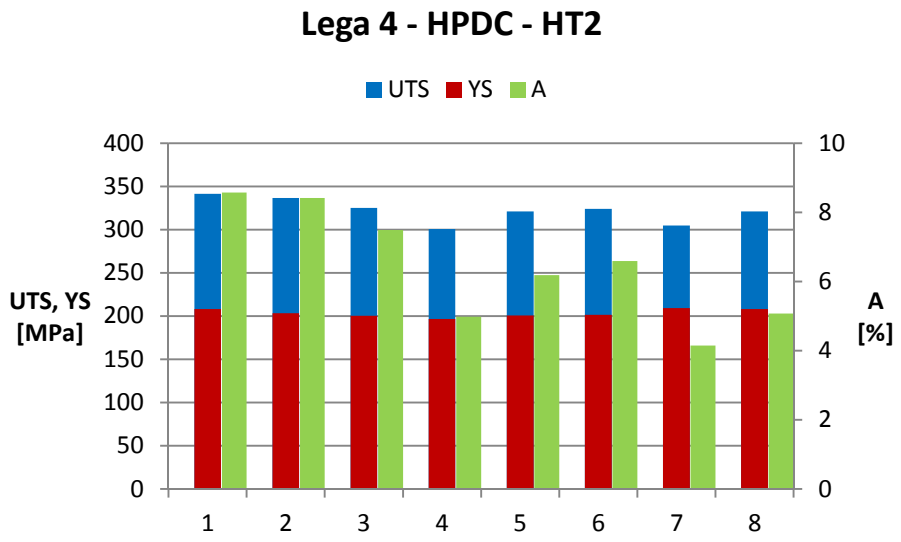

Figura 10: proprietà meccaniche della lega 4 dopo invecchiamento

I secondi sono stati sottoposti a trattamento termico di solubilizzazione e poi sono stati conservati a temperatura ambiente per 55 giorni. Due trattamenti di solubilizzazione differenti sono stati eseguiti. La lega dopo invecchiamento presenta proprietà meccaniche molto superiori, con carico di snervamento YS = 200 ÷ 208 MPa, carico di rottura oltre i 320 MPa e allungamento compreso tra 6 e 8 %. La presenza di difetti riduce il carico di rottura e l'allungamento a rottura di diversi provini. Non si riscontrano differenze nelle proprietà meccaniche derivanti dal diverso trattamento di solubilizzazione eseguito. Le prestazioni fatte registrare dalla lega invecchiata sono in linea con quanto riportato per la lega AA 206.0-T4.

La microstruttura della lega 4 prima del trattamento di solubilizzazione è dendritica e presenta le stesse fasi della lega 3, con l'aggiunta di una fase dovuta all'introduzione di Zn. Dopo trattamento di solubilizzazione, solo le fasi insolubili rimangono visibili, mentre Mg e $CuAl_2$ sono completamente solubilizzate.

Conclusioni

Il trattamento del fuso con miscela di Ar e O_2, oggetto di questa sperimentazione, non ha portato miglioramenti evidenti nelle proprietà meccaniche e nella microstruttura dell'alluminio. Apparentemente, tutto l'ossido che si forma durante il trattamento si accumula sulla superficie del fuso per galleggiamento e forma una scoria schiumosa di ossido e alluminio.

Le leghe realizzate a partire dall'alluminio trattato mostrano proprietà in linea con quanto riportato in letteratura, con alcune differenze attribuibili alle condizioni di colata e alla difettosità dei campioni. I dati confermano l'assenza di un beneficio tangibile dovuto al trattamento dell'alluminio fuso.

La criccabilità tipica delle leghe di Al-Cu è stata riscontrata sia in colata in conchiglia, sia in pressocolata. Nel secondo processo, l'aumento della temperatura dello stampo ha favorito la riduzione del fenomeno, consentendo di realizzare getti privi di cricche visibili a occhio nudo. Tuttavia, cricche interne rimangono presenti, in quantità limitate.

La sperimentazione descritta in questo lavoro trae ispirazione dai risultati presentati da David Weiss di Eck Industries alla 12° International Summer School on Light Alloys Casting, tenutasi a Vicenza presso il Dipartimento di Tecnica e Gestione dei Sistemi Industriali dell'Università di Padova nel luglio del 2011, riguardanti le prestazioni ottenute su una lega AA A206.0 rinforzata con particelle di Al_2O_3.

Tra tutti i metodi di produzione di compositi a matrice metallica descritti in letteratura o depositati come brevetti, molti richiedono l'impiego di materiali e attrezzature dai costi elevati e di difficile impiego in un ambiente produttivo convenzionale, talvolta non garantendo risultati ottimali.

Un processo sviluppato da Cecilia Borgonovo e Makhlouf M. Makhlouf, presso l'Advanced Casting Research Centre del Worcester Polytechnic Institute,

USA, ha permesso di produrre leghe Al-Li rinforzate da nanoparticelle di AlN utilizzabili in pressocolata. Il processo, per facilità di realizzazione e qualità dei risultati, è stato preso a modello per l'ideazione del trattamento qui sperimentato.

I risultati ottenuti dimostrano l'inefficacia di questo trattamento nelle condizioni in cui è stato eseguito. Tuttavia, sperimentazioni più approfondite su questo tipo di processi devono essere promosse al fine di favorire l'impiego di questi materiali in ambito produttivo.

Acknowledgements / Ringraziamenti

This work was partially developed at the *Giesserei Technologie Aalen* lab, at the Hochschule für Technik und Wirtschaft, Aalen, Germany. For this reason I would like to thank Prof. Kallien and the University of Aalen, especially the crew at the IRO, for the warm welcome and hospitality during the semester spent there. I would also thank the people at the laboratory, who helped me out with my project. Müjdat, Marcel, Vale, Alex, Dejan, Otto, Christian, Walter and Thomas, vielen Dank.

Un ringraziamento va al Prof. Bonollo per avermi offerto l'opportunità del progetto Erasmus e per avermi dato fiducia quando il progetto faticava ad avanzare.

Ringrazio gli amici che si sono fatti sentire nei mesi in cui parlare in italiano era un evento raro: Gael, Ilaria, Marco, Simone, Michele, Alberto, Matteo, Matteo e tutti quelli che nella fretta sto dimenticando.

Ringrazio la mia famiglia per il sostegno in questi due anni, specialmente per l'appoggio in questi ultimi, difficili mesi. Ringrazio soprattutto i miei genitori per avermi dato un sostegno incondizionato e una grande fiducia, anche quando la mia è mancata del tutto.

Infine, ringrazio Anna, perché è una donna meravigliosa.

1 Introduction

The research on new and improved materials has become a key factor in most of the engineering fields. Often, improving the behaviour of a material is the only possibility to reach better performances and to step beyond the previous limits of a given application. In mechanical engineering, this is true in high temperature applications, in components with high strength-to-weight requirements, in corrosive environments, in components subjected to wear and in many more cases. The need for new materials is become so high that material science is today one of the most brisk research fields.

One of the best strategies to achieve new performances is that of putting together two or more materials to gain the best of all of them and to reduce the weaknesses of each. It is not always a good solution and the interaction between the coupled materials plays a key role. This strategy is successfully applied in a great variety of composite materials based on polymer, metal or ceramic matrixes. Materials with extreme performances have been developed, though often at very high costs. Actually, the production problems and costs are the main limitations of these materials, which proved to be reliable in many demanding applications.

Among all the composite materials, metal-matrix composites (MMC) are becoming more and more attractive because of their proved good performances and the variety of processes they are suitable for. MMCs are usally composed of a metal matrix reinforced with a ceramic phase, in the form of particles, fibers or platelets, which can stand temperatures higher than the melting point of the matrix. This way, the casting and forming processes conventionally applied to metals are also available for MMCs. The ways MMC are fabricated are numerous. Two main categories can be individuated: the *in-situ* processes and the *ex-situ* processes. In the formers, the reinforcing phase is created within the matrix, in the latters, the reinforcing phase is firstly produced by independent process and secondly added to the metal matrix.[1]

Metal-matrix nanocomposites (MMNC) are becoming very popular because of the great performances reachable and the overcome of some limitations of MMCs, such as low fracture toughness and low machinability. In MMNC, the size of reinforcing particles is in the order of $10^{-9} \div 10^{-7}$ m at least in one dimension. Despite

their better performances, their production is more complex because of the difficulty of attaining a good dispersion of the nanoscale reinforcing phase.[2][3]

Particles of Al_2O_3 have been adopted as reinforcement in MMC to reach higher strength and hardness, higher elastic modulus and better performances at high temperature. Al_2O_3 acts both as mechanical reinforcement, increasing the hardness and the elastic modulus of MMCs, and as metallurgical reinforcement, promoting a refinement of the microstructure, which improves the overall mechanical behaviour of MMCs. Many processes have been employed to produce Al_2O_3-reinforced MMCs, both *in-situ* and *ex-situ*.[4]

Al-Cu alloys may be employed as metal matrixes for Al_2O_3-MMCs. Al-Cu alloys feature very high strength and good toughness, even at high temperatures. The adoption of Al_2O_3 particles as grain refining agents may improve the mechanical properties of these alloys and strongly reduce their hot cracking susceptibility. Improvements in hot cracking resistance by means of Al_2O_3 particles addition have already been verified.

In this work, an investigation on the possibility to produce Al_2O_3 particles within molten aluminium by means of an innovative melt treatment is carried out. The effects of the treatment on the mechanical properties of the treated alloy have been studied. Moreover, the results of employing the treated aluminium as master alloy for the production of Al-Cu alloys has been investigated. The alloys have been tested in permanent mold and high pressure die casting.

2 HPDC

Introduction to HPDC

High Pressure Die Casting (HPDC), also simply referred to as Die Casting, basically consists of forcing molten metal into a reusable steel mould, called a die, under the high pressure generated by a hydraulic plunger. The cavity of the die gives shape to the casting and can be designed to produce very complex parts with a high degree of dimensional accuracy and repeatability. The infinite variety of parts that can be manufactured, together with the good tolerances achievable and the number of alloys suitable for die casting, make this process absolutely versatile.

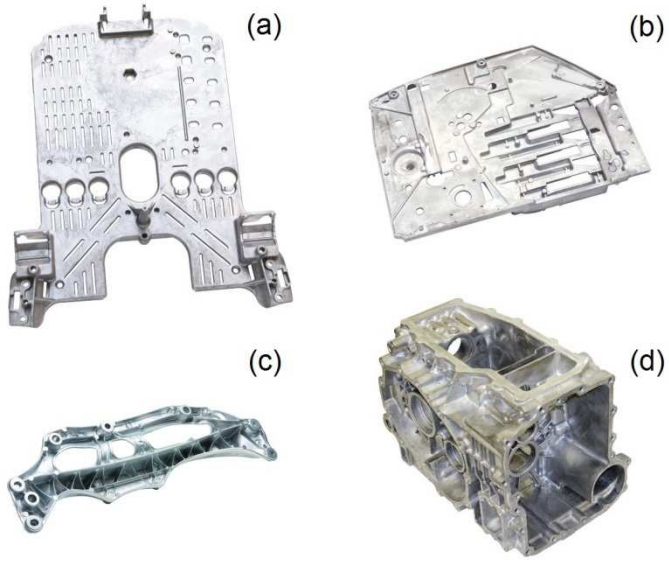

Figure 2.1: parts produced with HPDC: a dental chair component (a), a medical imager side wall (b), an engine base bracket (c) and a transaxle housing (d).

In addition, the production rate of die casting is very high and a HPDC cell can be completely automated, bringing its productivity to highest levels. Hence, die castings are among the highest volume, mass-produced parts in metalworking industry. For this reason, industries with high production volumes are those taking major advantage from this process: automotive first, but also consumer electronic devices, sport equipment, hardware, housewares and more.

History

HPDC is a relatively recent technology for the foundry industry, even if its history started in the middle of the 19th century, when a low-pressure, primitive version of it was patented for casting printing type. Towards the end of the century other shapes began to be developed and mass production of many products began in the early 1900s.

Initially used to cast tin and lead of various compositions, it's become a widely used process since the early decades of the 20th century, when these metals were substituted by the introduction of zinc and aluminium alloys, shortly followed by magnesium and copper. Many of the alloys still in use today were already available in the 1930s.

Long used in high-volume production of simple and cheap parts with limited structural function, today it well fits the production of components for more and more demanding applications. Over the last century, improvements in process, alloys and design of parts made HPDC very reliable and repeatable, allowing components as big and complex as engine blocks to be successfully cast.

Today, new technologies, such as vacuum assisted HPDC (Vacural) and semi-solid HPDC, coupled with better control over the process parameters, allow for the reduction of defects, especially gas porosities, to very low levels making heat treatments and welding of the castings available.[5]

Alloys for HPDC

Al-, Mg- and Zn-based alloys are the alloys with highest production volumes among those conventionally cast by HPDC. The fluidity and castability requirements and the resistance to hot tearing limit the number of alloys suitable for this process.

Aluminium alloys for HPDC mostly belong to the 4XXXX series, with Si as main alloying element, which provides the high fluidity necessary. Other alloying elements present in the die casting alloys of this series are Cu and Mg. Some Al-Mg alloys from the 51XXX series are also suitable.

Magnesium alloys have Al as main alloying element and Zn or Mn as secondary alloying element. AZ91, AM20, AM50 and AM60 are the four alloys commonly adopted.

Zinc alloys have Al as main alloying element, with wt.% of 4 or 8, and Cu as secondary element in some alloys. Mg is present in low content, from 0.015% to 0.05%. ZP0400, ZP0410, ZP0430 and ZP0810 are the alloys cast with HPDC process.

Copper, tin and lead alloys are also die cast, with lower production volumes.

The machine

In HPDC, molten metal is injected into the die under high pressure, generated by a plunger moved by a hydraulic cylinder. The machine that performs this process is composed of three main parts: the clamping unit, the die assembly and the injection unit. The injection mechanism makes the difference between hot-chamber and cold-chamber HPDC machines. The mechanism of the former is immersed in the molten metal bath within a furnace. It has a metal feed system, called a gooseneck, that is attached to the machine. A vertical plunger pushes the metal through the gooseneck to the die. This mechanism prevents oxidation of the melt and increase the productivity, if compared to the cold-chamber process. Hot-chamber machines are employed for alloys with low melting temperatures, such as zinc alloys.

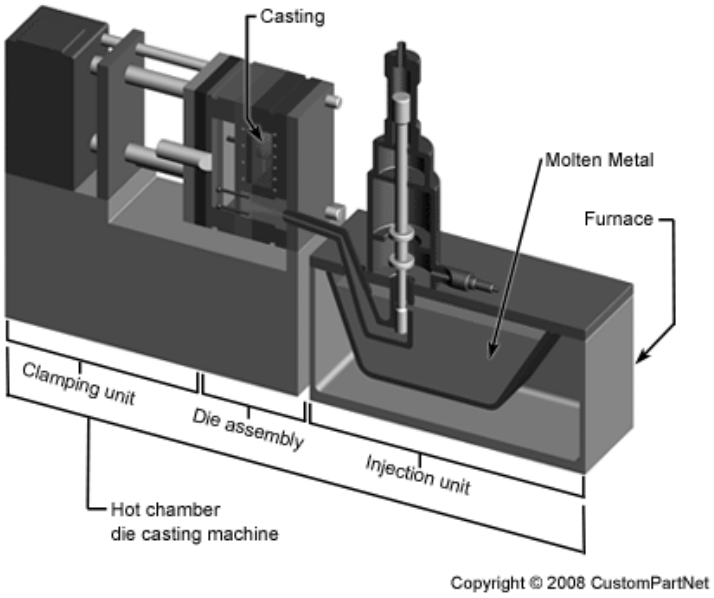

Figure 2.2: layout of a hot-chamber HPDC machine

The injection mechanism of the cold-chamber version is simpler: the plunger moves horizontally inside a steel cylinder, the shot sleeve, into which the alloy is poured through an opening on the upper side by means of a ladle. Cold-chamber

machines are usually adopted for alloys with high melting temperature, such as aluminium alloys.

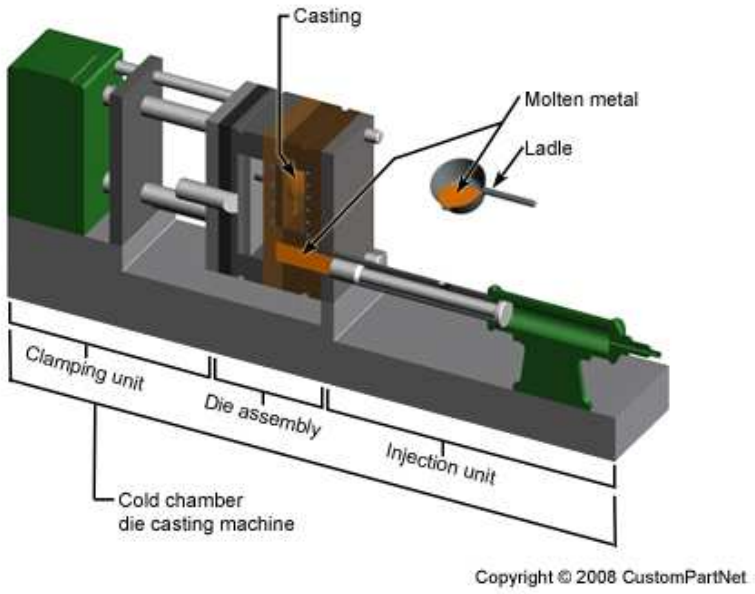

Figure 2.3: layout of a cold-chamber HPDC machine

The clamping unit is the same for hot- and cold-chamber machines: it is responsible for the reciprocating movement of the platen onto which half of the die assembly is mounted and for keeping the die closed when the molten metal is injected at very high pressure, up to 1000 bar in cold-chamber process. The clamping unit conventionally features a toggle mechanism, powered by a hydraulic circuit, but recently an innovative toggle-free system has also been implemented. The maximum clamping force is the most important characteristic of the machine, since it determines the size and the number of components that can be cast simultaneously: it must withstand the opening force generated by the molten metal pressed into the cavity, which is calculated as the product of the maximum injection pressure and the projected area of the cavity. In calculating the projected area, the overflows, the runners and the piston head have to be taken into account. Clamping force may reach 4500 t in cold-chamber machines and 800 t in hot-chamber machines.

The die assembly is made of two main parts, one mounted onto the movable platen, which can move horizontally to open and close the cavity into which the molten alloy is pressed, and one onto the fixed platen. The cavity is created by two inserts, the core insert and the cavity insert, mounted into the two halves of the assembly, the ejector die and the cover die respectively.

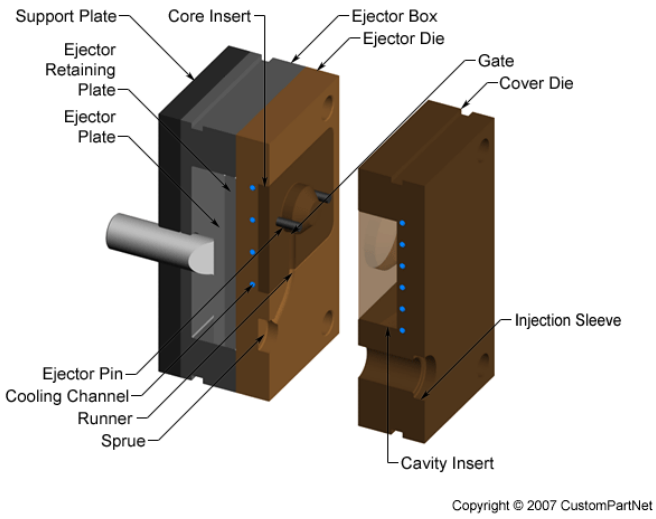

Figure 2.4: main components of a die assembly

This feature let the assembly be employed for many components, simply changing the inserts and the ejector pins, and allows for a cheaper substitution of the tool at the end of its life span or in case of damage. The cavity of the die gives its shape to the casting and includes a sprue, the runners, the gating system and the overflows. Overflows are necessary to confine oxide, born at the melt filling front, in volumes easily separable from the part. The ejector box is located between the cavity die and the movable platen. When the metal solidifies and the die is opened, the ejector pins push the casting out of the die, moved by a hydraulic actuator.[6]

The production cycle

The production cycle of HPDC can be divided into 5 steps:

1. **Clamping**: first, the die is cleaned from any scrap remained from the previous casting and is lubricated to facilitate the ejection of the next part. Then, the die is closed and the clamping system secures the movable platen in position.
2. **Injection**: the molten metal necessary to completely fill the cavity is transferred to the injection chamber, according to the hot- or cold-chamber scheme. When the metal is ready, the plunger inject it into the cavity. The plunger movement is divided into three phases: on the first phase, the plunger moves slowly through the shot sleeve and pushes the melt to the end of it; on the second phase, the melt is pushed at very high speed through the runners into the die cavity and

fills it completely; on the third phase, the piston applies a high pressure to the solidifying metal to compensate the volume contraction.

3. **Cooling**: the metal injected into the cavity cools down and solidifies completely.
4. **Ejection**: when the part is completely solidified, the clamping mechanism is released and the die is opened; then, the ejector pins push the casting out of the cavity.
5. **Trimming**: overflows, runners, sprue and any flash must be removed from the part.

Innovation in HPDC

From the first application with printing type to the modern employ in automotive industry, HPDC has been continuously improved to reach higher and higher quality and reliability. The pursuit of sound, complex and defect-free castings has pushed the research towards new technologies and variations to the conventional HPDC process.

Vacuum-assisted HPDC has been developed and adopted in industrial production to reduce the amount of air entrapped in the castings, as a consequence of the high turbulence of the molten metal, and the oxidation of the melt during the filling phase. Air and gas entrapped within the castings are the main obstacle to heat treatments and welding. Eliminating, or strongly reducing the presence of these defects is a key issue to expand the potential of HPDC.

A technology widely and successfully adopted to extract air from the cavity is the Fondarex process. Air is extracted from the cavity, during the injection phase, from a ventilation plate installed onto the die, connected to a vacuum circuit. The circuit is composed of a duct connecting the cavity to a tank, a solenoid valve placed in the duct, before the tank and a vacuum pump which generates vacuum inside the tank. The solenoid valve is activated when the injection chamber is sealed and air is extracted during the filling phase, reaching an internal absolute pressure of about 200 mbar. The circuit is protected by an auto-sealing valve, activated in case of molten metal flowing through the ventilation duct. A control over the air extraction flow is possible by means of a controlled choke valve installed between the duct and the

vacuum tank. Systems capable of extracting air also from the shot sleeve are available.

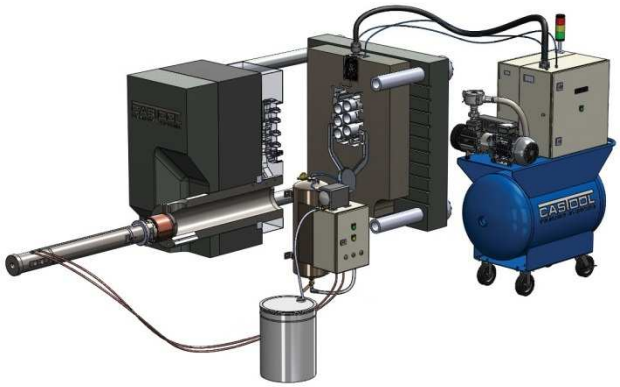

Figure 2.5: a vacuum system for extracting air both from the shot sleeve and the die cavity

Besides conventional pump-and-tank vacuum circuit, another technology has been applied to create vacuum atmosphere inside the cavity: a Venturi tube substitutes the pump with no need for a tank. The pressure drop generated at the smaller section of a Venturi tube is exploited to extract air from the cavity. An absolute pressure down to 300 mbar can be reached connecting the device to a conventional 6 bar compressed air line. This process, called StatVac and patented by Electronics GmbH, reduces the costs of the vacuum circuit and can be adjusted by an electronic control, to find the best vacuum curve for each die.

Figure 2.6: StatVac equipment by Electronics GmbH

Another implementation of the vacuum technology is represented by Vacural. The main difference with the technologies described above regards the melt dosing system: the injection chamber is connected to the holding furnace by a steel or

ceramic tube, depending on the molten alloy. This technology features the same vacuum system as that of Fondarex, but its application is double: in addition to the removal of air and gases from the cavity, vacuum is exploited also to dose the molten metal from the holding furnace before the injection phase. The metal is transferred to the chamber by the effect of the difference in pressure between the cavity, under vacuum, and the surface of the melt, at atmospheric pressure. The advantages are a lower oxide content, since it is taken from under the surface inside the holding furnace, and no need for an operator or a robot for the pouring of the melt into the shot sleeve.

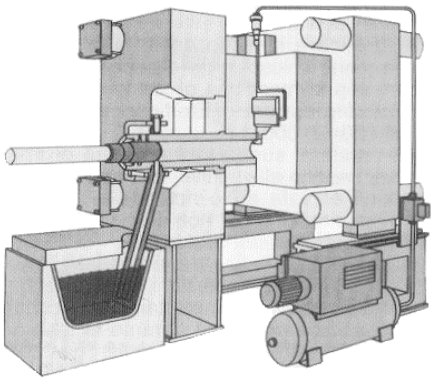

Figure 2.7: layout of a Vacural HPDC machine

Another improvement of HPDC came with the introduction of semi-solid casting technologies. A semi-solid metal is obtained when its temperature is situated between Solidus and Liquidus and the solidified fraction is dispersed in the molten fraction. Metal in this state behaves as a thixotropic fluid, keeping its shape unless a minimum shear stress is applied to it. Semi-solid metal is introduced into the shot sleeve and cast following the usual cycle. This process guarantees lower porosity content, a globular microstructure and improved mechanical properties of the castings. Also, the solidification temperature range is smaller, reducing the amount of volume contraction of the casting, with better control over dimensions and lower shrinkage porosity and cracking risk.

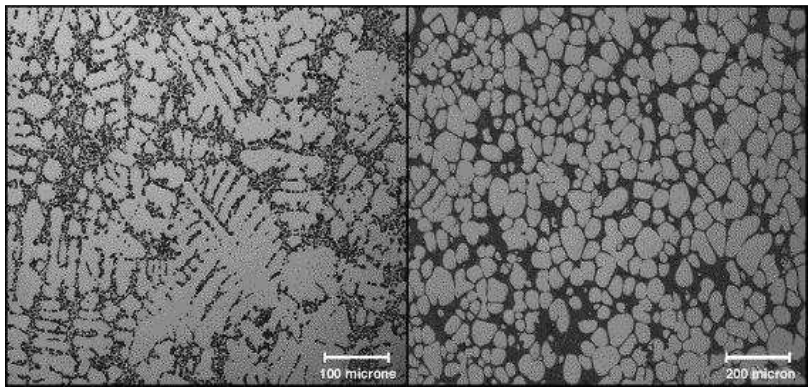

Figure 2.8: microstructure comparison between a convetional and a semi-solid die cast alloy

The semi-solid metal requires a preparation stage before casting, which may differ according to the technology adopted. In Rheocasting, conventional ingots are first completely molten and secondly stirred and cooled until the enthalpy of the melt is lowered to the required level. Thixocasting employs special billets already solidified with a globular microstructure, which are sawn and reheated before the casting. Other processes, such as Thixomolding and Rheo-diecasting, differ in this stage.

3 Al-Cu alloys

Introduction to Al-Cu alloys

Copper has been employed as addition in aluminium alloys almost since the beginning of aluminium industry, especially after the age hardening process was discovered. Age hardened Al-Cu alloys proved to be very strong and hard and some of them feature tensile strength and hardness comparable with those of low carbon steels: that means a specific strength three times bigger, being the density of aluminium alloys approximately 1/3 of that of steel. Besides the high strength, good elongation values are guaranteed, making these alloys reliable for damage tolerant design. Aluminium alloys containing Cu as major alloying element are widely adopted as wrought or cast alloys. High strength and hardness in a wide range of temperatures, from those typical of cryogenic applications to 200 °C and more (2219 –T81 shows a UTS of 572 MPa at −195 °C and of 200 MPa at 260 °C[7]), represent one of the key factors for the success of these alloys, together with a high creep resistance and a good machinability. On the other hand, some weaknesses, such as a poor corrosion resistance and a high hot-tearing susceptibility, affect these alloys, preventing their use in many applications.

History of Al-Cu alloys

The first one to discover such high mechanical properties of Al-Cu alloys was Alfred Wilm, in the early 20th century. As a metallurgist at the Zentralstelle für wissenschaftlich-technische Untersuchungen (Scientific and Technical Analysis Center) in Neubabelsberg, in 1903 he was commissioned a study to find an Al-based alloy to substitute brass in munitions.

Figure 3.1: Alfred Wilm (1869–1937)

He serendipitously found that the hardness of an Al based alloy containing Cu, Mn and Mg increased when left at room temperature for some days after quenching from over 500 °C. Deeper studies led to the definition of a specific composition with 3.5 to 5.5 wt.% Cu and Mg and Mn, both less than 1 wt.%, for which a patent was obtained. Dürener Metallwerke AG, a company in Düren, north-western Germany, acquired the license to produce this new alloy and in 1909 copyrighted the name *Duralumin*, nowadays still recognized, though AA 2017−T4 is the designation more commonly adopted. After Duralumin, many other alloys were developed, in which Cu is the main alloying element, both as casting alloys and wrought alloys. Soon these alloys were employed in aircraft construction, for structural components and engine blocks. German and American Zeppelin airships and Junkers' first all-metal military and passenger aircrafts, the Junkers J 7 and F13, took advantage of Duralumin to lose weight without losing strength.

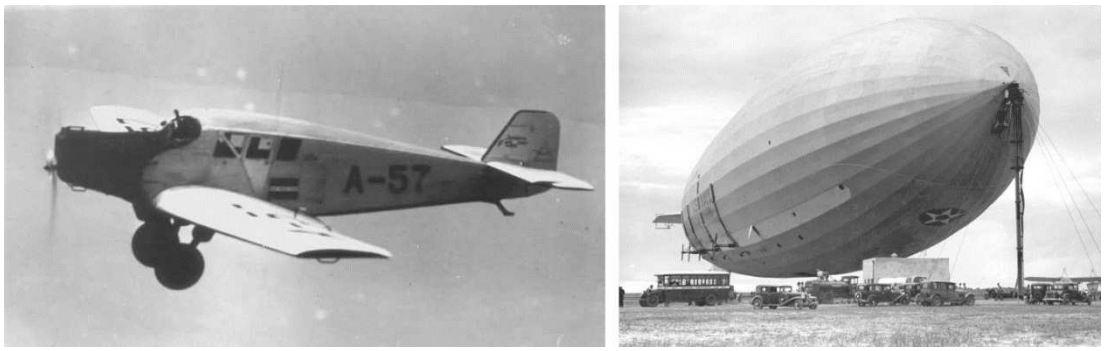

Figure 3.2: Duralumin was adopted in airplanes and airships for its stength, toughtness and lightness

It is believed that even the Wright brothers, together with their mechanic Charles Taylor, took advantage of this strengthening mechanism adopting an Al-Cu

alloy, namely Al 8 wt.% Cu, called P12, for the crank case of the engine of their first flying machine in 1903, though completely unaware of the age hardening process and of Mr Wilm's discovery.

In the meanwhile, automotive engineers started paying attention to aluminium alloys as well, since these new materials proved to be a key factor for lightening race cars and gaining the winning advantage in races. In 1901 Karl Benz produced the first race car powered by an engine with aluminium parts. Still, difficulties in metal working, lack of knowledge and high prices prevented aluminium alloys from being employed in mass car production. More recently, as aluminium alloys became more affordable, automotive industry started looking at them as an opportunity to lighten vehicles, thus improving fuel economy and overall dynamic performances. However, while in aerospace industry Al-Cu alloys have been successfully employed throughout all the 20^{th} century for their high strength and toughness, their use in automotive components was limited for many reasons such as poor weldability, low resistance to atmospheric corrosion and reduced castability, compared to those of other Al-based alloys.

Today Al-Cu alloys are widely employed in aerospace industry, especially for high temperature or cryogenic applications, such as liquid oxygen, helium and hydrogen tanks, and more generally wherever very high specific strength, even at high temperature, is required. They also find application in structural components of trucks and railway vehicles.[8][9]

Al-Cu stable phase diagram

The Al-Cu phase diagram is shown in figure 3.3:

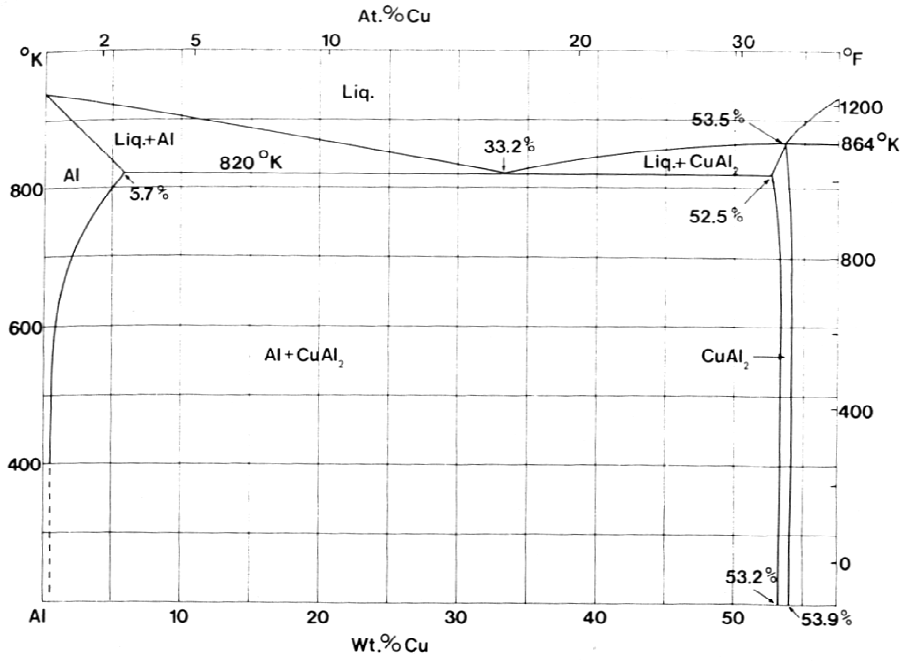

Figure 3.3: Al-CuAl2 phase diagram

Al-based alloys usually have Cu content that never exceeds 15 wt.%, thus only the Al-$CuAl_2$ section of the Al-Cu diagram is relevant. The eutectic point is located at a temperature of 548.2 °C (821.4 K) and a concentration of 33.2 wt.% Cu. This means that all the Al-Cu alloys commonly adopted in metal industry are hypoeutectic. The maximum Cu content soluble in solidified Al is 5.65 wt.% at eutectic temperature, while it falls to 0.3 wt.% approaching room temperature. In accordance with common nomenclature, pure Al phase is addressed to as "α" phase, while the stable $CuAl_2$ phase as "θ" phase.

The phase diagram shows the composition of the Al-Cu binary system at stable conditions. Thus, it is valid for alloys the temperature of which changes as result of a quasi-static process, where the whole alloy moves from a stable status to another. Given this hypothesis, the phase evolution of a certain alloy can be predicted following a vertical line corresponding to its composition.

As an example, the solidification of a Al-Cu alloy with Cu content lower than 5.65 wt.% will be shortly described:

1. over the Liquidus, all the alloy is fluid;
2. when the temperature decreases and reaches the Liquidus, at about 650 °C, the solidification of α and Cu in form of a solid solution begins. The

concentration of Cu in solidified α is determined by the Solidus at the same temperature;

3. as the temperature decreases, the concentrations of Cu in α and within the melt follow the Solidus and the Liquidus curves respectively. The growing grains become richer in Cu as a result of diffusive mechanisms;
4. when the temperature reaches the Solidus curve, all the alloy is solidified and the wt.% of Cu is equal to that of the initial molten alloy; Cu is homogeneously dissolved in α;
5. after further decreasing of the temperature, the solubility limit of Cu in α is reached and the content of Cu becomes too high to remain in solution. $CuAl_2$ starts precipitating as a fragile secondary phase within the α grains;
6. this precipitation continues with growing $CuAl_2$ precipitates until room temperature is reached.

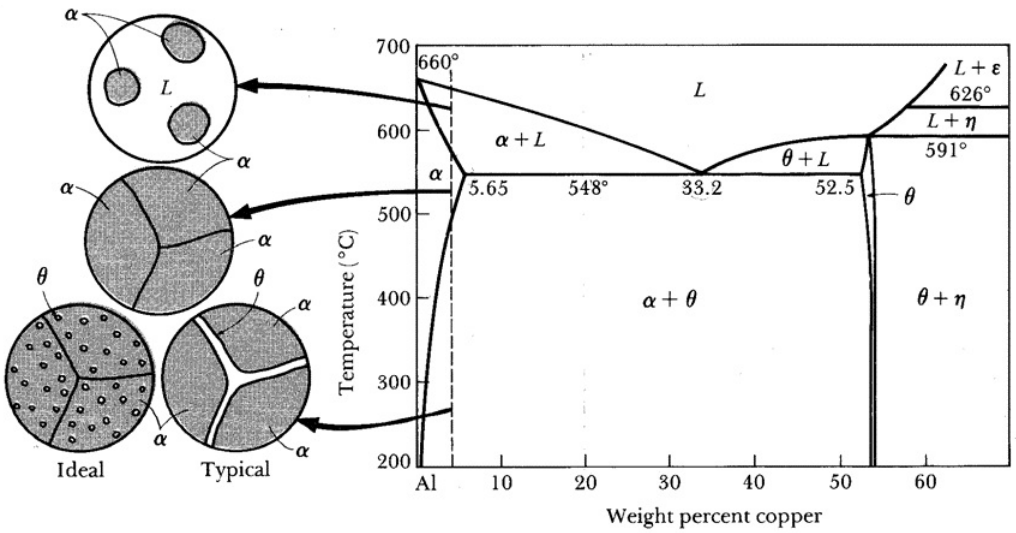

Figure 3.4: solidification of an Al-Cu alloy

Dynamics of foundry processes are far from being quasi-static and the cooling rates involved don't leave time enough for all the Cu in solution to move, by diffusive processes, through the solidified alloy. Hence, achieving a homogeneous and stable content of Cu throughout the grains is prevented. As a result, phenomena such as segregation and formation of supersaturated solid solutions take place in almost all the castings.

Segregation occurs when there is not enough time for Cu atoms to diffuse to the core of a solidifying grain. For that reason, at completed solidification, the outer regions of the grains will be richer in Cu than the cores. Possibly, at the final stages of solidification, the content of Cu in the still molten alloy may be so high to lead to the formation of eutectic phase at the grain boundaries.

When very high cooling rates are achieved, as in quench, the reduction in solubility of Cu in α phase is not followed by an equal diffusion of Cu atoms from within the grains. In short time, a too low temperature is reached that slows the diffusion and freezes the Cu atoms in a supersaturated solid solution of α + Cu. This is the starting point for the precipitation hardening mechanism.

Precipitation hardening of Al-Cu alloys

As accidentally discovered at the beginning of the 20th century, Al-Cu alloys achieve their great mechanical properties after heat treatment thanks to the precipitation hardening mechanism. Precipitation hardening, also called age hardening, occurs when a supersaturated solid solution is aged, naturally or artificially, to make a secondary phase precipitate in form of finely dispersed particles.

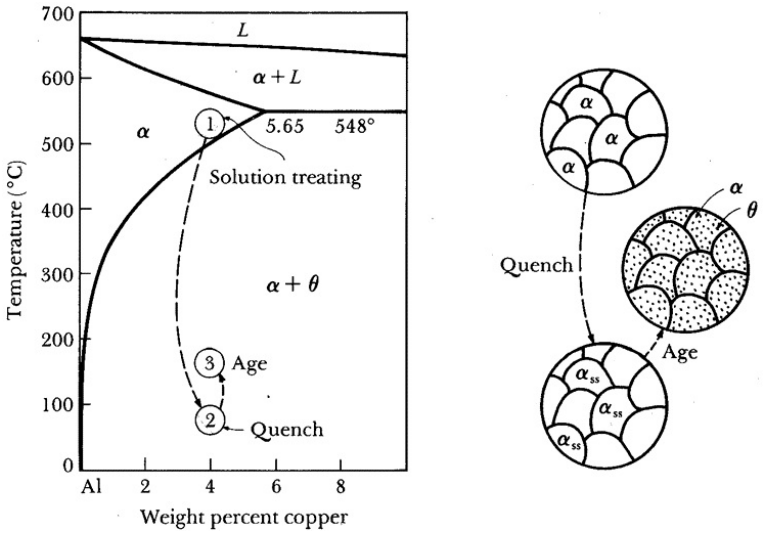

Figure 3.5: the precipitation hardening process

These particles act as obstacles to the movement of dislocations, which are responsible for the plastic deformation of metals. Hindering the movement of dislocations increases the amount of energy necessary to obtain a permanent

deformation of metals. The precipitate particles can be coherent, partially coherent or incoherent with the lattice of the main phase, and this changes the way dislocations are impeded. Coherent and partially coherent particles can be sliced by a moving dislocation, because of the continuity of the lattice, or can block the dislocation, that necessarily bows around it, with formation of another, ring-shaped dislocation. The latter is called the Orowan mechanism.

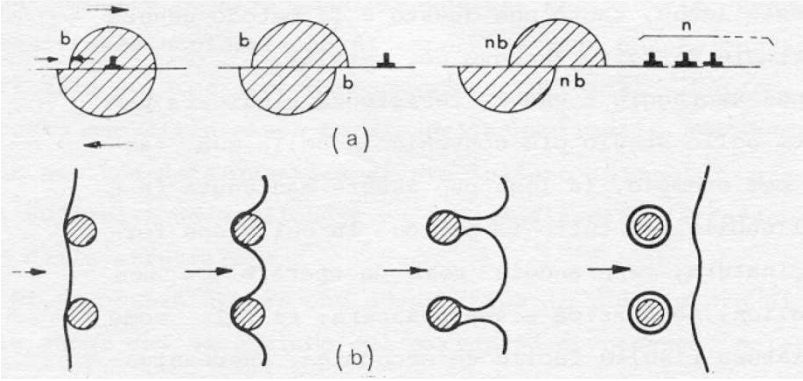

Figure 3.6: two mechanisms of overcoming precipitates

Whether a dislocation acts in one way or in the other is determined by the energy required for the two mechanisms: when the particles are small and closer to each other, the slicing mechanism is favourable; when they are bigger and farther from each other, the bowing one requires less energy. In figure 2.7 a qualitative description of the stress σ_y required to make a dislocation overcome a precipitate by the two mechanisms as function of the precipitate particles radius is shown:

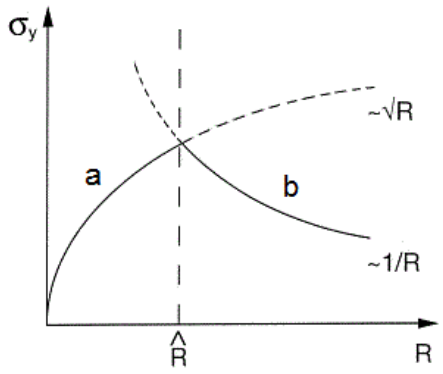

Figure 3.7: influence of precipitate radius on the stress σ_y

The maximum stress is required at a value $\hat{R}$ that makes the cutting stress and the bowing stress equal. It corresponds to the maximum hardening effect achievable through this process.

In case of incoherent precipitates, only the Orowan mechanism is viable and the particles radius should be as small as possible.

The resulting change in mechanical behaviour is shown in figure 2.8, where the S curve represents the behaviour of the alloy as supersaturated solid solution.

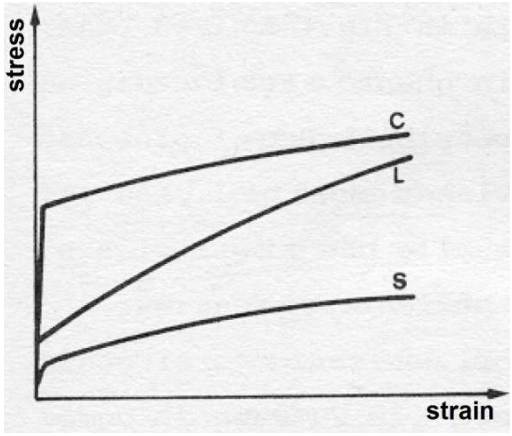

Figure 3.8: changes in behaviour due to different age hardening conditions

After precipitation hardening, the alloy may show two different behaviours: an increase in both yield and ultimate tensile strength occurs for precipitates with radius $R < \hat{R}$ (C curve in figure 2.8), because of the slicing mechanism acting from the beginning of plastic deformation; an increase of the ultimate tensile strength only occurs when $R > \hat{R}$ (L curve in figure 2.8), as consequence of a rapid work hardening, due to the formation of new dislocations via Frank-Reed Source mechanism.

For what concerns Al-Cu alloys, the phases generated as precipitates are different depending on the temperature and time of aging.

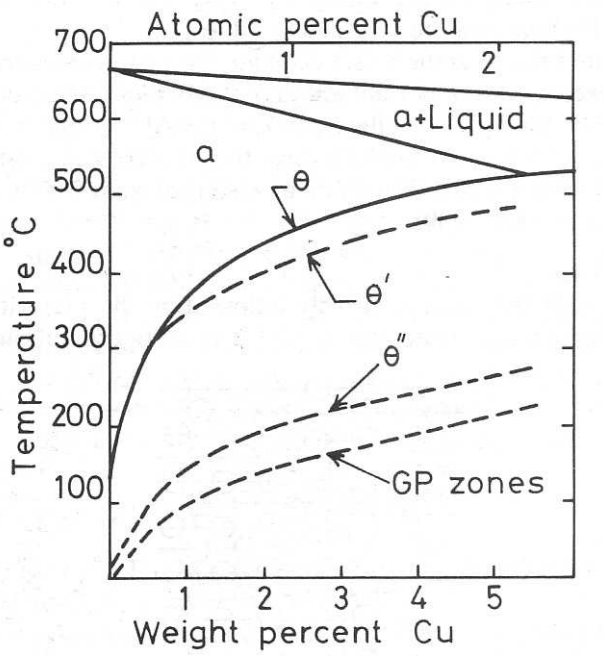

Figure 3.9: solvuses of Al-Cu phases

As shown in figure 3.9, 4 different phases may originate from heat treatment. They will be here shortly described:

- GP zones: Guinier-Preston zones are platelets of few layers of Cu atoms, less than 100 Å wide, coherent with the Al matrix but still responsible for a distortion of the lattice, due to the radius of Cu atoms that is 12 % smaller than that of Al atoms;
- θ" zones: these zones represent the evolution of GP zones: they are metastable precipitates, 20-50 Å high, 200 Å wide, with a tetragonal structure coherent with the matrix; being originated from existing GP zones, their central plane is made of Cu atoms only, while the concentration of Al atoms increase moving towards the outer planes, which are made of Al atoms; the structure is coherent;
- θ' zones: these precipitates originate within the matrix and partially from θ" zones as coarser particles with tetragonal structure, nominal composition equal to $CuAl_2$ and dimensions of 500 Å; the difference in atom spacing is no more bearable by the elastic deformation of lattice and a partial incoherence is originated as the elastic stresses are released;

- θ zones: these precipitates nucleate from θ' zones as a stable phase of $CuAl_2$; the structure is incoherent and their formation leads to the overaging of the alloy.

Controlling the formation of these phases is a key factor to obtain maximum performances from a heat treatment. Starting from a supersaturated solid solution, an initial hardening effect is given by the formation of GP zones. In a short period of time, GP zones are replaced by θ", with no change in hardness. As these zones develop, hardness increases again and short before reaching the maximum value they start to be gradually replaced by θ' zones, which are associated to a following decrease in hardness. If the treatment temperature is greater than 277 °C, θ' is replaced by stable θ and hardness falls back to values comparable with those of the initial solid solution.[10][11]

Commercial Al-Cu alloys

After one century of efforts in research and development of new and better compositions, today many Al-Cu-based alloys are available on the market, to meet the requirements of as many different applications. Here are listed some of the wrought and cast Al-Cu alloys more widely employed, together with their compositions and applications.[7]

Wrought alloys		
Nomenclature	Composition	Applications
2011	5.5 Cu 0.4 Pb 0.4 Bi	Wire, rod and bar for screw machine products. Application where good machinability and strength are required
2014	4.4 Cu 0.8 Si 0.8 Mn 0.5 Mg	Heavy-duty forgings, plates and extrusions for aircraft fittings, wheels and major structural components, space boost tankage and structure, truck frame and suspensions components. Applications requiring high strength and hardness including service at elevated temperatures
2017	4.0 Cu 0.6 Mg 0.7 Mn 0.5 Si	Now in rather limited use, chiefly for rivet. Used in components for general engineering purposes, structural applications in construction and transportation, screw machine products and fittings
2024	4.4 Cu 1.5 Mg 0.6 Mn	Aircraft structures, rivets, hardware, truck wheels, screw machine products, other structural applications

Table 3.1: wrought Al-Cu alloys

Cast alloys		
Nomenclature	Composition	Applications
AA 201.0	4.6 Cu 0.7 Ag 0.35 Mn 0.35 Mg 0.25 Ti	Structural casting members, aerospace housings, electrical transmission line fittings, truck and trailer castings and other applications where highest tensile and yield strengths and moderate elongation are required. Gasoline engines cylinder heads and pistons, turbine and supercharger impellers, rocker arms, missile fins and other applications where strength at elevated temperatures is important. Structural gear housings, aircraft landing gear castings, pump housings and other applications where high strength and high energy-absorption capacity are required
AA 204.0	4.6 Cu 0.25 Mg 0.17 Fe 0.17 Ti	Light- and heavy-duty impellers, structural parts for aerospace and automotive industry, ordnance parts for tanks, trucks and other equipment, lightweight high-strength hand tools, lightweight powertrain castings in auto and truck industry
AA 206.0	4.5 Cu 0.30 Mn 0.25 Mg 0.22 Ti	Structural castings in heat-treated temper for automotive, aerospace and other applications where high tensile and yield strength and moderate elongation are needed. Gear housings, truck spring hanger castings and other applications where high fracture-toughness is required
AA 208.0	4 Cu 3 Si	Manifolds, valve bodies and similar castings requiring pressure tightness. Other applications where good casting characteristics, good weldability, pressure tightness and moderate strength are required
AA 242.0	4 Cu 2 Ni 2.5 Mg	Motorcycle, diesel and aircraft pistons, air-cooled cylinder heads, aircraft generator housings and other applications where excellent high-temperature strength is required

Table 3.2: cast Al-Cu alloys

Limitations of Al-Cu alloys

Besides the very high mechanical properties achievable with Al-Cu alloys, they suffer from some weaknesses that prevent them to substitute other, less strong and though aluminium alloys in many applications. A higher tendency to hot cracking, poor weldability and lower corrosion resistance, compared to those of other commercial alloys, are the main reasons why they are not so widely adopted. Many studies analysed these problems in order to understand the causes and to find solutions to them.

Hot cracks, or hot tears, are generated in metal parts during solidification. They are generally composed of a main tear and numerous minor offshoots, which

follow intergranular paths, and the failure surface reveals a dendritic morphology. Many studies have been published regarding this phenomenon and many efforts have been spent in order to understand its causes and to find proper solutions. These studies show that hot cracking involves many variables, such as alloy composition, mold properties, casting design and process parameters. It is widely accepted that hot cracking is due to solidification shrinkage and thermal deformation developed during the solidification phase, though the exact mechanism is not completely understood. Two main groups of theories have been proposed: the first finds explanation to hot cracking in stress, strain and strain rate during solidification; these theories are related to the thermo-mechanical properties of alloys. The second group of theories is based on liquid film and lack of feeding and involves metallurgical factors. Though the basics of hot cracking are understood, there is still no agreement on what are its controlling factors.

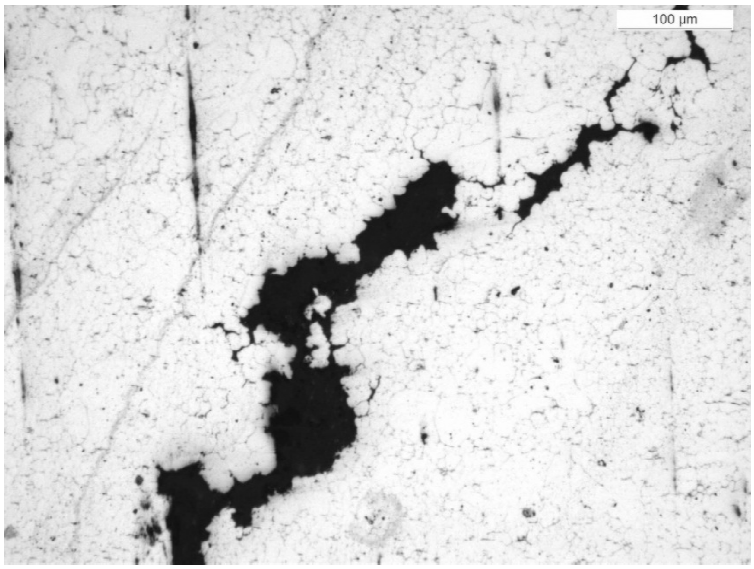

Figure 3.10: a hot crack originate on a die cast component

The attempts done to reduce hot cracking revealed that the microstructure plays a fundamental role in this phenomenon: a fine, globular or equiaxed dendritic microstructure proved to be effective in reducing or preventing hot cracking in Al-Cu alloys. Moreover, changing the mold temperature has a great influence on the behaviour of these alloys: a higher mold temperature reduces the severity of hot cracking because it promotes a uniform casting contraction and therefore alleviates stress concentration. Moreover, a higher mold temperature means a smaller thermal gradient, which reduces the columnar solidification and allows for the formation of

an equiaxed microstructure. The pouring temperature also affects hot cracking: a higher pouring temperature lead to a slower cooling rate and a coarser microstructure. Larger grains are less capable of accommodating stresses originated by thermal contraction and the liquid film is thicker between larger dendrites, increasing the hot cracking susceptibility.[13]

Poor weldability is a consequence of the high tendency to hot cracking of Al-Cu alloys. During solidification, hot cracks may occur at the weld bead, promoted by a directional solidification and the thermal stresses arising from the volume contraction. A solution to this problem is found in using a different, more hot cracking resistant alloy as filler.

Corrosion resistance in Al-Cu alloys is compromised by the galvanic interaction between α and $CuAl_2$ phases. Galvanic corrosion occurs at the interface between the phases, which have different electrical potential, when they are in contact with moisture naturally present in air. Under these circumstances, aluminium act as anode and $CuAl_2$ as cathode in a galvanic couple.

To prevent this corrosion mechanism, coatings and surface treatments are necessary. Usually, these alloys are painted or clad to protect the surface from atmospheric corrosion. A famous example is the Alclad process, patented by Alcoa, which consists of joining two layers of pure Al to a high-strength Al alloy plate to ensure a perfect insulation.

4 Experiment

Aims

Aim of this experiment is to investigate the possibility of creating Al_2O_3 particles within molten aluminium by means of an *in-situ* process. Furthermore, this experiment aims to verify whether the particles remain into the metal once solidified or not, and to measure the influence of particles on the mechanical properties of the metal.

Description of the experiment

The experiment consists of injecting a mixture of inert gas and oxygen into molten aluminium, which at the same time is stirred. The gas mixture is injected by means of a stirring impeller provided with small radial bores, connected to a motor by a tube through which the gas mixture flows from a mixing unit.

The hypotheses to be verified are that the wall of the bubbles is subjected to oxidation and that the stirring effect of the impeller generates turbulence high enough to tear the oxidized film, so letting the inert gas float to the top and keeping the aluminium oxide within the melt thanks to the stirring effect of the impeller. Using argon, heavier than air, as inert gas, a protective atmosphere generates over the melt, confined there by the walls of the crucible and continuously fed by the injected gas. The protective atmosphere prevents the oxidation of the melt surface by the oxygen normally present in air. The variables involved in the process are here reported:

- wt.% of O_2 in the gas mixture, x_{O_2};
- mass flow rate of the gas mixture, □;
- impeller rotating speed, ω;
- melt temperature, T_m;
- injecting/stirring time, t_p;

Changing the %wt O_2 of the mix could allow the thickness of the film to be controlled. On one hand, a thinner film is easier to tear and should lead to smaller particles. On the other hand, lowering this parameter brings higher processing times and requires a higher amount of inert gas to produce the same quantity of oxide.

The mass flow rate should be as high as possible to reduce the process time, but higher flow rates require higher pressures to compensate the increasing losses in the circuit and at the nozzles. Hence the gas mixing system has to be designed to stand these higher pressures. Moreover, high gas mass flow rates severely disrupt the free surface of the melt, causing drops to spill from the crucible, thus making the process dangerous for people and for the equipment.

The rotation speed of the impeller ω is to be set as high as possible, since a higher speed means more turbulence, better scattering of the bubbles, more stirring efficiency and higher shear rates. Nevertheless, when the melt is set in rotation, the free surface is deformed, assuming the typical vortex shape. For this reason, a too high rotation speed could push the aluminium towards the crucible edge and eventually make the melt overflow. To avoid such a risk, a safety margin should be taken.

The temperature of the melt T_m could affect the efficiency of the process because of its influence on the interaction between molten aluminium and aluminium oxide. The wettability of Al_2O_3 by molten aluminium has been proved to depend on the temperature[14]: increasing the temperature significantly reduces the contact angle. This implies a stronger adhesion between molten aluminium and the alumina layer, eventually affecting the entire process. Melt temperature also affects the costs of the process.

Once the mass flow rate and the %wt of O_2 are set, the injecting/stirring time t_p determines the amount of oxygen added to the molten metal. Directly related to that is the amount of oxide that may remain into the melt. Calculating the amount of oxygen M_o introduced is possible through the relation:

$$M_{O_2} = \dot{m} * x_{O_2} * t_p$$

For the same amount of oxygen, shorter process times can be achieved by increasing the mass flow rate and/or the wt.% of oxygen in the mixture and vice versa. A shorter process time is always to be preferred and could limit the particle agglomeration and floatation to the surface of the molten metal.

Experimental setups

The experiment was first run in small scale, by means of a hand-built equipment. Here is reported the description of the first setup.

The first small scale experiment was carried out by means of a Nabertherm© small induction furnace with a SiC crucible of approximately 2.5 litres capacity. It has a maximum power of 5500 W and is provided with an insulated cover having a 40 mm hole on its centre.

The impeller was machined out of a boron nitride block. Boron nitride is a refractory material, normally produced via hot pressing, capable of resisting temperatures up to 1800°C and resistant to thermal shocks. It is also free from solution in molten aluminium.

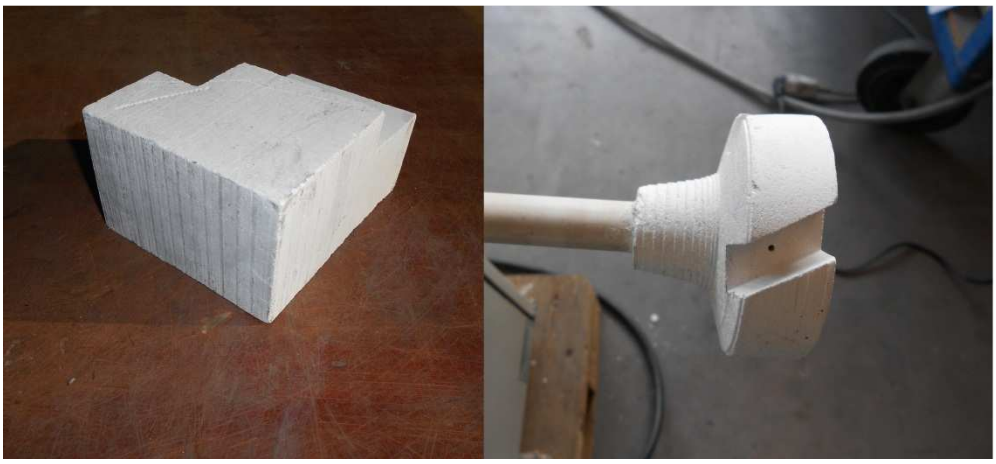

Figure 4.1: a block of boron nitride and the impeller machined

The geometry of the impeller has been designed to generate a downward flow of the molten aluminium that sweeps the bubbles away throughout the crucible. This feature is intended to improve the continuous stirring of the molten aluminium.

The impeller was machined with manually controlled turning and milling machines. After machining the impeller, 4 x Ø 1.5 mm radial bores were drilled to let the gas mixture flow out of the sides of the impeller.

The impeller was connected to an Al_2O_3 tube of 15 mm outer diameter and 2 mm wall thickness by means of a calcium silicate-based adhesive paste. Calcium silicate (Ca_2SiO_4) is a high temperature and fire resistant material, used for insulating and fireproof panels and adhesive and sealing pastes. In the form of adhesive it takes

at least 12 hours for curing and requires a first slow heating to avoid the formation of gas bubbles.

On the opposite side of the ceramic tube, a Ø 10 mm steel tube was inserted and glued with the same calcium silicate adhesive paste. This steel tube has two functions: first, the chuck of the stirrer allows tubes of 10 mm diameter maximum, hence the ceramic tube can't be directly installed on it; secondly, the top of the steel tube can be threaded for connection with the gas circuit.

Gluing the steel tube proved itself to be a complex task due to the need for a precise alignment of the two tubes, in order to reduce vibrations during the melt treatment. With an inner diameter of 11 mm, the ceramic tube is bigger and the steel tube moves inside it. To fix it in straight position and reach an acceptable accuracy, four longitudinal grooves were machined on the outer surface of the steel tube and four pieces of steel wire of 0.75 mm diameter were placed on the grooves, to act as centring tools for the tubes. The glue took more than 3 days to completely cure, because of the limited contact with air. Keeping the tubes near a heat source helped accelerating the curing phase.

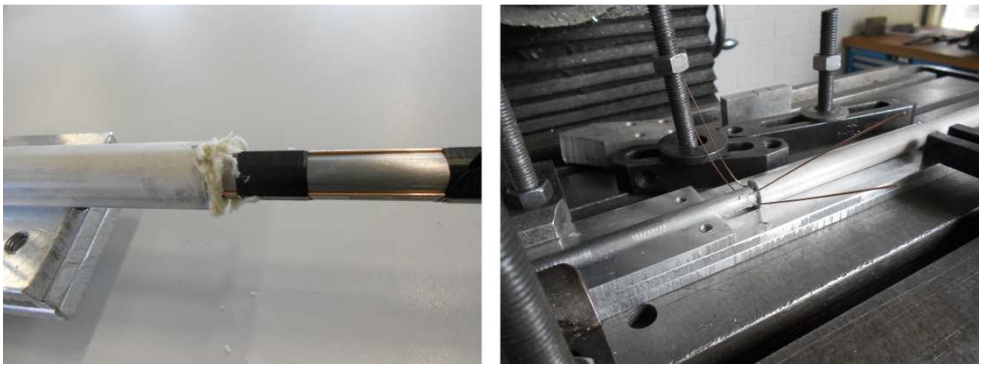

Figure 4.2: two phases of the gluing process

The stirrer used in this setup was an IKA EUROSTAR digital© overhead stirrer. Its rotation speed ranges between 50 and 2000 rpm, is controlled by a knob and shown on an LCD. As already mentioned, the chuck accepts shafts of Ø 10 mm maximum and an opening on the top allows the installation of a through shaft. The plate stand was fixed on the cover of the furnace by means of a custom fixing gear. This way, the whole stirring system remained in position when the furnace was opened.

On the threaded end of the steel tube a swivel joint was connected, that allowed the tube to rotate while connected to the gas mixing circuit.

Figure 4.3: the stirrer installed on the furnace

The gas mixing system is illustrated in picture n. It is composed of 2 cylinders, 2 mass flow meters/controllers, 1 pressure sensor and a control unit. The two cylinders are one of commercial grade argon, the other of PRAXAIR® Stargon O8®, a welding shield gas composed of 92 vol.% argon and 8 vol.% oxygen. Both the cylinders are provided with pressure regulators. The argon cylinder is connected to a Bronkhorst® LOW-Δp F-201D mass flow meter/controller, capable of controlling the flow rate in the range of 0 ÷ 2.23 l_n/min and working with pressures from 0 to 5 bar (relative). The other cylinder is connected to a Bronkhorst® EL-FLOW F-201AC mass flow meter/controller, with flow rate range of 0 ÷ 30 l_n/min and pressure range from 0 to 5 bar (relative). Both the outputs of the controllers are connected to a T-shaped joint, where the two gases mix and continue towards the stirrer. To this last segment of circuit is connected a Bronkhorst® EL-PRESS P-502C pressure meter/controller to measure the pressure right before the injection. All the three elements are linked to a Bronkhorst® E-7400 control unit that let the user read the measurements and adjust the flows. Both the flow meters can be set to work as controllers, when it is necessary to change the flow rate, or as sensors only, to prevent accidental modifications of the flow rate when not required.

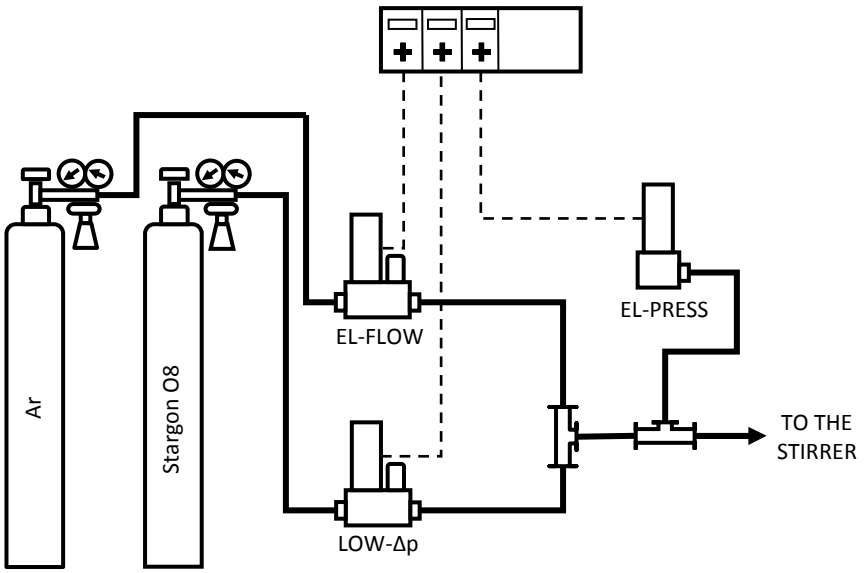

Figure 4.4: scheme of the gas mixing circuit

The two mass flow controllers use a thermal exchange sensor to measure the mass flow and a solenoid valve to control it. The thermal principle exploited for the measurement of the flow is dependent from the specific heat of the gas and from its density. For that reason, every mass flow controller is calibrated by the manufacturer to a specific gas. The two controllers here employed were intended to work with nitrogen, thus the calibration is different and the readout is wrong. Anyway, as suggested by the manufacturer, the read value can be converted to the actual value simply multiplying it to a conversion factor CF calculated with:

$$CF = \frac{C_{p_1} * \rho_1}{C_{p_2} * \rho_2}$$

in which C_{p_1} and ρ_1 are the specific heat and density at normal conditions (0°C, 101325 Pa, as specified on datasheet) of the calibration gas, while C_{p_2} and ρ_2 are those of the gas to be measured. These data can be retrieved from FLUIDAT®, a collection of routines to calculate physical properties of liquids and gases at any specified temperature and pressure, available on the manufacturer's website. This database is also capable of calculating properties of gas mixtures, such as the Ar + 8 vol.% O_2 mixture. For each Bronkhorst controller model, FLUIDAT® can directly calculate the CFs at different values of the valve opening, taking into account the geometry of the valve and its effect on the mass flow rate. Here are reported the values given by FLUIDAT® at 20°C and 5 bar (g):

	CF from N_2 to:	
% valve opening	Ar	Stargon O8®
10	1.394	1.356
25	1.390	1.362
50	1.387	1.373
75	1.389	1.385
100	1.397	1.397

Table 4.1: conversion factors for the different gases

Polynomial (for argon CFs) and linear (for Stargon O8® CFs) regressions of these values were made to describe the CF as a function of the valve opening *P*. By doing so, it was possible to iteratively calculate the proper CF, given the required mass flow rate of any of the two gases here employed.

The mass flow rate of Argon can be calculated as:

$$\dot{m}_{Ar} = CF_{Ar} * \dot{m}_{N_2} = CF_{Ar} * P * \dot{m}_{N_2,max}$$

so the valve opening *P* is:

$$P = \frac{\dot{m}_{Ar}}{CF_{Ar} * \dot{m}_{N_2,max}}$$

The equation works with Stargon O8® as well. Given a certain mass flow rate and assessing an initial value for the conversion factor, the resulting *P* is used to calculate the CF by the linear regression function. This new value substitutes the assessed one to recalculate *P* and the process goes on until the values converge.

A test of the small setup was made injecting pure argon in molten aluminium to verify the feasibility of the process, the maximum speed reachable with tolerable vibrations and an eventual excess of disruption on the free surface of the melt. A speed of 650 rpm proved to be bearable for the whole system and no melt spilt out of the crucible.

The bigger scale setup is illustrated in figure n. Two different induction furnaces were employed: a smaller, portable furnace, manufactured by OTTO JUNKER GmbH, of 12 kW maximum power, 900 °C max. temperature equipped with a 50 kg capacity crucible, and a bigger, fixed furnace, manufactured by Hindenlang GmbH, of 45 kW maximum power, whit a 300 kg capacity crucible. The

smaller one is controlled depending on the temperature measured by a thermocouple located in the furnace cavity, outside the crucible, which for that reason measures a temperature higher than that of the melt. To know and regulate the melt temperature, a second thermocouple was added. The thermocouple kept into the melt was protected by a silicon nitride tube.

The bigger furnace, on the contrary, is directly controlled by the thermocouple kept within the melt.

To stir the melt and to inject the gas, a portable degassing unit was employed. The machine is composed of a frame mounted on wheels, a vertical column, an horizontal arm that goes up and down the column moved by a chain, a graphite tube, at the end of which a graphite impeller is mounted, and a control unit. On the frame basement two gas cylinders usually find place: one is that of the inert or reactive gas that normally is injected to remove hydrogen and impurities, the other one contains a protective gas for the electric motor.

Figure 4.5: the big scale setup during the treatment

The impeller is connected to the graphite shaft by an hollow screw, through which the gas normally flows to the melt. To obtain smaller bubbles, the screw thread and hole were sealed with the calcium silicate adhesive and eight 2 mm diameter radial bores were drilled from the side walls of the impeller to the hollow core of the screw.

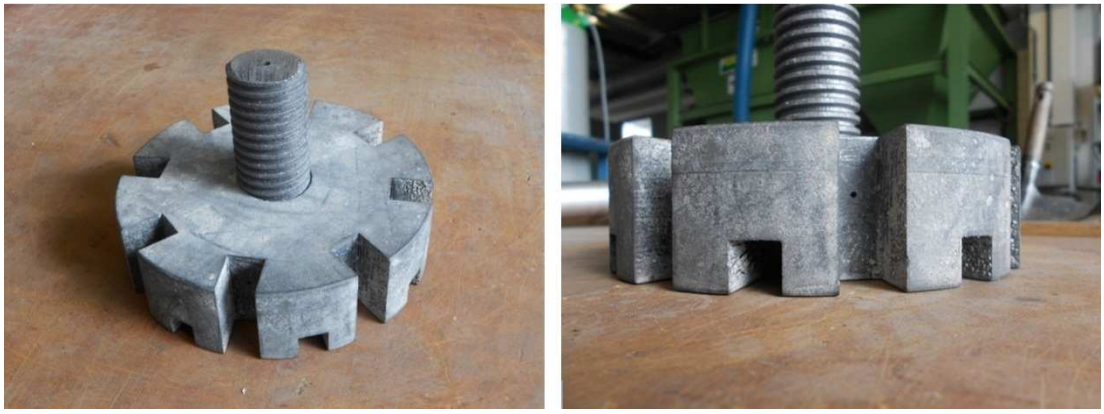

Figure 4.6: the Ø 185 mm impeller

This way, the gas flows from the mixing system to the control unit of the degassing machine, then to the impeller, through the graphite tube, and out of the bores to the melt.

The gas mixing system is the same as that used for the smaller setup, except for the Ar cylinder served as protective gas for the degassing unit. Hence, Ar + 8 vol.% O_2 was injected without further dilution with Ar.

Calculation of the gas mixture to inject

The relationship between the amount of injected gas and the consequently generated aluminium oxide is here illustrated.

The relative atomic mass of Al and O are respectively:

$$A_r(Ar) = 26.9815$$

$$A_r(O) = 15.9994$$

The relative molecular mass of Al_2O_3 is then:

$$M_r(Al_2O_3) = 2 * A_r(Ar) + 3 * A_r(O) = 101.9612$$

The wt.% of oxygen in aluminium oxide is:

$$X_O = \frac{(3 * A_r(O))}{M_r(Al_2O_3)} = 0.4707 = 47.07\%$$

This means that 0.4707 g of O are required to create 1 g of Al_2O_3. At this point, it is

FLUIDAT® was employed once again to retrieve the data necessary to calculate the mass of oxygen in 1 l_n of Stargon O8®. This gas mix contains 8 vol.%

oxygen. The ratio between argon and oxygen densities at equal temperature and pressure is, after FLUIDAT®:

$$\theta = \left(\frac{\rho_{Ar}}{\rho_{O_2}}\right)_{\substack{0°C \\ 1\ atm}} = \frac{1.784\ kg/m^3}{1.429\ kg/m^3} = 1.2484$$

The ratio θ remains the same changing temperature and/or pressure. Calculating the wt.% of oxygen and argon in Stargon O8® is now possible:

$$\frac{vol.\%\ Ar}{vol.\%\ O_2} * \frac{\rho_{Ar}}{\rho_{O_2}} = \frac{wt.\%\ Ar}{wt.\%\ O_2} = \frac{1}{wt.\%\ O_2} - 1$$

from which comes:

$$wt.\%\ O_2 = \frac{1}{\frac{vol.\%\ Ar}{vol.\%O_2} * \frac{\rho_{Ar}}{\rho_{O_2}} + 1} * 100 = 6.51\%$$

and:

$$wt.\%\ Ar = 100 - wt.\%\ O_2 = 93.49\%$$

The last step is represented by the calculation of the mass of 1 l_n of Stargon®. According to the densities provided by FLUIDAT®, the density of Stargon O8® is:

$$\rho_{Stargon\ O8} = \left(vol.\%\ Ar * \rho_{Ar} + vol.\%\ O_2 * \rho_{O_2}\right)/100 = 1.756\ kg/m^3$$

where all densities are intended at 0°C and 1 atm (a). Every 1 l_n of Stargon O8® contains then 1.756 g of gas, the 6.51% of which is oxygen, namely 0.114 g/l_n.

With this value an estimation of the processing time needed to create a certain amount of Al_2O_3 is now possible. The following path explains how to do it.

Let M_{Al} be the initial mass of aluminium and $wt.\%\ Al_2O_3$ the desired percentage in weight of aluminium oxide within the molten metal, with respect to the total amount of material (aluminium + aluminium oxide), as shown in this expression:

$$wt.\%\ Al_2O_3 = \frac{M_{Al_2O_3}}{M_{Al} + X_O * M_{Al_2O_3}} * 100$$

At denominator, only the mass of oxygen is added to the initial mass of aluminium, since the aluminium composing the oxide is already taken into account in

M_{Al}, no matter if it's transformed into oxide. Arranging the last formula, the mass of oxide to create is:

$$M_{Al_2O_3} = \left(\frac{wt.\%\ Al_2O_3}{100 - X_O * wt.\%\ Al_2O_3}\right) * M_{Al}$$

and the oxygen to be injected is:

$$M_{O_2} = X_O * M_{Al_2O_3}$$

Dividing M_{O_2} by 0.114 g/l_n, the mass of Stargon O8® to inject, expressed in normal litres, is finally found. Furthermore, dividing this last value by the mass flow rate set on the control unit, the injecting time is obtained.

Melt treatment procedure

The first step into this experiment was carried out by means of the smaller setup described above. The procedure followed is here described.

The commercially pure aluminium supplied by Rheinfelden ALLOYS GmbH & Co. KG was analysed by a BRUKER Q4 TASMAN CCD-based spark optical emission spectrometry (S-OES) to verify the level of purity and the content of other elements within the alloy supplied. Three measurements were done on three different regions of the specimen and the average values are considered representative of the real content. The following table shows the average content of each element measured:

Si 0.066%	Fe 0.215%	Cu 0.0021%	Mn <0.0020%	Mg 0.00036%	Cr <0.0020%
Ni 0.0043%	Zn 0.0031%	Ti <0.0010%	B 0.0069%	Cd <0.00050%	Co <0.0010%
Li 0.00070%	Mo <0.0010%	Na 0.00052%	P <0.0020%	Pb <0.0050%	Sn 0.0029%
Sr <0.0010%	V 0.0024%	Zr <0.0020%	Sb <0.0070	Al 99.65%	

Table 4.2: composition of the supplied alloy

As expectable, the main impurity in aluminium is Fe because of its very high affinity with Al and the difficulty in removing it. Anyway, the level of purity meets the specifications stated by the supplier.

After the positive analysis of the composition, 2250 g of material were cut from an ingot and loaded into the crucible while still cold. Then the furnace was turned on and set to a temperature of 730 °C. The impeller was installed on the stirrer over the lid of the furnace so to get preheated by the heat raising from inside the furnace before starting the injection process. When the aluminium was completely molten, pure argon was blown on the top of the crucible to create an inert atmosphere and the oxide layer over the melt was removed. The melt was so ready to be stirred.

To prevent molten aluminium from penetrating into the bores of the impeller, a flow rate of 3 l_n/min of pure argon was set before dipping the impeller into the melt. Then the stirrer was lowered along the stand rod to a previously measured height and the impeller resulted completely submerged by the molten metal. After checking the absence of contact between the impeller and the crucible walls, the stirrer was turned on and set to 650 rpm and the F-201D controller was set to a flow rate of 2.150 l_n/min, a value that, converted by the right CF, equals 3 l_n/min of Stargon O8®. Then the argon controller was set to 0 and a timer started measuring the processing time.

The treatment was interrupted three times, after 45, 85 and 120 minutes respectively, to cast three tensile specimens. These treatment times corresponded to a wt.% of Al_2O_3 in the melt of 0.1, 0.2 and 0.3%. At each interruption, the gas was switched to pure argon again, the stirrer was stopped and lifted and fixed to a higher position on the stand rod, so to extract the impeller from the melt, and the furnace lid was opened. The impeller appeared wrapped by a foamy mixture of oxide and molten aluminium all the times. Some of the same foamy material was above the molten metal inside the crucible, floating because of its lower density. A fine grey powder also appeared on the surfaces and on the inner side of the lid, apparently originated within the crucible.

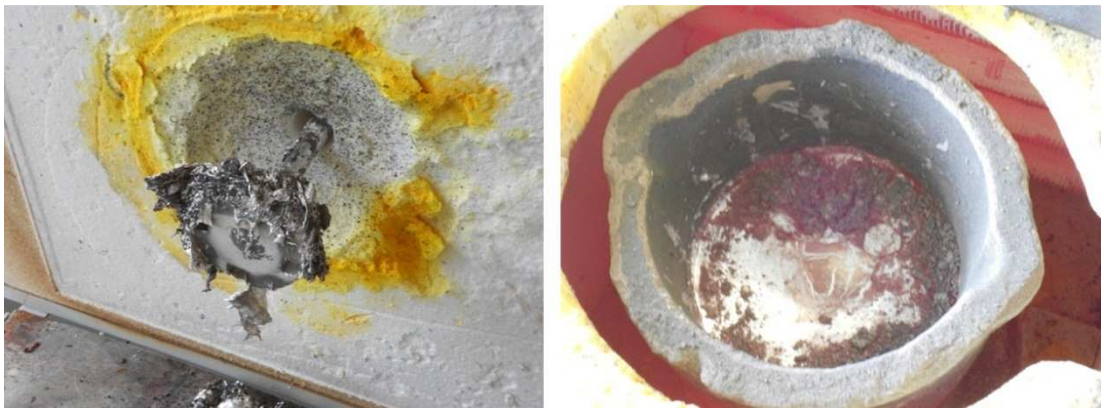

Figure 4.7: slag solidified around the impeller and the oxide powder on the crucible

The slag around the impeller was removed before it solidified. All the slag removed from the impeller and the cast specimens were weighed to estimate the remaining amount of material into the crucible, in order to calculate the time necessary before for the next casting.

Once the third specimen was cast, short after restarting the treatment, the ceramic tube broke near the top of the impeller. The reason for this break probably is a too high thermal stress on the tube where it was reached by the free surface of the melt, due to the high thermal gradient. Given the low reliability of the small setup, it was decided not to build another alike and to move to the bigger scale one for the following tests.

For the following test, the furnace of 50 kg capacity was employed. The planned test consisted in stirring and injecting gas for as long as possible, casting a sample every 30 seconds by taking some metal directly from the crucible with a ladle, without stopping the process. First, the treatment was made injecting Ar only. Three different molds were employed, since the time elapsing between one casting and the next was too short to let the casting solidify completely.

Four ingots of the same pure aluminium as that used for the previous test were first weighed and then loaded inside the crucible. The temperature of the cavity was set to 790 °C and the furnace was left on overnight. The morning after, the aluminium was completely molten and the thermocouple located inside the protective tube in direct contact with the melt indicated a temperature of 730 °C. As for the smaller furnace, before starting the process, the furnace cavity and the crucible were filled with pure argon and the oxide layer over the melt was removed.

Then, the degassing unit was placed in position and turned on. The bottom position of the moving arm had already been verified while the crucible was still empty, to prevent the impeller from touching it. The machine lowered the arm carrying the impeller until the set bottom position was reached. In the meanwhile, a limited gas flow, automatically controlled by the machine, kept the impeller bores free. Once in position, the impeller was set in rotation and the gas flow was switched to its maximum by the electronic control. The rotation speed was regulated in order not to let the aluminium vortex reach the edge of the crucible, keeping a safety margin. It was set to 350 rpm.

The degassing unit stopped automatically after approximately 11 minutes, because of the previously set working time. The horizontal arm got back to the rest position and then the process was started again. This could not be avoided, since the machine cannot work continuously. After 15 minutes, the level of melt into the crucible reached the impeller and part of it was not covered by the melt anymore. At that point the treatment was stopped.

Another series of specimens were cast injecting Ar + 8 vol.% O_2. As for the series treated with Ar, specimens were cast taking melt directly from the crucible, by means of a ladle, and the treatment was carried out for as long as possible. This time, each specimen was cast after 1 minute and only one mold was employed.

The procedure followed was the same as for the treatment with Ar. The process was interrupted and restarted twice because of the degassing unit ending its working cycle. As happened with the smaller impeller, a foamy slag grew around the graphite tube during the treatment and slowly reduced the clearance between the crucible wall and the slag itself.

Figure 4.8: slag wrapped around the graphite tube

Because of that, after 30 minutes it was not safe to insert the ladle into the crucible and the treatment was stopped.

When the graphite tube cooled down to room temperature, it was taken off the machine and the agglomerate of aluminium and oxide was removed using a gas torch to melt it down.

The treated material remained into the crucible was adopted to create and cast alloys as described in chapter 4. The foamy material floating over the molten aluminium was removed before adding the alloying elements. Figure n. illustrates its structure:

Figure 4.9: slag removed from the surface of melt

The gas bubbles seem to float and agglomerate on the surface forming a foam of aluminium and oxide. A dark oxide layer covers the rough surface of the slag. It looks like an agglomerate of oxidized metal particles.

Production of specimens

The alloys produces after this melt treatment were tested casting tensile specimens in permanent mold and machining other tensile specimens from die cast plates. Four alloys were cast and three of them had Cu as main alloying element. In figure n. a series of permanent mold cast specimens is shown.

Figure 4.10: permanent mold cast tensile specimens

The treated pure aluminium was cast in permanent mold only, while the other alloys produced were cast in permanent mold and die cast.

HPDC equipment

A Weingarten® GDK 200 cold chamber die casting machine was employed for the trials. The machine is capable of 200 tons clamping force. The clamping system is a conventional toggle mechanism moved by an hydraulic cylinder. The horizontal clearance between the tie bars measures 490 mm, which is the limit for the width of the die, since its installation on the machine is made from above, by means of a gantry crane or a bridge crane.

Figure 4.11: Weingarten GDK 200 HPDC machine

The geometry of the die is designed to produce a 150 x 100 x 3 mm plate. The cavity is composed of a round sprue, a runner, the plate, a wide overflow and the vacuum duct. All these volumes are machined on the cavity insert, which is located in the ejector plate, on the movable platen side.

Figure 4.12: die employed for the production of die cast plates

The core insert is completely flat and is mounted into the other die, on the fixed platen side. This feature simplifies the production and reduces the cost of the die. On the upper part of both the plates, two more inserts create a chilled vent to protect the vacuum circuit. These two inserts are made of copper and can be water- or oil-cooled.

The vacuum circuit is connected to the top of the copper insert on the fixed platen side. An in-line filter, composed of a steel hollow cylinder filled with steel wool, provides further protection to the circuit. A hose connects the outlet of the filter to an Electronics GmbH StatVac vacuum unit. This unit provides vacuum through a Venturi tube connected to the 6 bar compressed air line. It receives the shooting signal from the control panel of the die casting machine and synchronises the opening of the solenoid valve that let the compressed air flow through the Venturi tube.

A computer collects the process data coming from the sensors installed on the machine: the speed of the plunger, it's position, the pressure applied to the plunger and the vacuum pressure. The data are processed by DASYlab.

Castings

Circular cross-section tensile specimens were cast in permanent mold. Except for the castings of pure aluminium after the melt treatment, all the alloys suffered from hot cracking near the risers, as shown in figure n.:

Figure 4.13: hot cracks in permanent mold cast specimens

Hot cracks strongly affected also the die cast plates too:

Figure 4.14: hot cracks on a die cast plate

A reduction in hot cracks was obtained increasing the mold temperature from 160 °C to 220 °C. Increasing the mold temperature made the solidification phase longer. Initially, the extractor pins remained stuck into the overflow.

Figure 4.15: mark of the ejector pin on the overflow of a die cast plate

To avoid this inconvenience, the solidification time set on the machine control was increased.

During the last series of castings, a drop of the melt temperature occurred because of a change in the set temperature of the furnace, from 720 °C to 680 °C. As a consequence, the hot cracks presence in the plates increased, probably because of a lack of fluidity of the alloy. The temperature of the furnace was set back to 720 °C and the cracks presence decreased progressively during the following castings.

Heat treatment

Some of the plates produced by HPDC were heat treated to induce a natural aging of the alloy. The plates were introduced into a pre-heated treatment furnace and extracted after the set cycle. All the plates presented blistering defects on the surface, due to the presence of gas porosities inside the plates.

Figure 4.16: blisters on the surface of a heat treated die cast plate

5 Results of material testing

Materials and treatments

To investigate the effects of the treatment performed, four alloys and different treatment conditions were tested.

Alloy 1 is the pure aluminium as supplied by the foundry. Alloy 2 is obtained by adding Cu to Alloy 1 after melt treatment. Alloy 3 and 4 are two alloys with compositions close to that of 206.0 commercial cast alloy, obtained adding alloying elements to the already treated Al, as for the second alloy.

The compositions of the alloys are here reported:

Alloy	Composition, wt.%									
	Cu	Mn	Mg	Zn	Ti	Fe *	Si *	other *		Al
								each	total	
1	-	-	-	-	-	0.22	0.07	<0.007	0.06	bal.
2	4.61	-	-	-	-	0.22	0.07	<0.007	0.07	
3	4.99	0.45	0.37	-	-	0.24	0.08	<0.008	0.07	
4	4.98	0.42	0.27	0.1	0.023	0.20	0.28	<0.008	0.07	

Table 5.1: chemical composition of the tested alloys (* = impurity)

Note: Fe content in all the four alloys and Si content in alloys 1, 2 and 3 are present in the Al ingots supplied; Si content in alloy 4 is due to some residual alloy remained on the crucible walls after a previous usage.

Table 5.2 shows the parameters of treatment and the casting processes adopted for each tested alloy.

Alloy	Injected gas		Treatment time	Melt temp.	Stirring method		Casting process	
	Ar	Ar + 8 vol.% O_2			Ø 72 mm 650 rpm	Ø 185 mm 350 rpm	permanent mold	HPDC
1	●	●	0 – 15, 0 – 30, 45, 85, 120 min	730 °C	●	●	●	-
2	-	●	30 min	730 °C	-	●	●	●
3	-	●	30 min	730 °C	-	●	●	●
4	-	●	90 min	730 °C	-	●	●	●

Table 5.2: treatment parameters and casting processes tested for each alloy

Alloy 1: commercially pure Al

The first series of specimens of alloy 1 was obtained after treatment with the Ø 72 mm impeller setup. The parameters of the melt treatment are:

Injected gas:	Ar + 8 vol.% O_2
Duration of treatment:	45, 85 and 120 min
Gas flow rate:	3.1 l_n/min
Melt temperature:	730 °C
Impeller diameter:	Ø 72 mm
Rotation speed:	650 rpm

Four tensile strength test specimens were cast before the treatment and after 45, 85 and 120 minutes respectively. The results of tensile test are displayed in figure 5.1. Note: A_g indicates the permanent elongation at the point of maximum load.

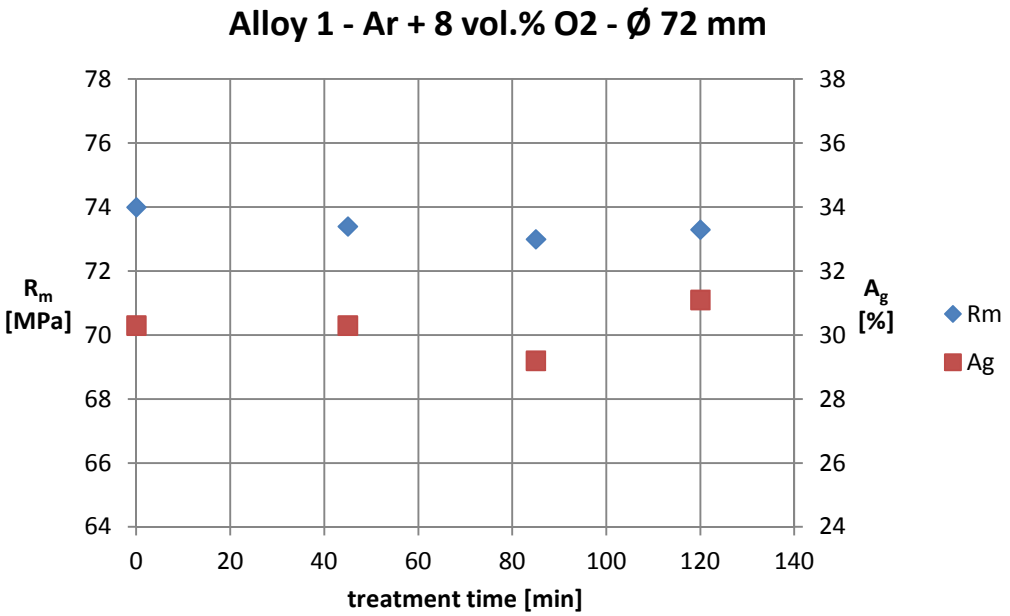

Figure 5.1: mechanical properties of alloy 1 – melt treatment with Ar + O_2 – Ø 72 mm impeller setup

The values of R_m and A_g don't seem to be affected by the process and the small changes from one specimen to the other don't show a clear trend. No strengthening effect can be attributed to the treatment so far.

Two other series of specimens of alloy 1 treated with Ø 185 mm impeller were made: one injecting Ar only, the other one injecting Ar + 8 vol.% O_2. Each series was cast taking molten alloy directly from the crucible during the treatment.

The parameters of the treatments are:

Injected gas	Ar	Ar + 8 vol.% O2
Duration of treatment	15 min	30 min
Gas flow rate	17.5 l_n/min	17.5 l_n/min
Melt temperature	730 °C	730 °C
Impeller	Ø 185 mm	Ø 185 mm
Rotation speed	350 rpm	350 rpm

When injecting Ar, each specimen was cast every 30 seconds. Since this time was not enough for a complete solidification of the castings, three molds were employed in rotation, to allow each casting to solidify before opening the mold. The three molds are different in size: for that reason, results of tensile strength test are divided into three groups, according to the diameter of the central section of the specimens. Figures 5.2 and 5.3 show the data resulting from the tensile strength tests:

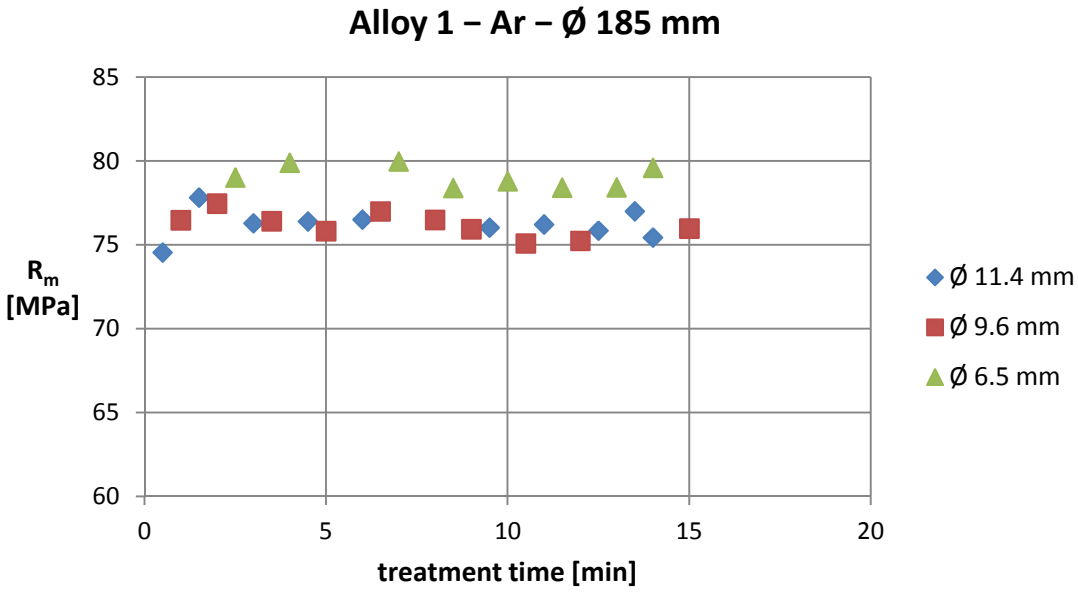

Figure 5.2: ultimate tensile strength of alloy 1 − melt treatment with Ar − Ø185 mm impeller setup

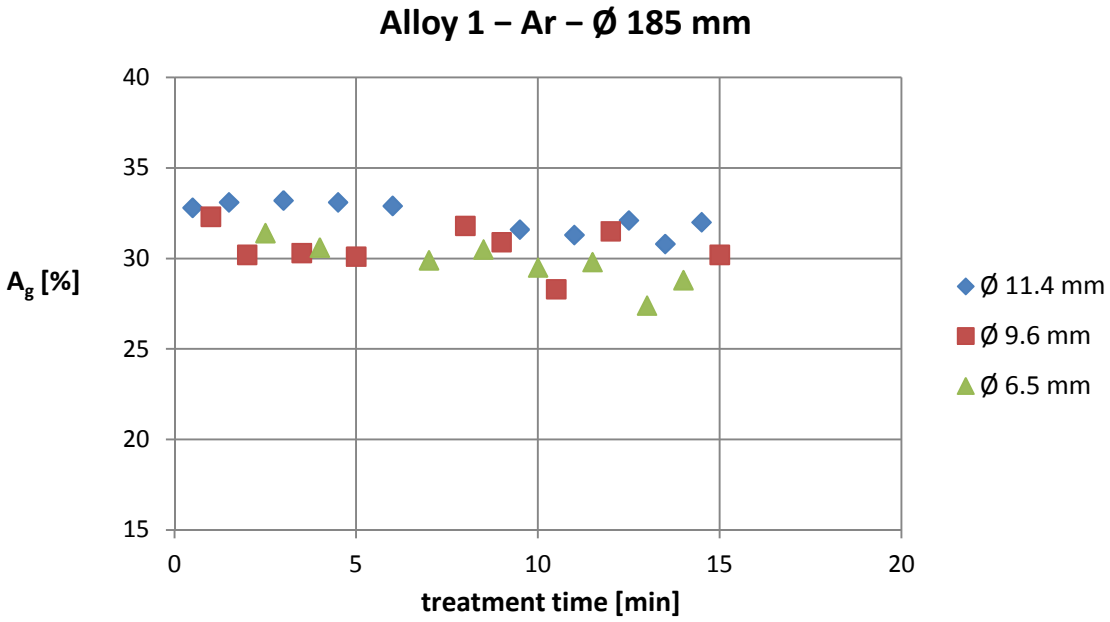

Figure 5.3: permanent elongation at maximum load of alloy 1 − melt treatment with Ar – Ø 185 mm impeller setup

When injecting Ar + 8 vol.% O_2, each specimen was cast every minute: this way the Ø 11.4 mm mold could be employed for all the castings. The difference in duration is due to technical limits related to the pouring technique. Both the treatments were interrupted when no more specimens could be cast, as described in section 4.

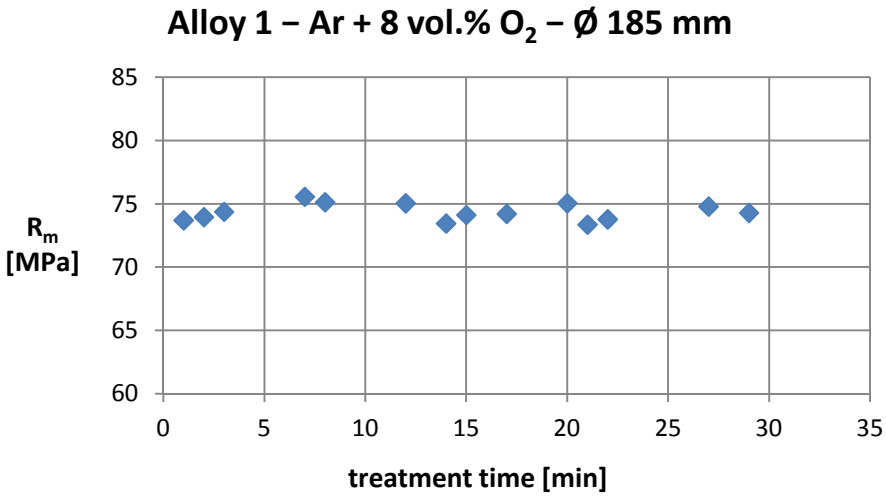

Figure 5.4: ultimate tensile strength of alloy 1 − melt treatment with Ar and O_2 – Ø 185 mm impeller

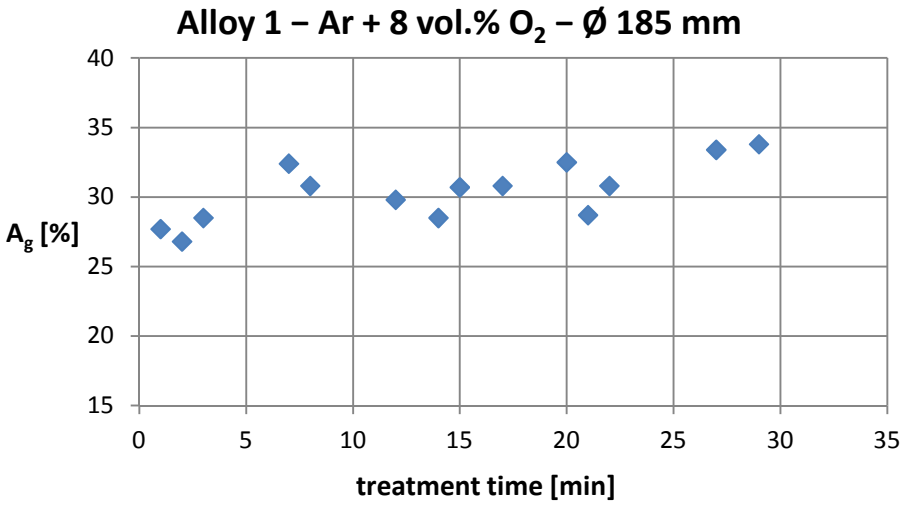

Figure 5.5: elongation at maximum load of alloy 1 − melt treatment with Ar and O_2 – Ø 185 mm impeller

The results show that the ultimate tensile strength of the alloy is not influenced by the duration of treatment, both with Ar and Ar + O_2.

A difference in strength is evident from Ø 11.4 mm to Ø 6.5 mm specimens in the series treated with Ar (figure 5.2). The difference is probably due to a faster solidification which leads to a finer microstructure.

On the other hand, elongation at maximum load is generally lower for smaller specimens (figure 5.3). This fact may suggest the presence of shrinkage porosities due to a poor feeding of the central cavity when a faster solidification occurs. Nonetheless, no such difference is noticeable from Ø 11.4 mm to Ø 9.6 mm diameter specimens. More generally, elongation tends to slightly decrease with longer treatment times for all the specimens, regardless of the mold size.

The specimens of the alloy treated with Ar + O_2 show a lower UTS when compared to the specimens of the same size, treated with Ar only. The difference is small and remains through all the treatment time, suggesting no influence due to the treatment:

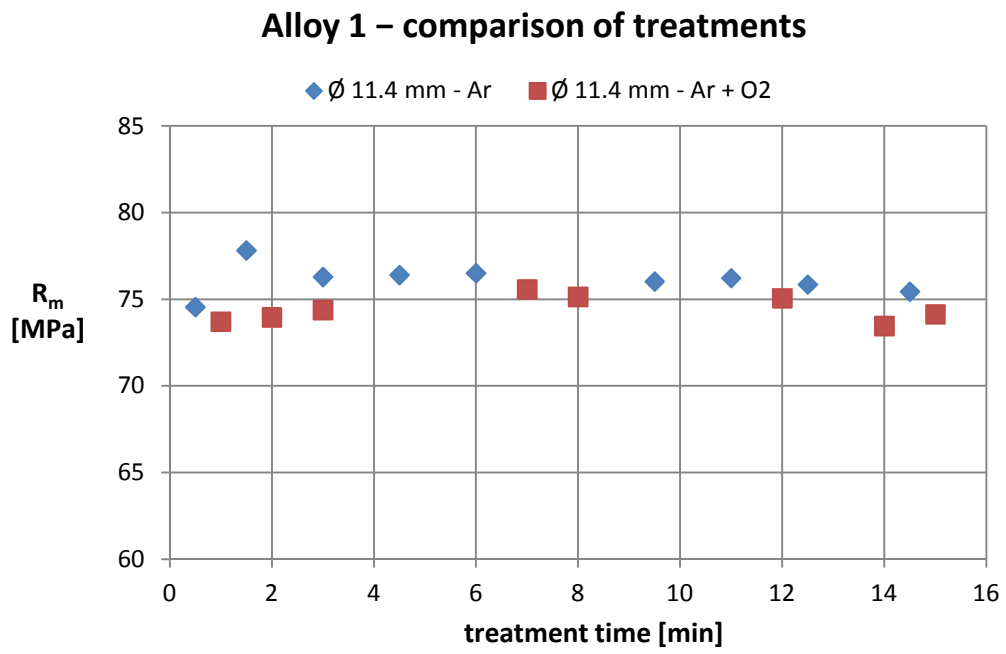

Figure 5.6: R_m comparison between alloy 1 treated with Ar and alloy 1 treated with Ar + O2

As visible in figure 5.5, the elongation at maximum load increases during treatment when the injected gas is Ar + O_2, even if only after 30 minutes of treatment it reaches the values obtained from the specimens treated with Ar.

The data on elongation show a high scattering: to investigate the causes of this data distribution, the linear trend of A_g values was calculated as function of the treatment time and its effect subtracted. The resulting values $A_{g,TF}$ are compared to those of R_m:

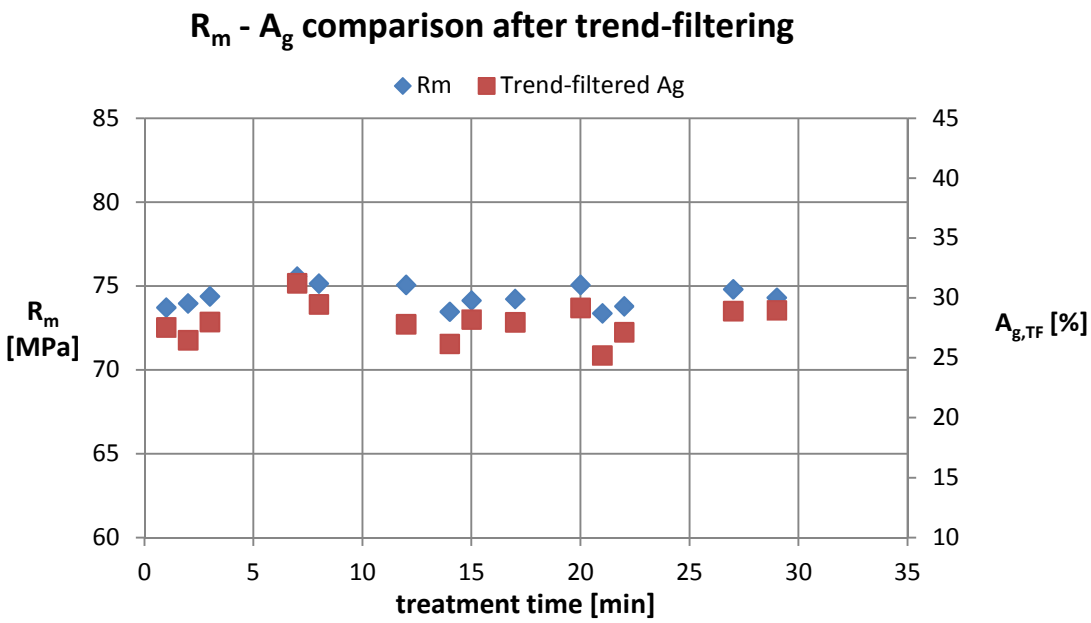

Figure 5.7: comparison of R_m and A_g variability in alloy 1 after trend-filtering of A_g values − melt treatment with Ar + O_2 − Ø 185 mm impeller

Apparently, both R_m and A_g are influenced by common factors. A cause for the drop both in strength and elongation can be found in the amount and distribution of porosities: the reduction in cross-section affects the ultimate tensile strength and is heavier if porosities are concentrated in the same region of the specimen, for example as a consequence of the shrinkage on a hot spot; at the same time, big porosities may promote an early necking of the specimens.

From the CT images, the internal porosity can be evaluated and related to the mechanical behaviour. Some of the specimens treated with Ar + O_2 were analysed through CT and their images are shown in figure 5.8. Apparently, a finer and more dispersed porosity, especially if distributed throughout the length of the specimen, is a favourable condition for higher strength and elongation. Though, the specimen cast after 8 minutes presents high strength and elongation even with shrinkage cavities similar to those of specimens cast after 1 and 21 minutes.

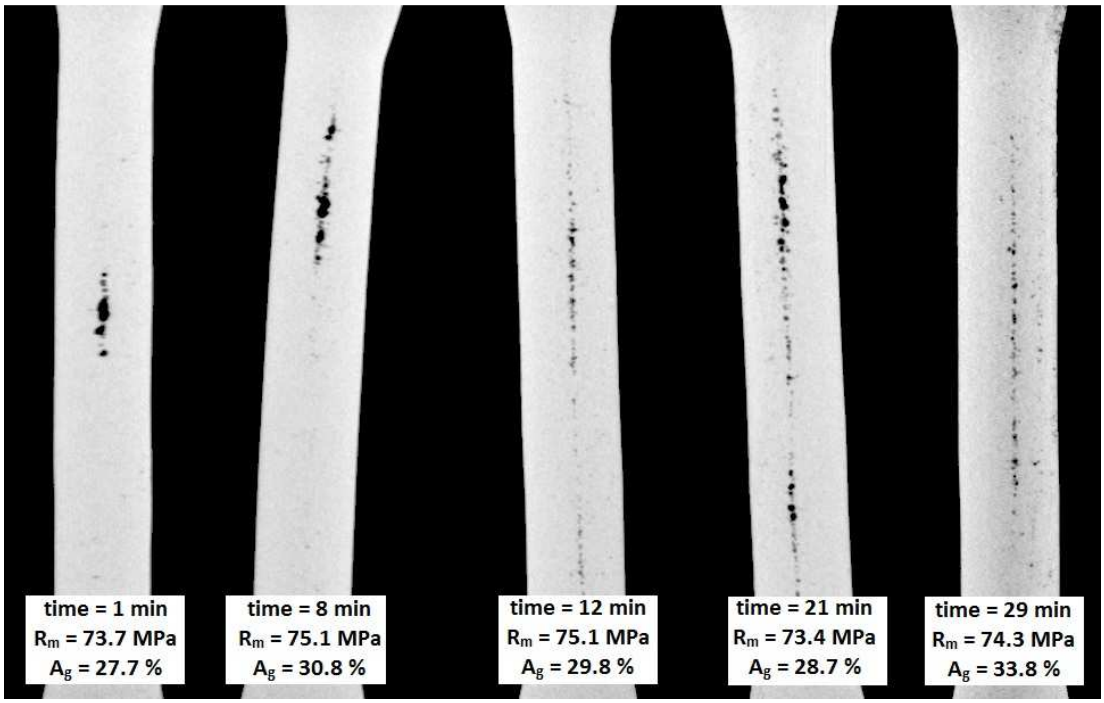

Figure 5.8: CT images showing the internal porosity of some of the tensile specimens of alloy 1

Apparently, in specimens cast after 1, 8 and 21 minutes, a hot spot originated and led to the formation of a shrinkage cavity.

The results can be divided in three groups: the specimens cast from time 0 to 12 min, those from 14 to 20 and those from 21 to 29. Strength and elongation drop at the beginning of each group and then slowly increase again. The reason is a short interruption of the treatment after 13 and 20 minutes respectively: the pauses let the mold cool down to a lower temperature and that may be the cause for a poor feeding of the central section of the specimens because of an early solidification of the sides. The same happened for the first specimens of the series, since the mold was at room temperature before the first casting. Hence, the differences in strength and, partially, in elongation can be the result of the variation of the mold temperature.

The positive trend of elongation can be explained with a progressive reduction in hydrogen and impurities content thanks to the degassing and cleaning effects of the gas bubbles.

From the tensile tests data no clear strengthening effects are observed: the values are close to those of the specimens treated with Ar.

Porosity was evaluated also by means of Archimedes' balance. The results are apparently in contrast with the mechanical behaviour of the specimens, since porosity grows higher for higher treatment times.

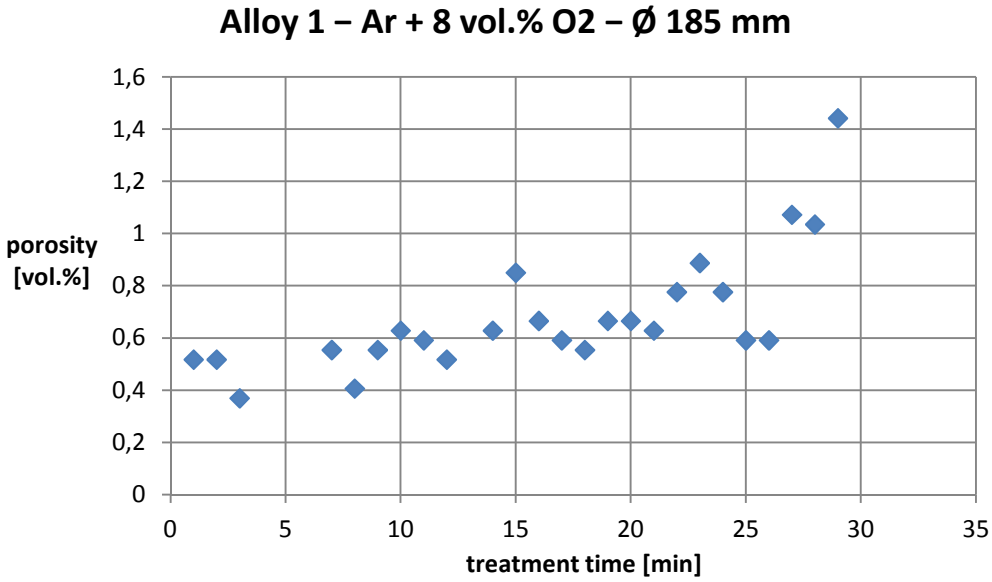

Figure 5.9: porosity content of tensile specimens of alloy 1 − melt treatment with Ar + O_2 – Ø 185 mm impeller

The porosity measured takes into account the grip sections of the specimens too. From the observation of CT images, a variability in porosity of these sections is visible, both at the core and near the surface, and this is the explanation for the higher porosity of some specimens.

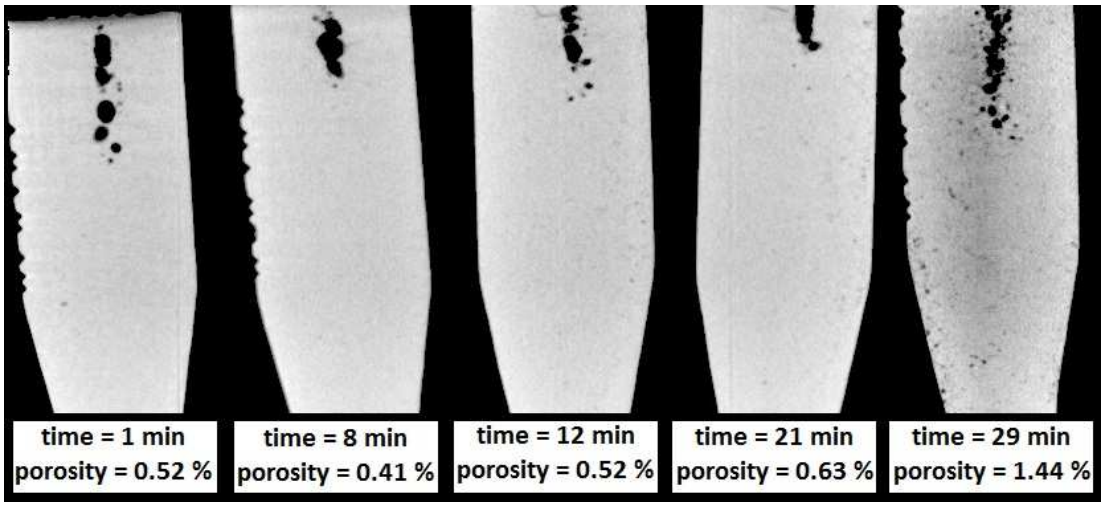

Figure 5.10: CT images of the grip sections of tensile specimens of alloy 1 − melt treatment with Ar + O_2 – Ø 185 mm impeller

The higher porosity of the last specimens is supposedly due to the pouring technique: since taking molten metal from the crucible had become difficult because of the reduced clearance between the wall and the slag around the graphite tube, the ladle was filled with melt taken from the surface, where more gas was still dispersed within.

The microstructure of alloy 1 without treatment and after both the treatments was observed by means of an optical microscope. Samples were taken from the grip sections of the specimens. Micrographs of alloy 1 before the treatment show a high quantity of gas porosities. As observed by means of CT images, the grip sections always present higher porosity contents because of the longer solidification time, causing an accumulation of trapped air and hydrogen.

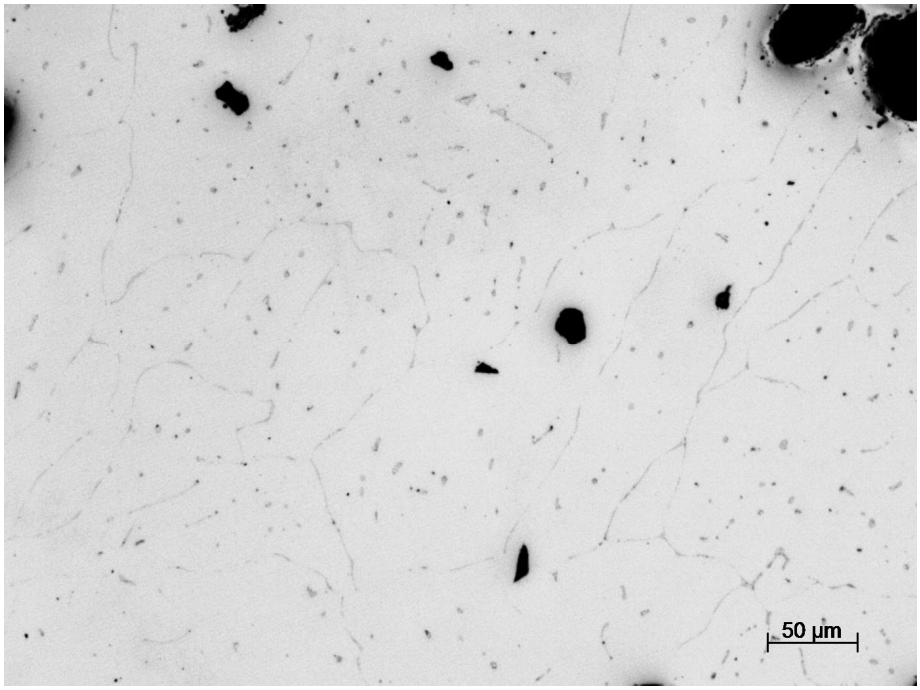

Figure 5.11: microstructure of alloy 1 − no melt treatment − 100x

Higher magnifications show the presence of an Al/Al_3Fe eutectic phase nucleated at the grain boundaries and inside the grains. Some regions show a higher content oh this phase, some other are poorer.

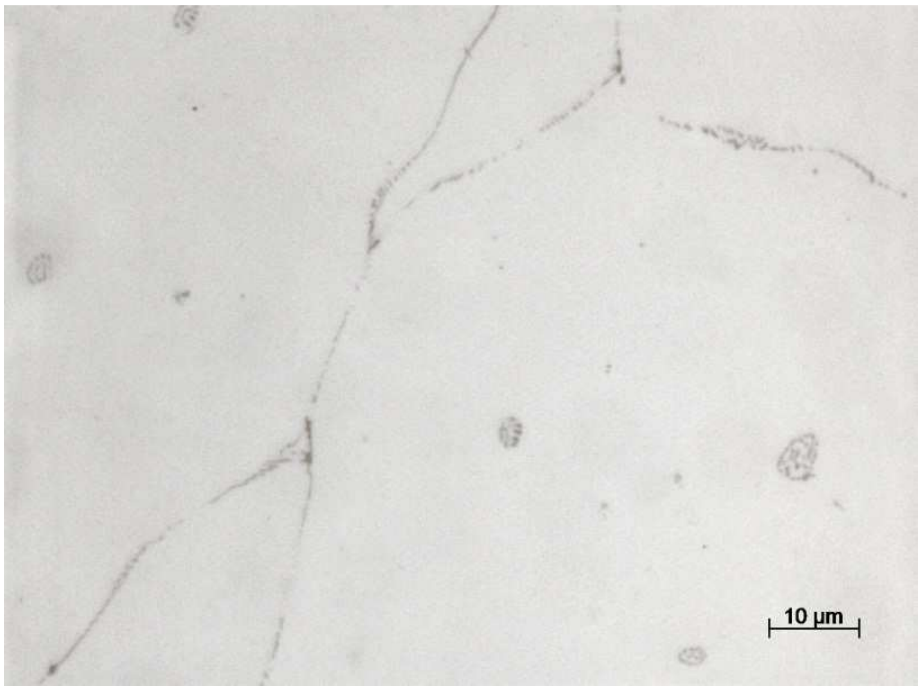

Figure 5.12: microstructure of alloy 1 − no melt treatment − 1000x

Figure 5.13 shows a micrograph from the specimen treated for 120 minutes with the Ø 72 mm impeller:

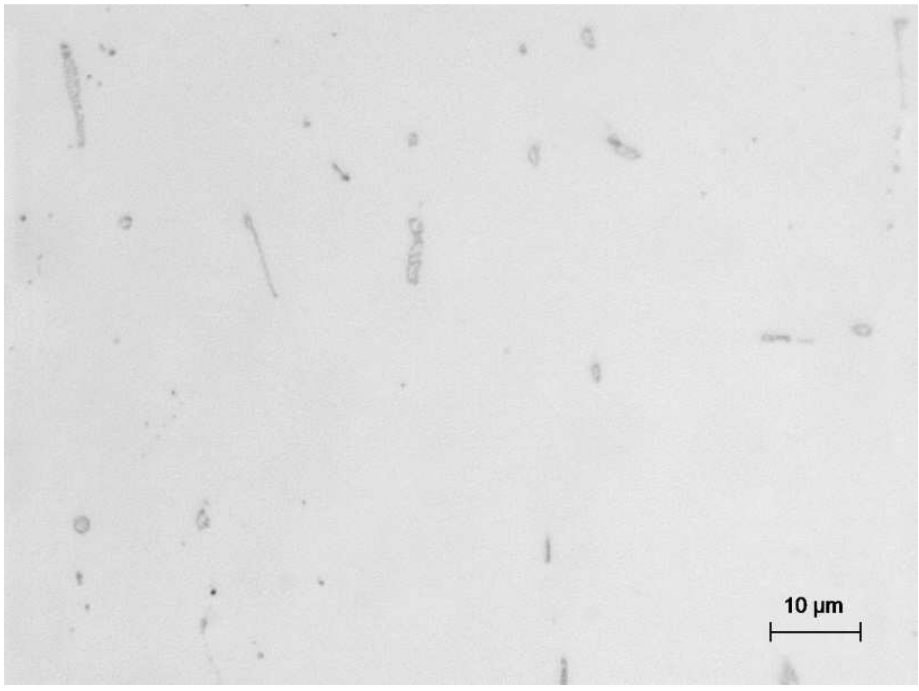

Figure 5.13: microstructure of alloy 1 − melt treatment with Ar + O_2 – Ø 72 mm impeller setup − 1000x

After treatment with Ar + O_2, the microstructure is almost the same, with regions where Al/Al_3Fe eutectic is present with finer distribution within the grains

and nearly absent at the grain boundaries and regions where the phase is present only at the boundaries.

The same microstructure was found also in the specimens treated with the larger impeller, as shown in figure 5.14:

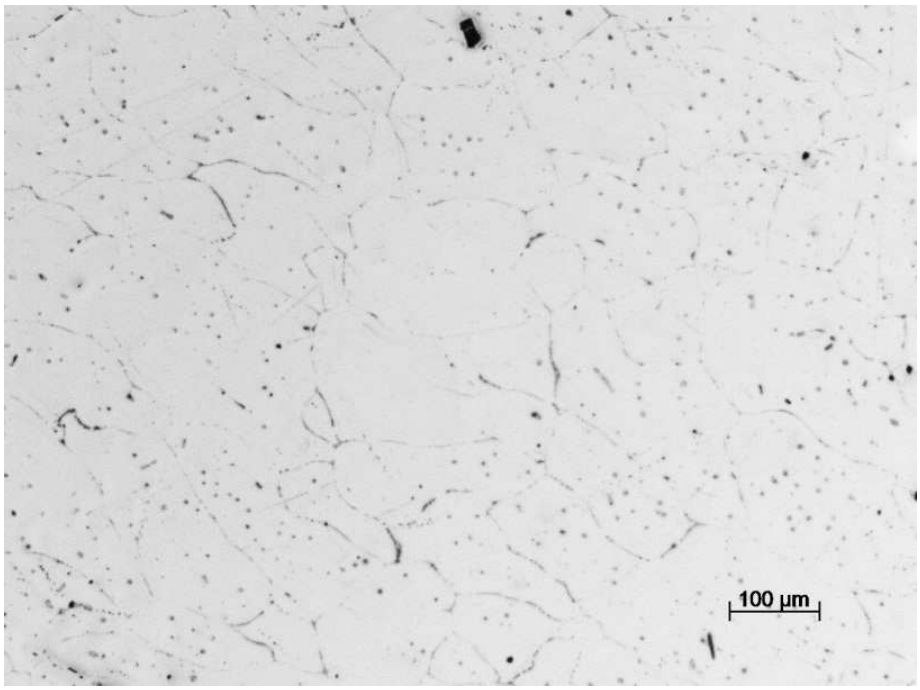

Figure 5.14: microstructure of alloy 1 − melt treatment with Ar + O_2 − Ø 185 mm impeller – 100x

The Al/Al_3Fe eutectic solidifies in round-shaped zones within the grains, as seen in alloy 1 without melt treatment.

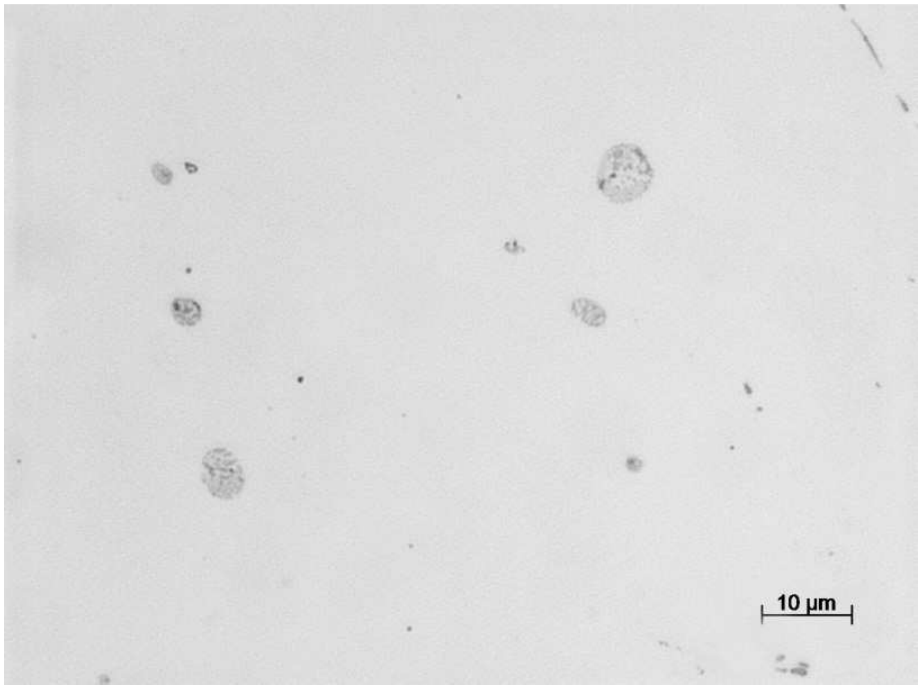

Figure 5.15: microstructure of alloy 1 − melt treatment with Ar + O_2 – Ø 185 mm impeller − 1000x

Alloy 2: AlCu4.6

Alloy 2, which composition is reported in table 5.1, was fabricated starting from already molten alloy 1, treated with Ar + O_2. Pure copper was added to reach the final composition. The alloy was tested both with permanent mold casting and in HPDC. The melt treatment parameters are:

Injected gas:	Ar + 8 vol.% O_2
Duration of treatment:	30 min
Gas flow rate:	17.5 l_n/min
Melt temperature:	730 °C
Impeller diameter:	Ø 185 mm
Rotation speed:	350 rpm

Alloy 2 – Permanent mold

A series of five tensile specimens with a circular section of 11.4 mm radius was cast in permanent mold and tested. The results are shown in figure 5.16.

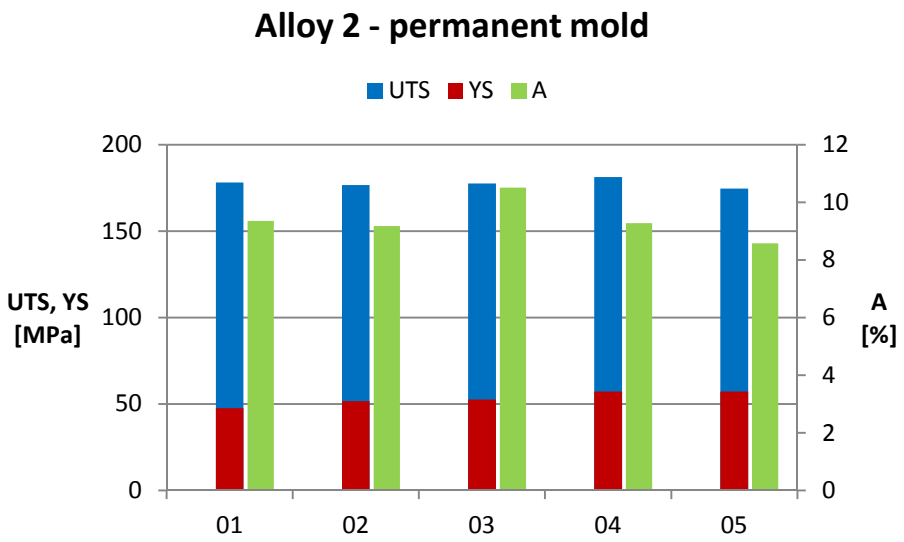

Figure 5.16: mechanical properties of permanent mold cast alloy 2

The ultimate tensile strength of all the specimens ranges from 174.6 to 181.3 MPa. Elongation is more variable, ranging from 8.6 to 10.5%, with an increment of 22%. Again, the variability could be ascribed to the different amount of defects of each specimen.

The strengthening effect of Cu added as alloying element is evident, even at as-cast condition. UTS is more than double of that of alloy 1, at the expense of the elongation, reduced to less than 1/3.

As a reference, the mechanical properties of EN AC-21100 cast in permanent mold have been considered. Its composition and mechanical properties are reported in tables 5.3 and 5.4:

EN AC-21100 − Composition (wt.% according to EN 1676)										
Si	Fe	Cu	Mn	Mg	Cr	Ni	Zn	Pb	Sn	Ti
0.18	0.19	4.2 5.2	0.55	-	-	-	0.07	-	-	0.10 0.30

Table 5.3: chemical composition of EN AC-21100 as specified in EN 1676 standard

EN AC-21100 – Mechanical properties (as fabricated)		
$R_{p0.2}$ [MPa]	R_m [MPa]	A [%]
70	170	5

Table 5.4: minimum mechanical properties of as-fabricated EN AC-21100 cast in permanent mold

The composition of alloy 2 differs from that of AC-21100 in Ti content, which is lower than the minimum indicated, while Fe content slightly exceeds the maximum admitted. Nonetheless, it can be a suitable alloy for a useful comparison.

Ultimate tensile strength and elongation reach the specified minimum values, while yield strength is constantly lower. A reason for the limited yield strength could be the degree of porosity, which reduces the effective cross-sectional area of the specimens.

CT images reveal a porous zone in the centre of the cross-section. Compared to those of alloy 1, porosities are finer and occupy a wider area of the section, forming a spongy zone. Specimens 4 and 5 also seem to have a higher porosity content, with larger cavities. This is due to the dendritic structure of the alloy. This zone could justify the lower yield strength and sounder specimens may reach a yield and ultimate tensile strength and an elongation higher than those achieved in these tests.

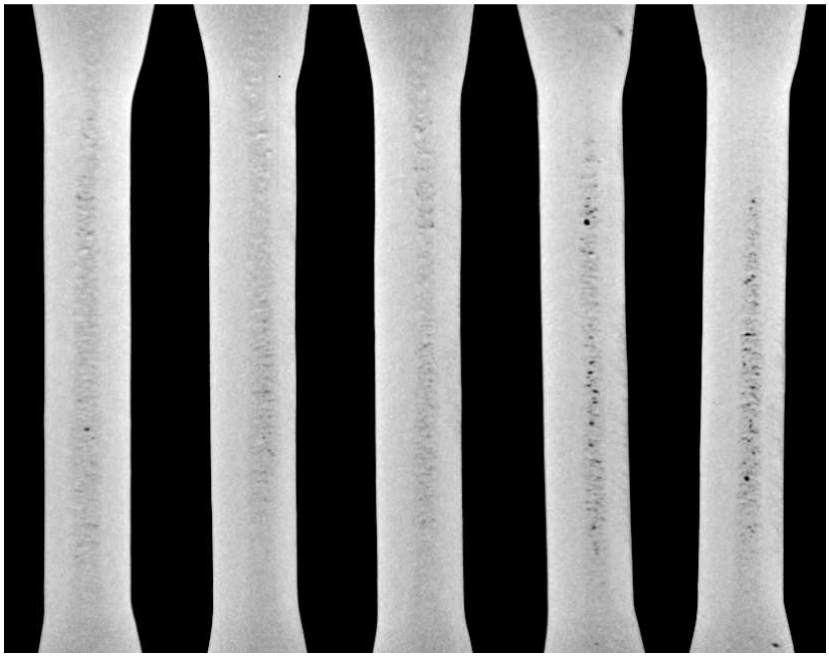

Figure 5.17: CT images of permanent mold cast specimens of alloy 2

As a further confirmation, the yield region of the stress-strain curves of these specimens is wide and there is no clearly defined yield point. Test made on HPDC specimens revealed, on the contrary, a precise value of the stress at which the permanent deformation starts: the difference is presumably due to the fact that each

part of the permanent mold cast specimens yields at a different load, according to its actual cross-sectional area.

Density measurements were performed to assess the porosity of the specimens. In figure 5.18, the estimated porosity is shown:

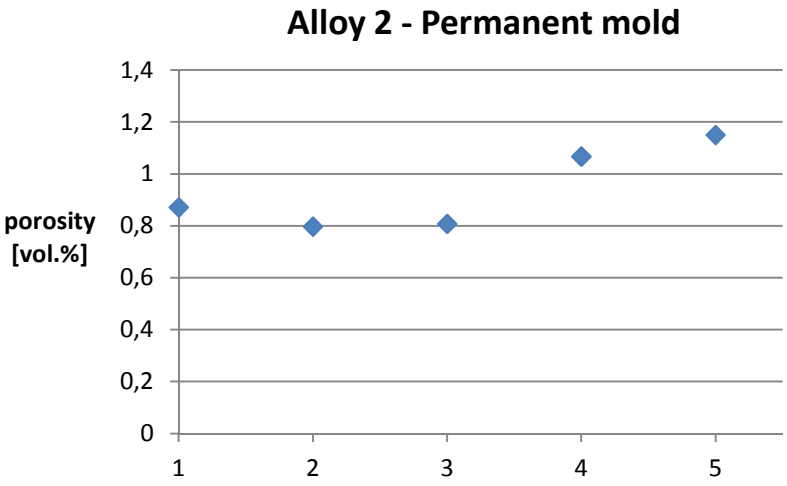

Figure 5.18: porosity content of alloy 2 specimens cast in permanent mold

The values confirm what was visible from CT images: specimens 4 and 5 have a higher porosity. Though, no relations between porosity and mechanical properties have been found.

All the specimens had hot cracks, located at the end of the grip sections, near the risers. CT images didn't reveal any crack in the central part of the specimens, as confirmed by the tensile tests, since all the specimens achieved similar UTS values.

Tensile test curves of all the specimens showed an irregular evolution of the stress, with a "saw toothed" profile, as displayed in figure 5.19.

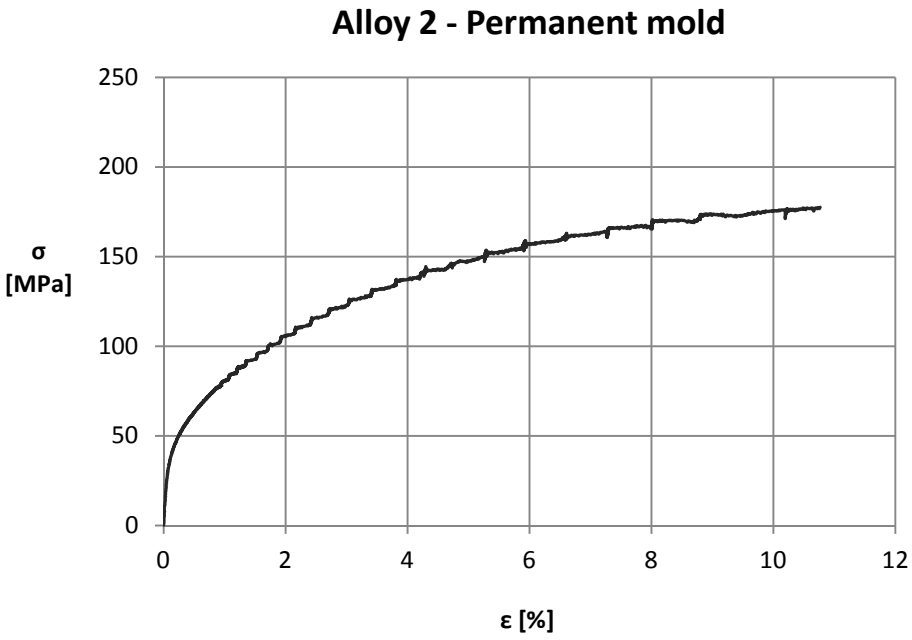

Figure 5.19: a stress-strain curve of permanent mold cast alloy 2, showing the "saw-tooth" behaviour

This strain behaviour may be the consequence of the progressive failure of the strong and fragile $CuAl_2$ phase segregated at the grain boundaries.

Alloy 2 - HPDC

A series of 45 tensile specimens machined from 13 die cast plates of 3 mm thickness was tested. The castings obtained by HPDC were strongly affected by hot cracks. Those visible by naked eye were discarded, though many had internal cracks not visible from the surface. As a consequence, the majority of tensile tests ended before reaching the actual stress bore by the alloy. In figure 5.20 the results of tensile tests are presented: each circle indicates the ultimate tensile strength R_m and the elongation at fracture A of a specimen.

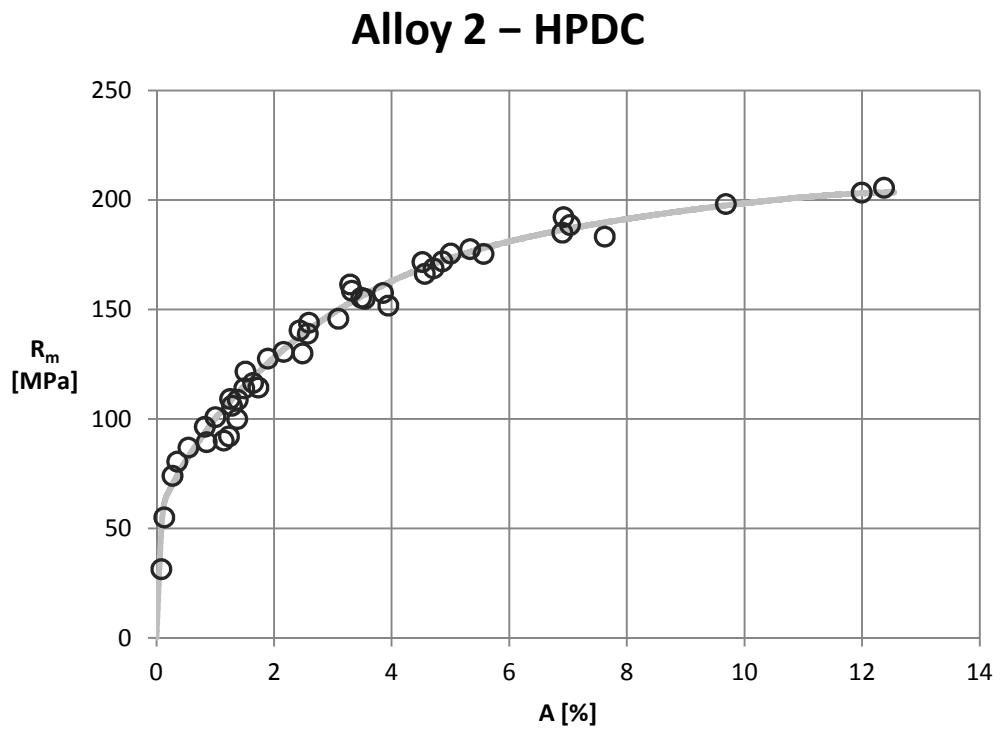

Figure 5.20: distribution of failure points of die cast alloy 2 specimens

The variability of data indicates a strong presence of defects affecting the mechanical properties of most of the specimens. Though, all the circles lie quite close to the stress-strain curve of the strongest, suggesting that the mechanical behaviour of this specimen is representative of the strength and toughness of the alloy 2 when free of defects.

Compared to the values reached by the same alloy cast in permanent mold, strength and elongation of die cast alloy 2 are higher, as predictable considering the higher cooling rate of the castings, which leads to a finer microstructure.

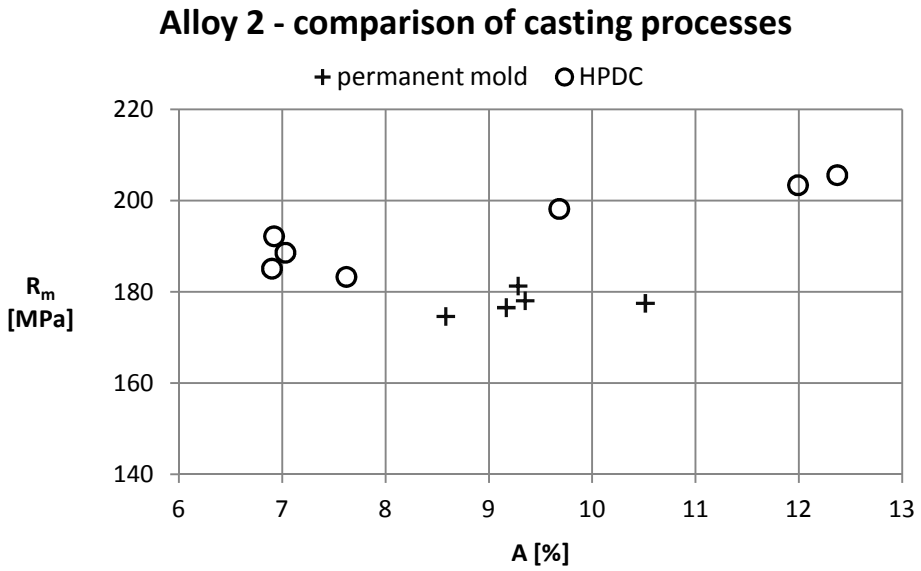

Figure 5.21: mechanical properties of alloy 2 - comparison of casting processes

Stress-strain curves show an irregular profile, as those of permanent mold cast specimens. A stress-strain curve is reported as example.

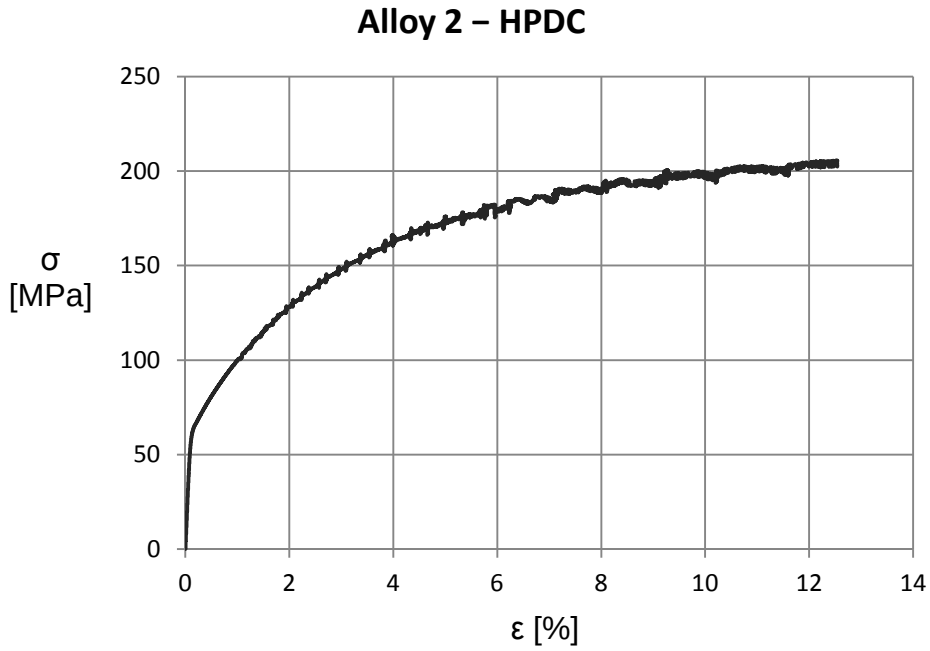

Figure 5.22: stress-strain curve of die cast alloy 2, showing the same "saw-tooth" behaviour as for permanent mold cast specimens

Finding the same behaviour even using two different tensile test machines confirms that this damaging mechanism is a characteristic of the alloy.

Micrographs of the permanent mold cast alloy 2 show a dendritic microstructure with Al/Al_3Fe eutectic and $CuAl_2$ solidified between the dendrite arms. Some interdendritic voids due to the shrinkage were also found.

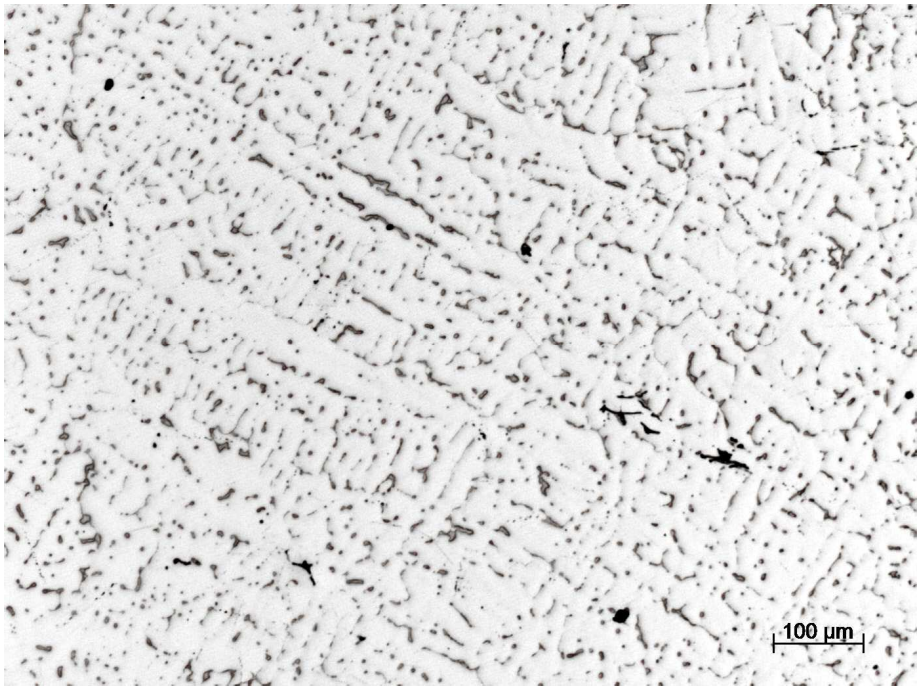

Figure 5.23: microstructure of alloy 2 − permanent mold casting − 100x

At higher magnifications, the different phases are clearly distinguished:

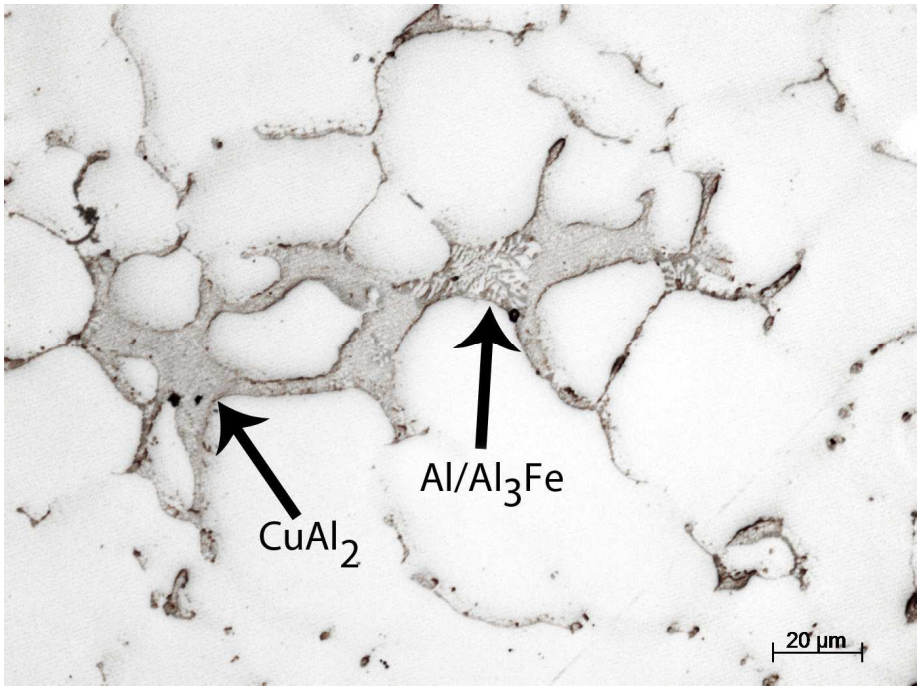

Figure 5.24: microstructure of alloy 2 − permanent mold casting − 500x

The Al/Al_3Fe eutectic is no more present within the grains, but only at the boundaries, together with $CuAl_2$.

The microstructure of die cast alloy 2 is evidently finer, thanks to the higher cooling rate:

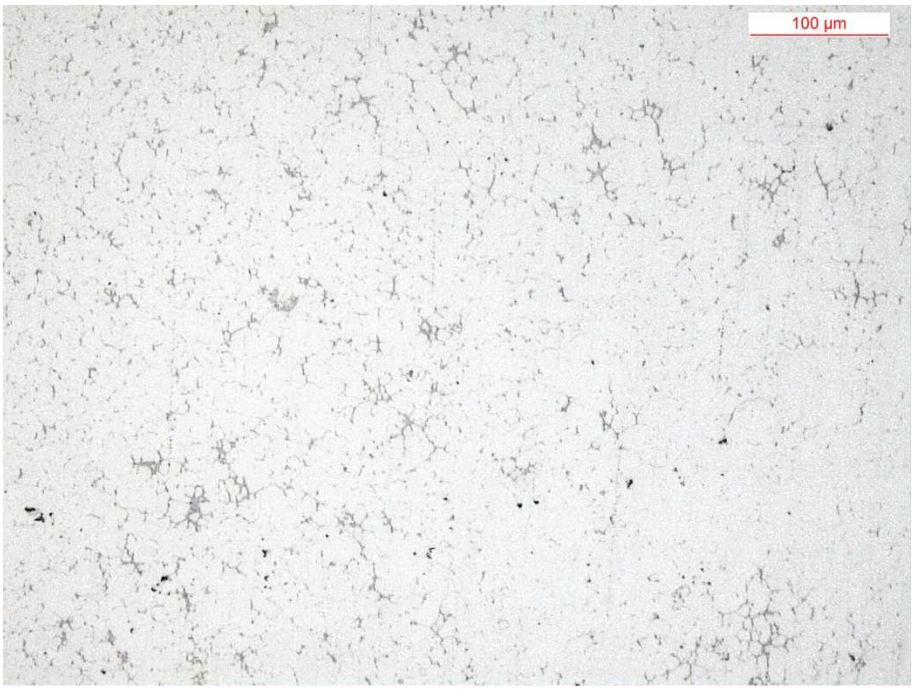

Figure 5.25: microstructure alloy 2 – HPDC − 100x

Dendrites are no more evident as in permanent mold cast specimens.

Alloy 3 – AlCu5MnMg

As for alloy 2, alloy 3 was obtained from already treated alloy 1, adding all the other alloying elements. The composition is reported in table 5.1. Cu and Mg were added as commercial grade pure metals, while Mn was added in form of a master alloy of Al with 25 wt.% Mn. The alloy was tested both with permanent mold casting and HPDC. The parameters of the melt treatment performed are:

Injected gas:	Ar + 8 vol.% O_2
Duration of treatment:	30 min
Gas flow rate:	17.5 l_n/min
Melt temperature:	730 °C
Impeller diameter:	Ø 185 mm
Rotation speed:	350 rpm

Alloy 3 – Permanent mold

To test the mechanical properties of alloy 3 in permanent mold, seven tensile specimens were cast. All of them presented hot cracks at the end of the grip sections, the same position and shape of those in alloy 2 specimens. The specimens were sawn so to avoid the cracked parts to remain in the grips.

The tensile test data of the seven specimens are reported in figure 5.26:

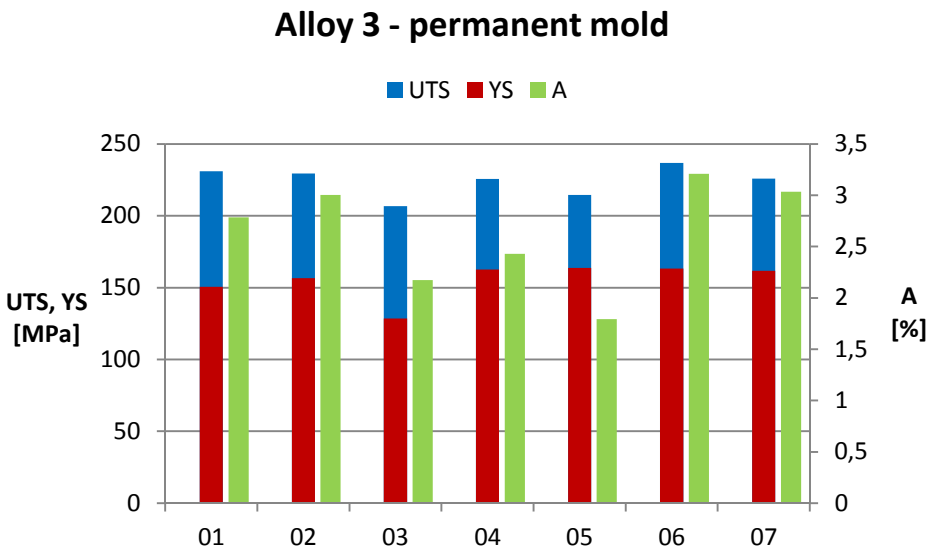

Figure 5.26: mechanical properties of permanent mold cast alloy 3

The addition of Mn and Mg, together with a higher content of Cu, improved the strength of the alloy, but sensibly reduced the elongation at fracture, compared to alloy 2.

The distribution of data suggests a higher content of defects compromising the properties of some specimens. To verify the porosity content, the specimens were observed through CT and the images reveal a porous zone similar to that of alloy 2.

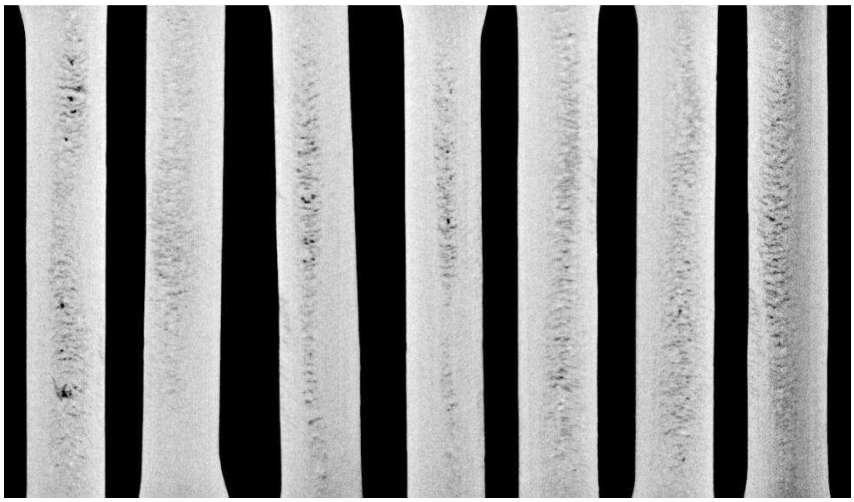

Figure 5.27: CT images of permanent mold cast alloy 3

Apparently, the content is higher but the density measurements made with Archimedes' balance indicate a porosity content lower than that of the specimens cast with alloy 2.

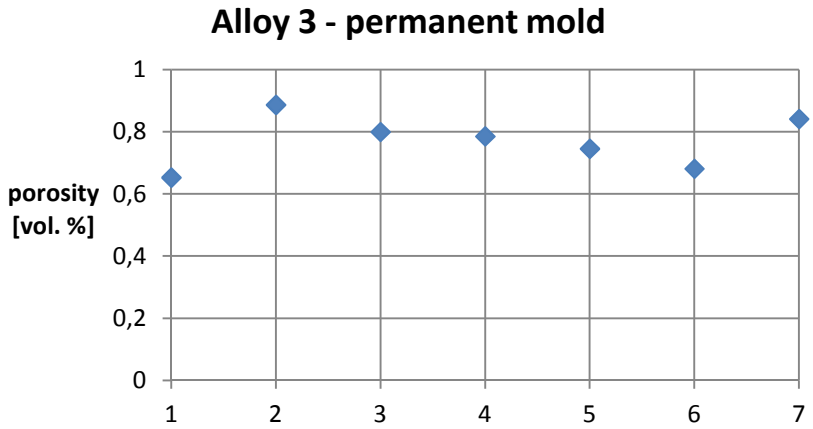

Figure 5.28: porosity content of the specimens of permanent mold cast alloy 3

The mechanical properties of alloy EN AC-21000, which composition is similar to that of alloy 3, as provided by Raffmetal S.p.a., are reported as a reference:

EN AC-21000 − Composition (wt.% according to EN 1676)										
Si	Fe	Cu	Mn	Mg	Cr	Ni	Zn	Pb	Sn	Ti
0.20	0.35	4.2 5.0	0.10	0.15 0.35	-	0.05	0.10	0.05	0.05	0.15 0.30

Table 5.5: chemical composition of EN AC-21000 alloy as specified in EN 1676 standard

EN AC-21000 – Mechanical properties		
$R_{p0.2}$ [MPa]	R_m [MPa]	A [%]
165 - 195	195 - 235	1 - 4

Table 5.6: mechanical properties of EN AC-21000 as provided by Raffmetal S.p.a.

The UTS and elongation at fracture of alloy 3 are close to the upper limits of those of AC-21000, but the yield stress hardly reaches the lower limit. The differences in composition, especially the presence of Mn and the absence of Ti could be responsible for the different yielding point.

Alloy 3 – HPDC

Flat tensile specimens were machined from 10 die cast plates of 3 mm thickness. As for alloy 2, many hot cracks were visible from the surface. A smaller geometry of the specimens was adopted to avoid the cracks more easily. After machining, the specimens produced were analysed by x-ray imaging to detect and discard those with defects. In figure 5.29, an x-ray image is shown. Cracks are visible in both the two specimens in the middle.

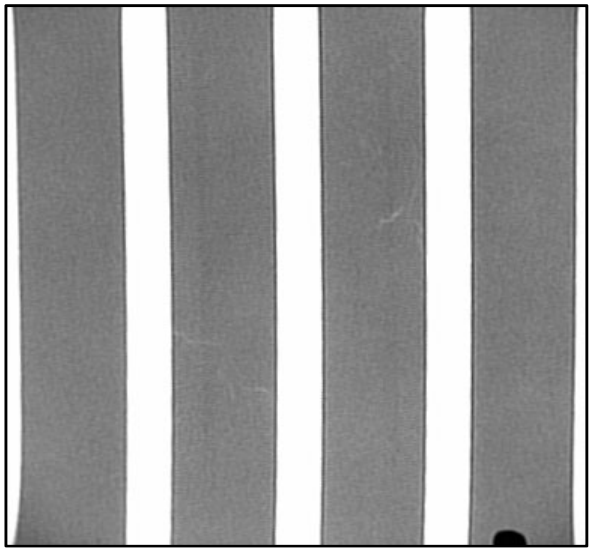

Figure 5.29: x-ray images of die cast alloy 3 specimens, showing hot cracks inside the two samples in the middle

In figure 5.30, the results from the tensile tests are shown:

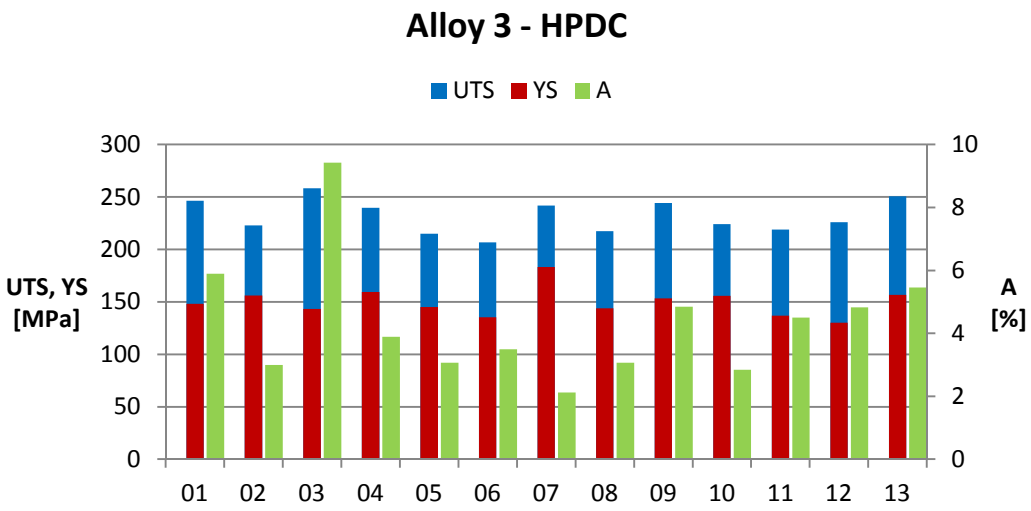

Figure 5.30: mechanical properties of die cast alloy 3

Analysing the data, a great variability of results appears: most of the tests ended with an elongation at fracture of 2% to 6%, a too wide range to assess the real elongation of the alloy. In addition, one specimen reached 9.42%.

The variability of properties shown by alloy 3 as HPDC is mostly attributable to the presence of defects, affecting the damaging mechanism, since yield stress is more stable. It may be also due to an inhomogeneous distribution of alloying elements within the melt. To be noticed is that the lower elongation value is that of the specimen with higher yield strength, suggesting the presence of an excess of alloying elements, forming strong though fragile phases at the grain boundaries. The origin of an inhomogeneous concentration could be a too short time elapsed from the moment of adding elements into the furnace to the moment when castings were performed.

Comparing the two casting processes, the influence of the process is evident on the elongation values, which are lower for permanent mold cast specimens. The yield behaviour is also different: permanent mold cast specimens present a wide yielding range without a clear yield point, while HPDC specimens have a yield point where the strain increases at approximately constant load and then the stress grows with strain again, until the failure point is reached. Two curves are reported as examples:

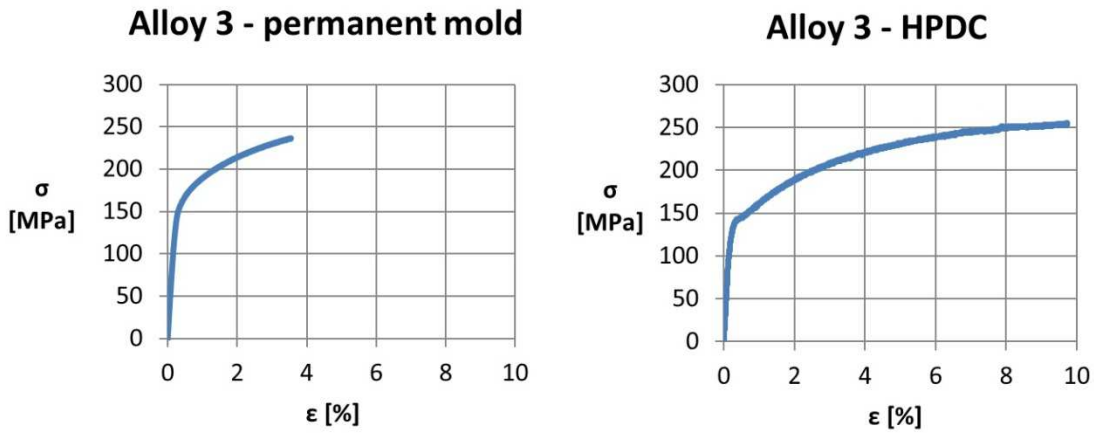

Figure 5.31: comparison of the yielding behaviour of permanent mold and die cast alloy 3

Despite this difference in yielding behaviour, the yield strength of the specimens doesn't differ strongly when the two casting processes are compared: permanent mold castings have an average of 155 MPa, while HPCD specimens yield at an average of 149 MPa. Apparently, the finer microstructure obtained by HPDC doesn't improve the yield strength of the specimen, probably because the yielding mechanism is more related to the presence and dimension of secondary phases at the grain boundaries than to the grain size of the primary phase. On the other hand, ultimate tensile strength is slightly higher in HPDC specimens, with average values of 224 MPa for permanent mold casting and 232 MPa for HPDC.

To be noticed is that the stress-strain curves of alloy 3 don't exhibit the toothed profile shown in alloy 2 curves. Mn and Mg additions probably change the damaging mechanism of the alloy.

The microstructure of permanent mold cast alloy 3, observed with an optical microscope, appears as in figure 5.32.

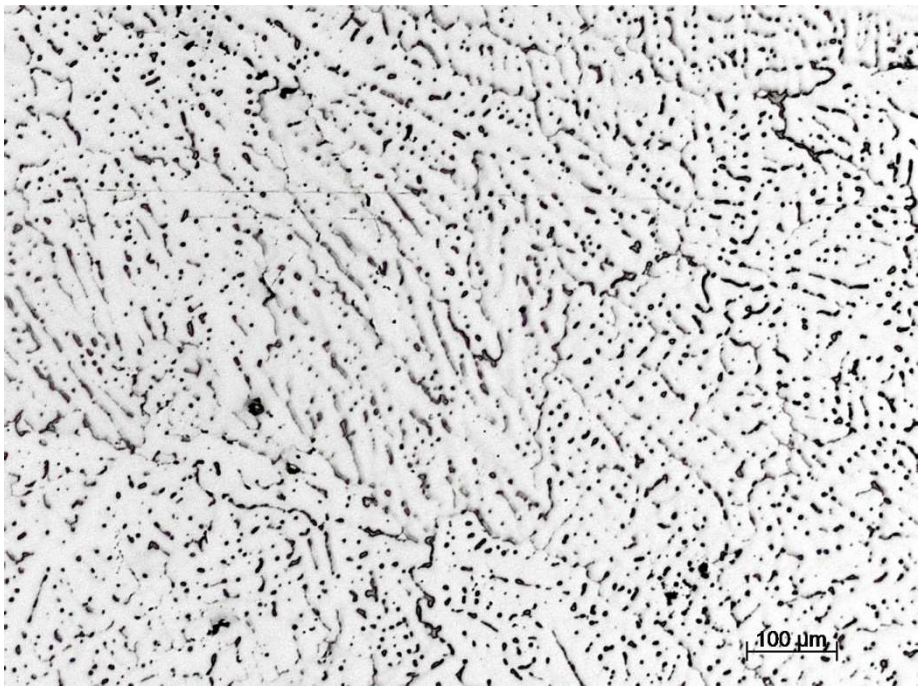

Figure 5.32: microstructure of alloy 3 − permanent mold casting − 100x

The microstructure is dendritic. The phases at the interdentritic regions were observed at higher magnifications:

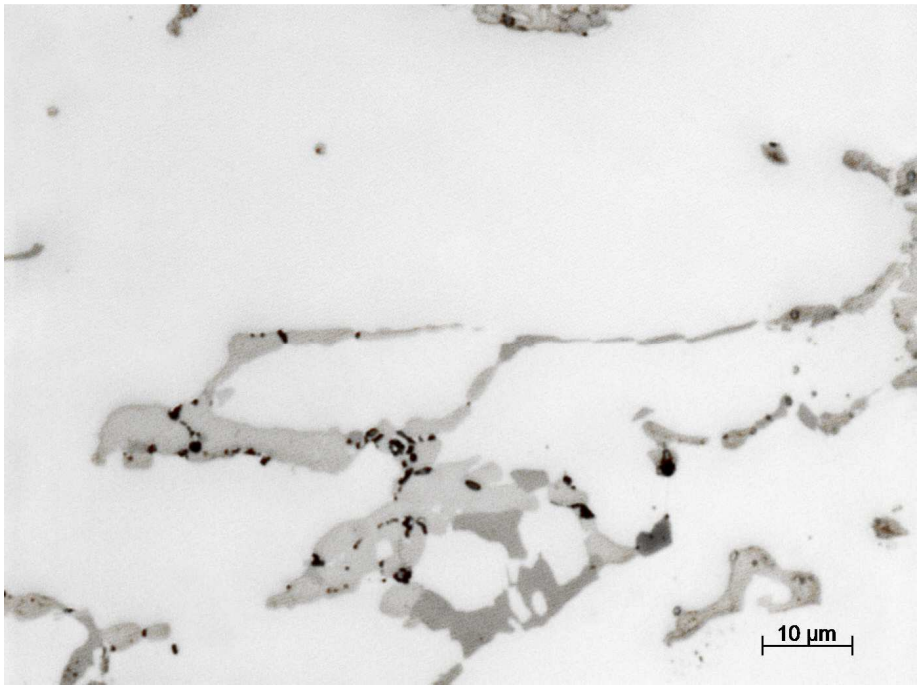

Figure 5.33: microstructure of alloy 3 − permanent mold casting − 1000x

Mg particles, the small black points, solidify close to the $CuAl_2$ phase, in light grey. Mn and Fe are concentrated in the dark grey phases.

As for alloy 2, die cast alloy 3 has a finer and less dendritic microstructure, as observed in figure 5.34:

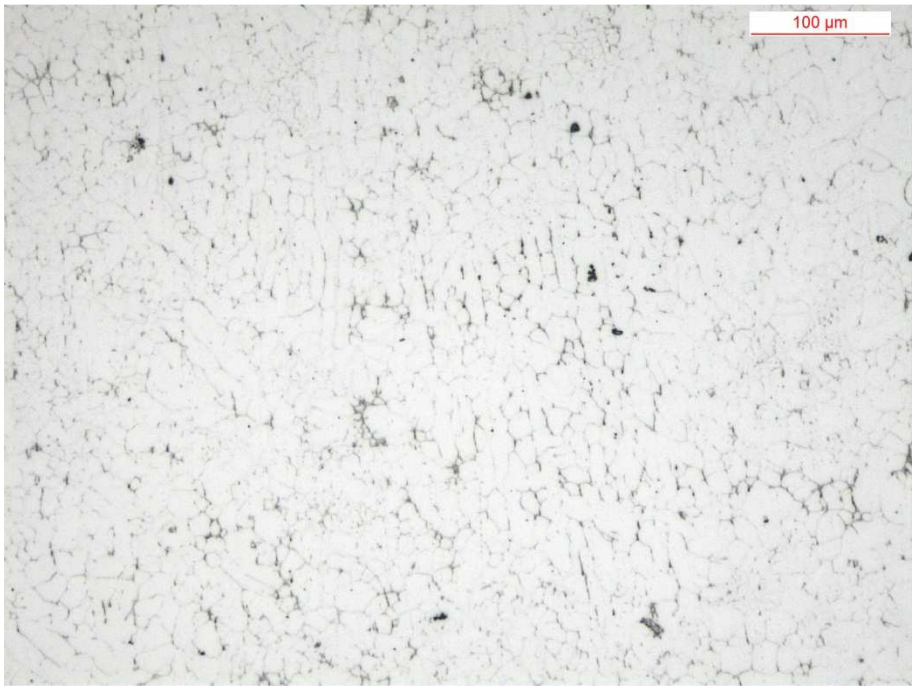

Figure 5.34: microstructure of alloy 3 – HPDC − 100x

Alloy 4 – AlCu5MnMg

The composition of alloy 4 is close to that of alloy 3. The differences are a lower Mg content (0.27% instead of 0.37%), an addition of 0.1% Zn and of 0.023% Ti. The Si content of alloy 4 is due to some residual on the crucible left from the previous usage. The Ti was added as AlTi5 grain refining alloy.

The alloy was fabricated after treating the molten aluminium with Ar + O_2. The parameters of the melt treatment were:

Injected gas:	Ar + 8 vol.% O_2
Duration of treatment:	90 min
Gas flow rate:	17.5 l_n/min
Melt temperature:	730 °C
Impeller diameter:	Ø 185 mm
Rotation speed:	350 rpm

The alloy was tested both as permanent mold casting and HPDC. Additionally, two series of HPDC specimens were heat-treated.

Alloy 4 – Permanent mold

A series of tensile specimens were cast in permanent mold. Some of them solidified before completely filling the mold cavity. Only four of them were tested and the obtained data are reported in figure 5.34.

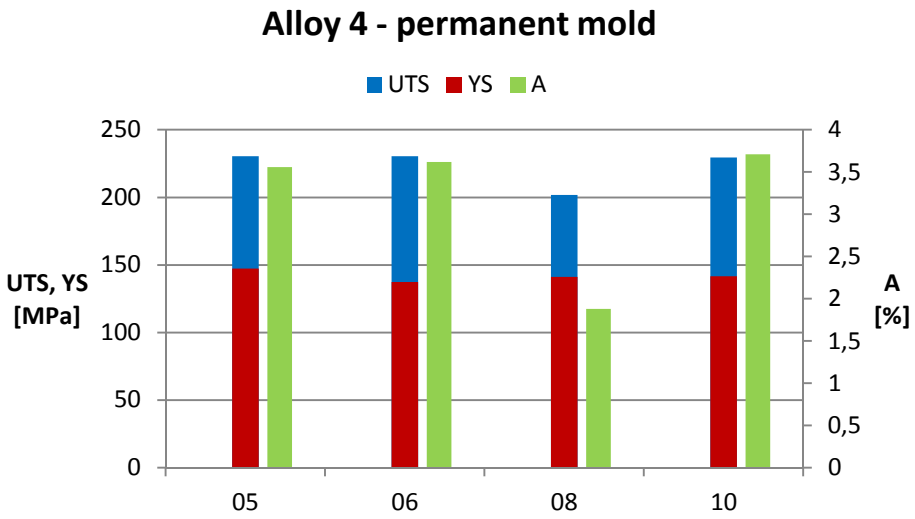

Figure 5.35: mechanical properties of permanent mold cast alloy 4

Three of the four tested specimens have the same mechanical behaviour, with very close values. The earlier failure of specimen nr. 08 is attributable to the presence of defects. Compared to alloy 3 cast in permanent mold, the mechanical properties are similar. The addition of Ti as grain refiner is too low to determine a real improvement. It is proved that 0.15% Ti is the minimum content for these alloys in order to obtain a consistent enhancement of the microstructure.

Alloy 4 – HPDC

Three series of tensile specimens were machined from die cast plates. The higher mold temperature reduced the hot cracking phenomenon and the majority of the plates appeared free of visible cracks. Nevertheless, smaller, internal cracks were still present, as revealed by x-ray images.

A series of ten plates was machined to obtain 40 specimen in as-cast condition; another series was solution heat-treated for 2 hours at 515 °C and then for 45 minutes at 525 °C before machining the specimens; the third series was solution heat-treated for 2 hours at 515 °C and then for 90 minutes at 525 °C[15]. The plates

were cooled in air. All the specimens were tested 55 days after the treatment, during which the treated ones were subjected to natural aging.

Alloy 4 – heat treatment specifications	
designation	times and temperatures
HT1	120 min at 515 °C + 45 min at 525 °C cooled in air natural aging for 55 days at room temperature
HT2	120 min at 515 °C + 90 min at 525 °C cooled in air natural aging for 55 days at room temperature

Table 5.7: designation and parameters of the performed heat treatments

The heat-treated plates presented blistering defects on the surface after the treatment.

X-ray images were taken to select the specimens free of internal defects, such as oxide films or hot cracks, and all the defective specimens were discarded. Though, not all the defects were detected, because of their size or orientation. Thus, some of the tested specimens broke at the early stages of the test. The data of such tests were discarded.

Tensile tests data of the non-treated specimens are illustrated in figure 5.36:

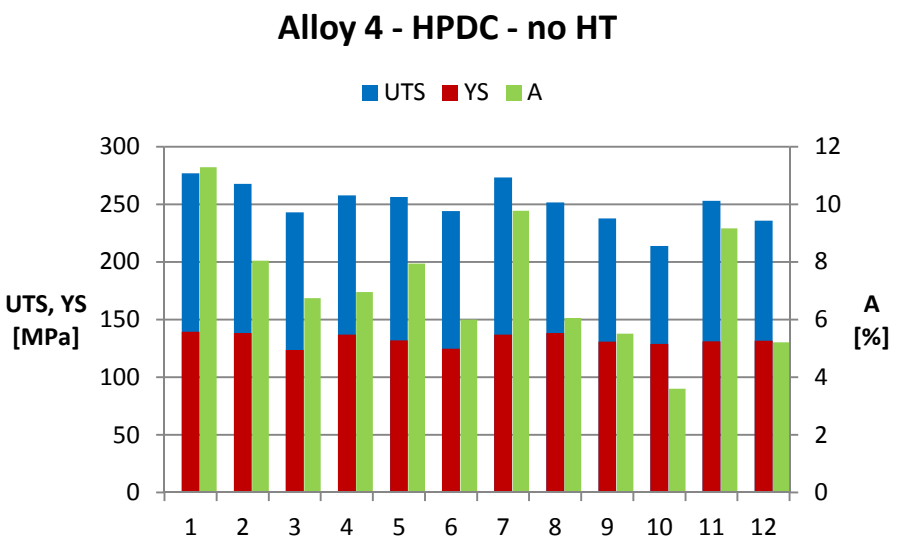

Figure 5.36: mechanical properties of HPDC alloy 4 without heat treatment

Alloy 4 without heat treatment shows a stable value of the yield stress, with an average of 132.7 MPa. UTS and elongation at fracture change with higher variability, depending on the amount of defects located on the fracture surface.

Comparing these data with those from the permanent mold cast specimens of the same alloy, a higher UTS is reached, with an average value of 250.9 MPa, 28 MPa higher. Elongation shows a wide range of values and the highest values reached in HPDC are more than three times those reached in permanent mold. The higher soundness of HPDC specimens really improves their toughness. Yield stress of HPDC specimens is slightly lower than that of the permanent mold ones. Comparing the stress-strain curves, the same difference observed in alloy 3 appears: permanent mold specimens yield within a wider range of stresses, while HPDC specimens have a well-defined yield point.

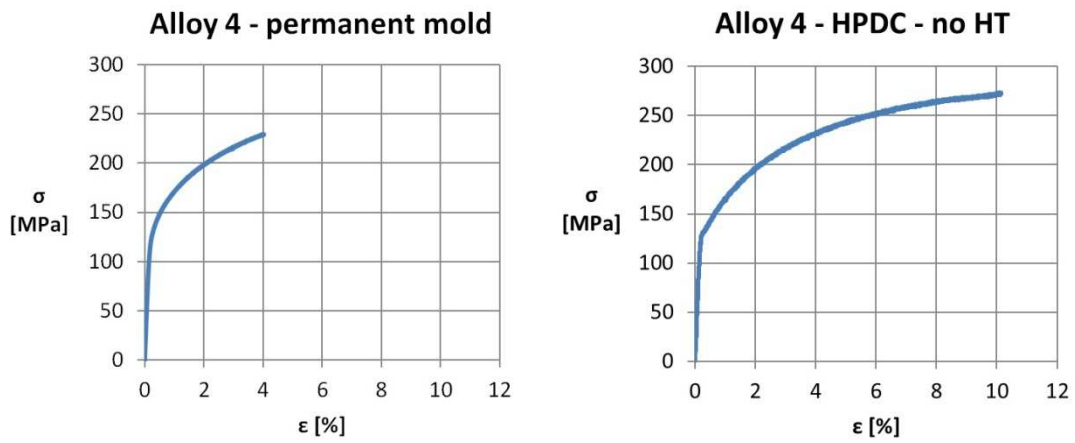

Figure 5.37: comparison of the yielding behaviour of permanent mold and die cast alloy 4

When compared to HPDC alloy 3, data appear more stable, with higher UTS and elongations and a slightly lower YS. The stability of data suggests a more homogeneous distribution of alloying elements, especially because of the repeatability of yield stress measurements.

The mechanical properties of the heat treated series are shown in figure 5.38 and 5.39:

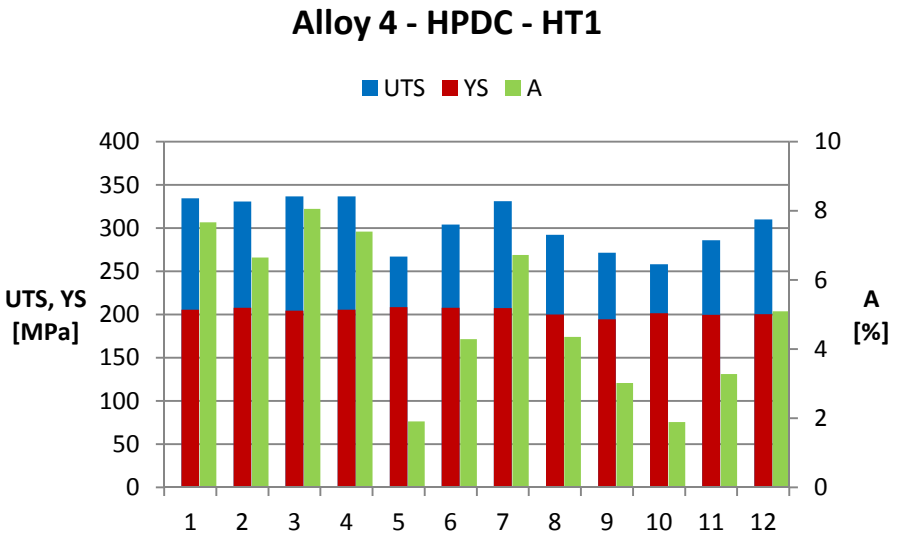

Figure 5.38: mechanical properties of die cast alloy 4 after HT1

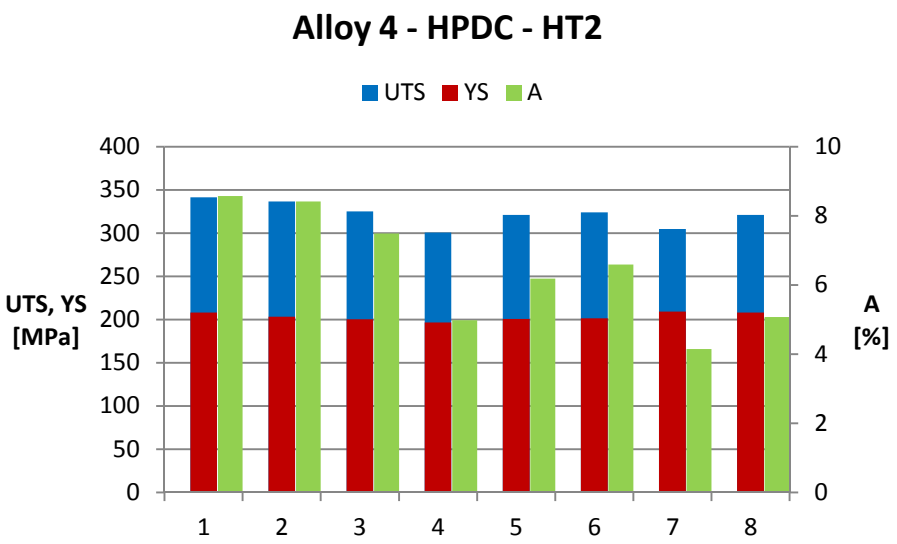

Figure 5.39: mechanical properties of die cast alloy 4 after HT2

From these data, it seems that the different holding times between the heat treatments have not determined any difference in final mechanical properties of the alloy after natural aging. Apparently, the solution process was already completed after 45 minutes at 525 °C.

The aging process strongly improved the strength of alloy 4, though keeping a good level of toughness. The mechanical properties of permanent mold cast AA 206.0 T4 alloy, as stated in ASM Handbook, are reported for a comparison:

AA 206.0 − Composition (wt.%)						
Si	Fe	Cu	Mn	Mg	Zn	Ti
0.10	0.15	4.2 5.0	0.20 0.50	0.15 0.35	0.10	0.10 0.30

Table 5.8: chemical composition of AA 206.0 alloy as reported in ASM Handbook

AA 206.0 T4 – Mechanical properties		
$R_{p0.2}$ [MPa]	R_m [MPa]	A [%]
207 (165)	345 (275)	10 (6)

Table 5.9: mechanical properties of AA 206.0 T4 as reported in ASM Handbook (minimum values between parenthesis)

UTS and YS of many die cast specimens achieve the values specified for the AA 206.0 T4 alloy. The elongation is lower in all the tests performed, probably because of the defects content, especially oxide films and gas porosities.

To be noticed is that the right part of all the diagrams of the HPDC alloy 4 presents lower mechanical properties. That part corresponds to specimens machined from plates richer in hot cracks. As described in section 4, this happened together with a progressive drop in melt temperature, which probably reduced the fluidity of the alloy.

The microstructure of alloy 4 cast in permanent mold is shown in figure 4.40:

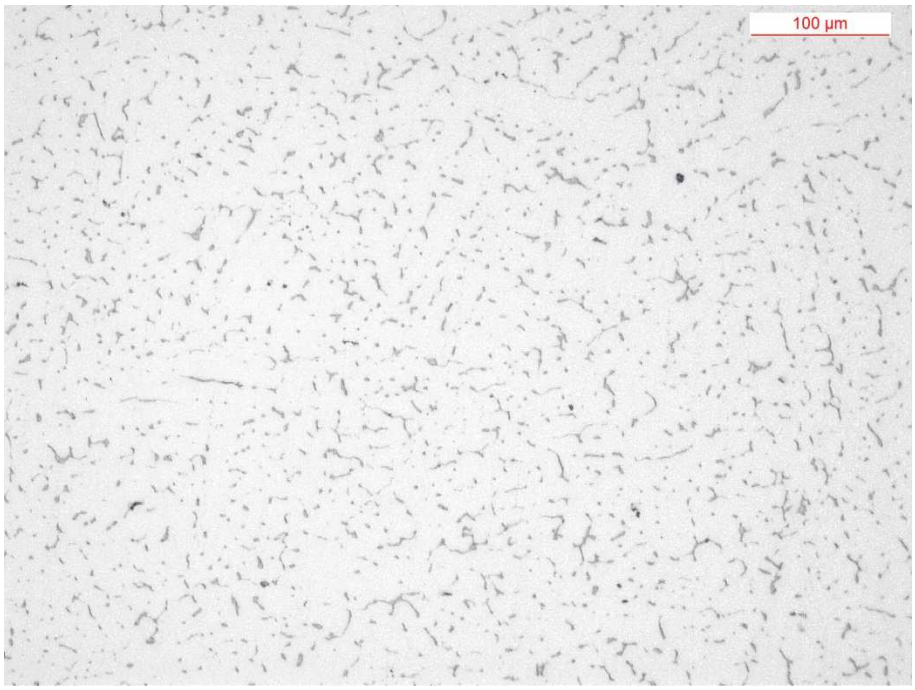

Figure 5.40: microstructure of alloy 4 − permanent mold casting − 100x

The microstructure appears dendritic, though dendrites are not so evident. This micrograph was taken from the last specimen cast, when the mold was at higher temperature: this may have promoted the formation of equiaxed dendrites. The distribution of secondary phases follows the interdendritic spaces. The phases are visible at higher magnifications:

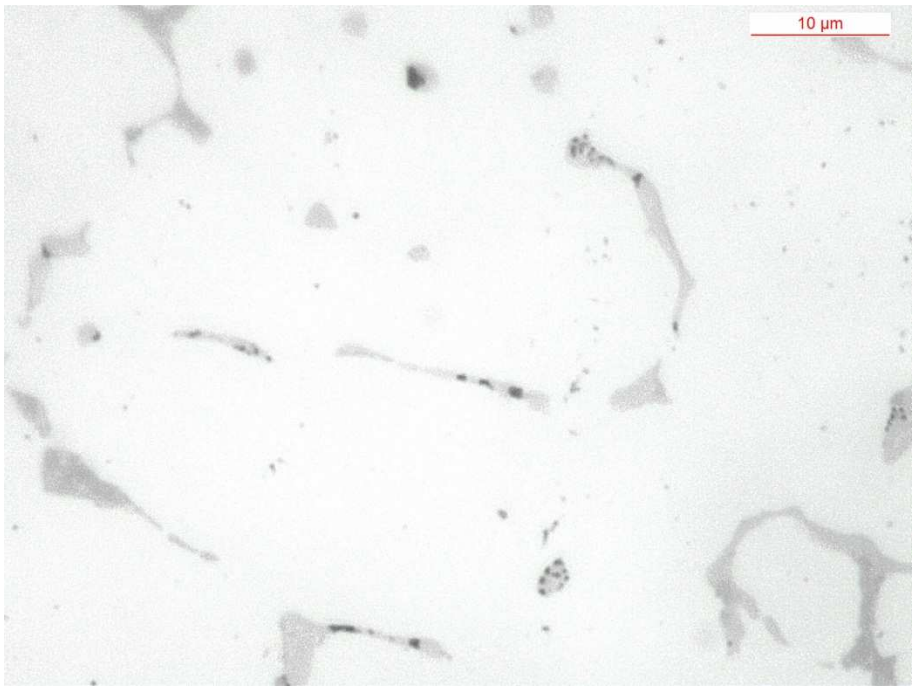

Figure 5.41: microstructure of alloy 4 - permanent mold casting - 1000x

As seen in alloy 3, CuAl2 is present in light grey regions with black spots of Mg, while Fe and Mn solidify in the dark grey phases.

Micrographs of die cast alloy 4 without heat treatment present some differences from to those of alloy 3. The microstructure is slightly finer, probably thanks to the addition of AlTi5 grain refiner, and a new phase appeared, which may be related to the addition of Zn.

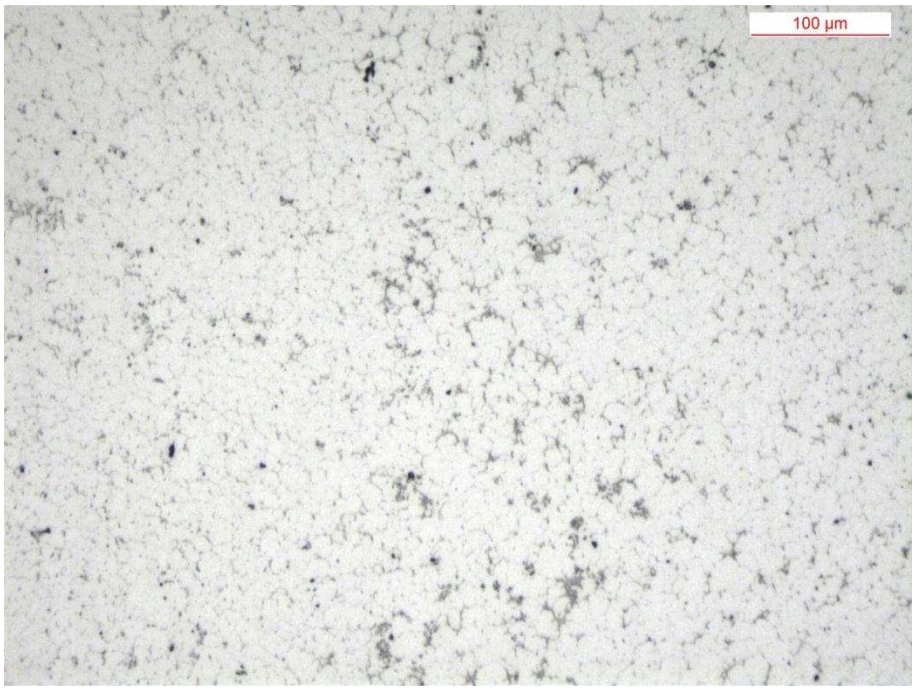

Figure 5.42: microstructure of alloy 4 − HPDC − no heat treatment − 100x

The new phase appears as a fine eutectic with Mg particles apparently solidified within. It is visible at higher magnifications, together with the other already seen phases:

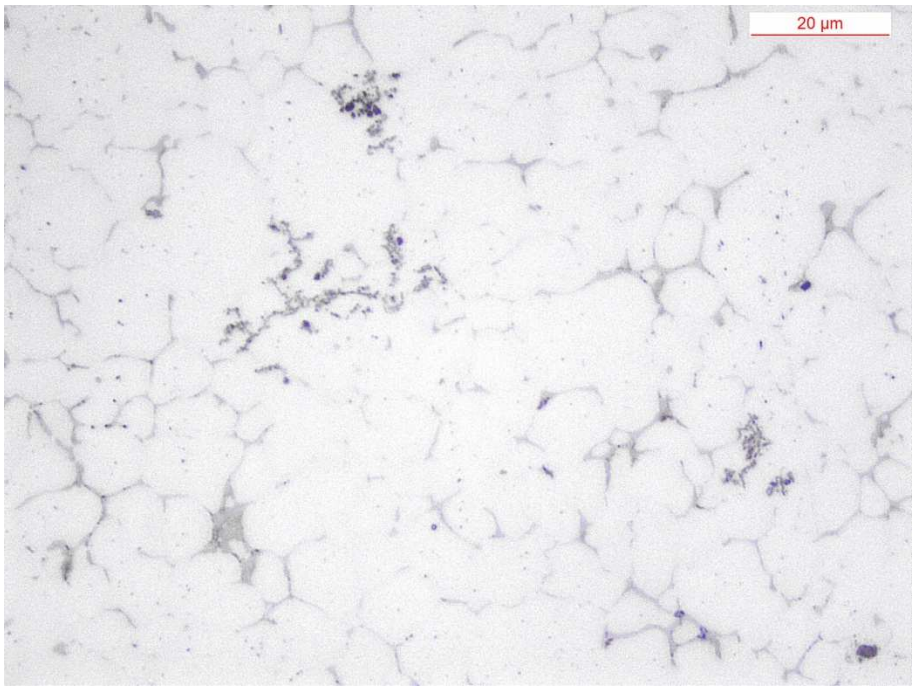

Figure 5.43: microstructure of alloy 4 − HPDC − no heat treatment − 500x

After heat treatment, the microstructure changes radically, as visible in figure 5.44:

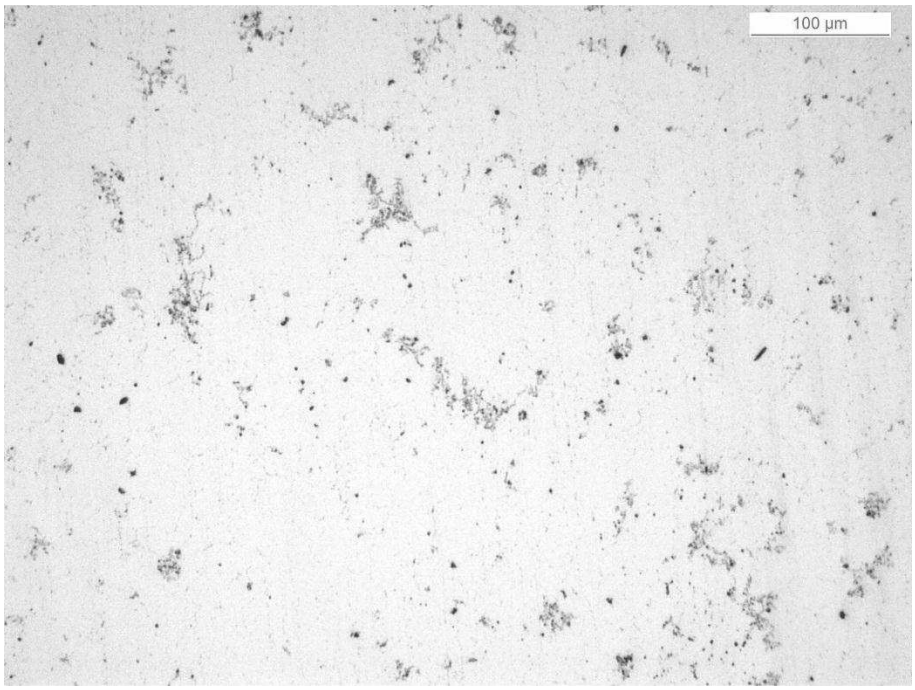

Figure 5.44: microstructure of alloy 4 − HPDC − HT1 − 100x

The solution heat treatment completely dissolved CuAl2 and the grain boundaries are no more visible. Only the insoluble phases, containing Fe and Mn, remain clearly distinguished.

After the longer heat treatment, the structure is similar:

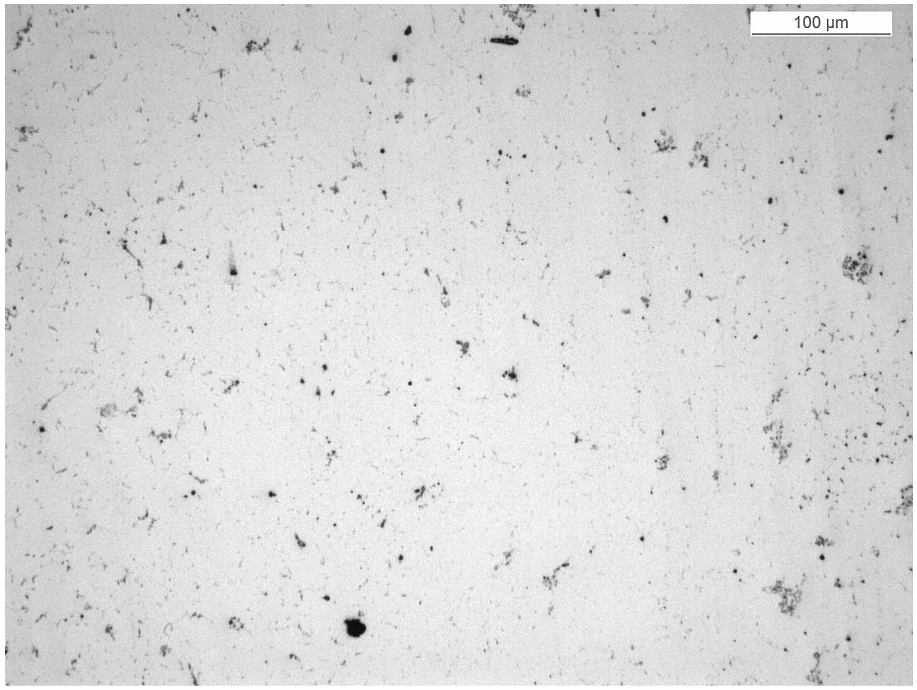

Figure 5.45: microstructure of alloy 4 - HPDC - HT2 - 100x

Apparently, a lower content of insoluble phases is present. Grain boundaries are not visible and only some insoluble phases are clearly distinguished.

Conclusions

The experiment was carried out in different conditions and with different parameters. In all the circumstances, the melt treatment produced a foamy slag which floated on the melt surface. The slag originates from the agglomeration of oxidized aluminium which floats because of its lower specific gravity and possibly because of the gas entrapped within.

The mechanical properties reached by alloy 1 after melt treatment with Ar and with Ar + O_2 do not present relevant differences. A positive evolution of the elongation in specimens cast during the treatment with Ar + O_2 is observed, though the values reached are comparable to those of the same alloy treated with Ar.

Influences of the mold size, temperature and porosity content and distribution were found on the mechanical properties of the alloy.

The microstructure of alloy 1 is characterized by the presence of an Al/Al_3Fe eutectic phase solidified at grain boundary and in round zones within the grains. No appreciable changes were found between the alloy without melt treatment, the alloy treated with Ar and the alloy treated with Ar + O_2. The impeller size had no influence on the microstructure.

Tests on alloy 2 showed the strengthening effect of Cu addition as alloying element. UTS and YS are improved with expense of the elongation. The measured values of UTS and A of permanent mold cast specimens agree with the specifications of EN AC-21100 alloy, while the YS is lower. Die cast specimens reach higher strength and elongation but suffer from the presence of many defects, especially hot cracks, which strongly affect the actual strength.

Both permanent mold and die cast alloy 2 show a “saw-toothed” profile of stress-strain curves. The damaging mechanism of the $CuAl_2$ phase may be the cause.

The microstructure of alloy 2 is dendritic and $CuAl_2$ solidify at the interdendritic spaces, together with the Al/Al_3Fe phase. HPDC have a finer microstructure due to the higher cooling rate.

Alloy 3 reached higher strength but lower elongation, compared to alloy 2. The additions of Mn and Mg and the higher content of Cu sensibly increased the

yield stress. Defects influenced the variability of values. A low homogeneity of composition is proposed as cause for this variability of data. Mechanical properties of permanent mold cast alloy 3 were compared to EN AC-21000 alloy: UTS and elongation reached the specified ranges, while YS was slightly lower. Die cast alloy 3 shows the same variability of data. Its mechanical properties are strongly influenced by the defects content.

The yielding behaviour of alloy 3 is different, depending on the casting process. Only die cast specimens show a defined yielding point.

The microstructure of alloy 3 is dendritic, with $CuAl_2$ and Mg phases alternated to Fe- and Mn-rich phases. Die cast microstructure is evidently finer and more equiaxed.

Alloy 4 cast in permanent mold show mechanical properties similar to those of alloy 3. Die cast specimens without heat treatment reached higher UTS and elongation, thanks to the finer microstructure, but a YS slightly lower. The same difference in yielding behaviour between the casting processes, as in alloy 3, is detected.

Heat treated alloy 4 really improved the mechanical properties thanks to the natural aging process. UTS and YS after both the solution heat treatments and the natural aging period reached the specified values for AA 206.0 T4 alloy. No difference in mechanical properties emerged between HT1 and HT2. Elongation is constantly lower than the optimal value, but higher than the minimum specified. The explanation is found on the defectiveness of the specimens.

The microstructures of alloy 4 revealed the presence of a phase not detected in the other alloys, supposedly due to the addition of Zn, in addition to the other phases already shown in alloy 3. In heat treated microstructures CuAl2 and Mg are not detectable anymore.

In general, no strengthening effect can be attributed to the melt treatment investigated. Apparently, all the oxide generated during the treatment remains on the melt surface. The mechanical properties of the Al-Cu alloys tested are not influenced and the hot cracking susceptibility was not improved. No Al_2O_3 particles were seen in micrographs.

A reduction of hot cracking was achieved by increasing the mold temperature in HPDC process. Moreover, the melt temperature influences the hot cracking process. Increasing the melt temperature also reduced the formation of cracks.

The research presented in this work was inspired by the lecture by David Weiss from Eck Industries at the 12th International Summer School on Light Alloys Casting, held in 2011 in Vicenza, at the Department of Engineering and Management of the University of Padova. He reported on the production of an AA A206.0 casting alloy reinforced with Al_2O_3 particles.

The research for an affordable, effective and feasible process available to produce similar reinforced alloys revealed that many techniques have been developed and patented, though the majority require complex equipment, expensive materials or process conditions far from those conventionally available in foundries. Some of them involve the impregnation of porous preforms made of ceramic materials. Other techniques involving chemical reactions and multi-stage processes were also found: a process involving CuO and aluminium proved to be effective in producing Al_2O_3 particles through addition of CuO in stirred molten aluminium at 1273 K. Al_2O_3 were obtained also adding $NH_4AlO(OH)HCO_3$ directly into molten aluminium.

Among all, a process, successfully applied in production of AlN-reinforced Al-Li alloys, appeared interesting for its feasibility: a work by Cecilia Borgonovo and Makhlouf M. Makhlouf from the Advanced Casting Research Centre at Worcester Polytechnic Institute reports on the production of Al-Li/AlN die-castable nano-reinforced alloy by injecting a mixture of N_2 and NH_3. The process is effective in producing the AlN particles homogeneously dispersed in Al-Li alloy matrix and it is also scalable. In addition, the process appeared feasible at the Giesserei Technologie Aalen laboratory, at the Hochschule für Technik und Wirtschaft in Aalen, Germany, where the present work has been developed.

The results of this work proved that its application to the production of Al_2O_3 reinforcing particles in molten aluminium is not possible. Though, the research for affordable processes has a key role in spreading the adoption of these innovative materials.

References

[1] K.U. Kainer, *Basics of Metal Matrix Composites*

[2] C. Borgonovo, *Aluminum Nano-composites for Elevated Temperature Applications*, Worcester Polytechnic Institute, Worcester, USA

[3] C. Borgonovo, Makhlouf M. Makhlouf, *Synthesis of die-castable nano-particle reinforced aluminium matrix composite materials by in-situ gas-liquid reactions*, Worcester Polytechnic Institute, Worcester, USA

[4] A.A. Hamid, P.K. Ghosh, S.C. Jain, S. Ray, *Processing, Microstructure, and Mechanical Properties of Cast In-Situ Al(Mg,Ti)-Al_2O_3(TiO_2) Composite*, Metallurgical and Materials Transactions A, vol. 37A, Feb. 2006

[5] North American Die Casting Association - www.diecasting.org

[6] CustomPartNet – www.custompartnet.com/wu/die-casting#equipment

[7] *ASM Handbook*, ASM International, vol. 2

[8] UC RUSAL – www.aluminiumleader.com/en/around/transport

[9] I. J. Polmear, *Aluminium Alloys - A century of age hardening*, Materials Forum Vol. 28 – 2004

[10] J.R. Greer, *Handout AlCu*, www.jrgreer.caltech.edu

[11] Prof. F. Bonollo, *Leghe di alluminio: approfondimenti metallurgici – Trattamenti termici*, Dipartimento di Tecnica e Gestione dei Sistemi Industriali - Università di Padova, Vicenza, Italy

[12] *Alcan AA206 Primary Foundry Alloys*, Alcan Primary Products Corporation Inc.

[13] S. Li, *Hot Tearing in Cast Aluminium Alloys: Measures and Effects of Process Variables*, Worcester Polytechnic Institute, Worcester, USA

[14] S. Bao, K. Tang, A. Kvithyld, M. Tangstad, *Wettability of Aluminum on Alumina*, Metallurgical and Materials Transactions B, vol. 42B, Dec. 2011

[15] E.G. Fuchs, A Roósz, *TTD-Diagrams for the Homogenization of As-Cast Structures*, Z. Metallkunde, Vol. 63, pp. 211-214 (1972)

[16] Prof. F. Bonollo, *Prodotti Metallurgici Innovativi e Multifunzionali*, Dipartimento di Tecnica e Gestione dei Sistemi Industriali - Università di Padova, Vicenza, Italy

[17] www.matweb.com

[18] www.keytometals.com

[19] www.aviometal.com

[20] www.wikipedia.org